



ANAIS - CBrAVIC 2020

XLI CONGRESSO BRASILEIRO DE APLICAÇÕES DE VÁCUO NA INDÚSTRIA E NA CIÊNCIA

Nazir Monteiro dos Santos

sbvdiretoria@gmail.com

Foz do Iguaçu/PR



APRESENTAÇÃO	05
PROGRAMAÇÃO	12
RESUMO DAS PALESTRAS	
Perspectives of modified PECVD technique of DLC growth for new R&D&I demands	17
Vladimir Jesus Trava-Airoldi	
Asymmetric bipolar pulsed plasma: a new approach for cold plasma densification and process control	18
Luis César Fontana	
Thermochemical treatments of stainless steels	19
Rodrigo P. Cardoso, Cristiano J. Scheuer, Fernando I. Zanetti, Igor G. Zanella, Leonardo L. Santos, Lauro M. Ferreira, Adriano D. dos Anjos, Carlos E. A. Feitosa, Aécio F. Mendes, Laércio Malfatti, João F. F. Lima, Tarciana D. Toscano, Silvio F. Brunatto	
Nanostructural characterization of β -Ti-Nb-Zr ternary alloy coatings produced by magnetron co-sputtering	21
E. David Gonzalez, Angelo Luiz Gobbi, Conrado R. M. Afonso, Pedro Augusto de Paula Nascente	
RESUMO DOS TRABALHOS PREMIADOS	
A global model study of argon plasma chemistry used as propellant of a gridded ion thruster	23
Bernardo Vieira Magaldi, Rodrigo Sávio Pessoa, Argemiro Soares da Silva Sobrinho	
Development of a methodology for measuring the evolution of duplex stainless steel low-temperature plasma nitrided phases expansion using confocal laser scanning microscopy	29
Carlos Eduardo Alves Feitosa, Rodrigo Perito Cardoso, Silvio Francisco Brunatto	
Effect of manganese on the mechanical properties of Ti-15Mo-Mn alloys	31
Giovana Collombaro Cardoso, Mariana Luna Lourenço, Carlos Roberto Grandini	
RESUMO DOS TRABALHOS APRESENTADOS	
Estimation of layer thickness of plasma nitrided martensitic stainless steels with machine learning techniques	33
Giovanni Corsetti Silva	
Carbon nanotubes functionalization through electrical discharge across a mixed of nanotubes with solid chemical compounds	35
Teresa Tromm Steffen, Daniela Becker, Luis César Fontana, Peter Hammer	

Development and test in pilot-scale of a thermal plasma reactor for the production of carbonaceous materials from coal tar pitch	37
Eduardo Petraconi Prado, Felipe De Souza Miranda, Gisele Amaral Labat, Gilberto Petraconi, Maurício Ribeiro Baldan	
A global model for DC magnetron sputtering	39
Júlia Karnopp, Julio César Sagás	
Effects of oxygen addition on atmospheric pressure plasma jet parameters.....	41
Fellype do Nascimento, Kleber Petroski, Ananias Alves Barbosa, Konstantin Kostov	
Evaluation of the aggregation of sugarcane bagasse residue in the manufacture of soil-cement bricks.....	43
Samyra De Oliveira Figueira Da Silva, F. M. T. Sampaio, Antônio Renato Bigansolli	
Development of algorithm to study troposphere and low stratosphere instabilities from radiosonde observations	45
Elson de Campos, Marco Antonio Ridenti, Marisa Roberto, Alysson Brhian de Souza Muniz Silva, José Ricardo Abalde Guedes, Alessandro José de Abreu	
Synthesis of graphene on nickel oxide by PECVD	47
Larissa Solano de Almeida, Andressa L. O. Pinto, Marcos D. Manfrinato, Luciana Sgarbi Rossino	
Study of the added nitrogen effect on the diamond-like carbon film in the film electric characteristic.....	49
Mateus da Silva Pereira, Larissa Solano de Almeida, Marcos Dorigão Manfrinato, Luciana Sgarbi Rossino	
Cold plasma jet improve tissue repair in wounds infected by multispecies biofilms	51
Maria Alcioneia Carvalho de Oliveira, Aline da Graça Sampaio, Thalita Mayumi Castadelli Nishime, Kostantin Georgiev Kostov, Cristiane Yumi Koga-Ito	
Effect of the interlayer on duplex treatments properties	53
Miguel Rubira Danelon, Marcos Dorigão Manfrinato, Luciana Sgarbi Rossino	
Association of atmospheric pressure cold plasma and nystatin on <i>Candida albicans</i> biofilms.....	55
Lady Daiane Pereira Leite, Maria Alcioneia Carvalho de Oliveira, Thalita Mayumi Castaldelli Nishime, Konstantin Georgiev Kostov, Cristiane Yumi Koga-Ito	
Nitrided austenitic stainless steel: the importance of characterizing the submicrometrical region.....	57
Danilo Olzon-Dionysio, Solange de Souza, Sylvio D. de Souza, Maristela Olzon-Dionysio	
Effects of cold atmospheric plasma on the healing process of dermal ulcers infected by multispecies biofilms	59
Maria Alcionéia Carvalho de Oliveira, Aline da Graça Sampaio, Thalita Mayumi Castaldelli Nishime, Konstantin Georgiev Kostov, Cristiane Yumi Koga-Ito	
Analysis of epoxy/granite composites using FTIR	61
Jorge Luiz Siqueira-Costa-Neto, Guilherme Soares Damasceno, Antônio Renato Bigansolli, Belmira Benedita de Lima-Kühn	
Study of the corrosion resistance of DLC film with multilayers of organosilicone and silicon oxide	63
César A. A. Júnior, Marcos Dorigão Manfrinato, Luciana Sgarbi Rossino	

Global model of argon ICP discharge: effects of reaction set on collisional energy	65
Júlia Karnopp, Rodrigo Sávio Pessoa, Julio César Sagás	
Microestrutura de filmes Ti(1-x)Al(x)N obtidos no modo metálico e no modo composto via <i>magnetron sputtering</i>	63
Abel André Cândido Recco	
Mechanical spectroscopy of hot-rolled Ti-Zr-Mo-Ag alloys	68
Renata Carolina Araujo de Camargo, Diego R. N. Correa, Jhulienne Elen Torrento, Carlos Roberto Grandini	
Hallow cathode effect caused by sample-support arrangement on plasma immersion ion implantation of nickel aluminum bronze AMPCO M ₄	70
Bruna C. E. S. Kurelo, Gelson B. de Souza, Silvio Francisco Brunatto	
ASTM CA6NM martensitic stainless steel plasma assisted hybrid heat-thermochemical treatment: first results for carbon-expanded austenite surfaces	71
Felipe Jedyn, Rodrigo Perito Cardoso, Silvio Francisco Brunatto	
Structure proposed to lead with data sensor based	73
Leandro Colevati dos Santos, Sebastião Gomes dos Santos Filho, Maria Lúcia Pereira da Silva	
On the polymerization processes of 2-metil-2-oxazoline plasma polymer (pp-oxazoline)	75
Pedro William Paiva Moreira Júnior, Felipe Vicente de Paula Kodaira, Rogério Pinto Mota	
Cariogenic multispecies biofilms were inhibited by cold atmospheric plasma	77
Leandro Figueira, Maria Alcioneia Carvalho de Oliveira, Marcia Hiromi Tanaka, Thalita Mayumi Castadelli Nishime, Konstantin Kostov, Cristiane Koga-Ito	
Cold atmospheric plasma inhibits <i>Escherichia coli</i> biofilms formed on PVC specimens	79
Ellen Rodrigues de Souza Reis, Konstantin Georgiev Kostov, Cristiane Yumi Koga Ito	
Chemical and mechanical characterization of Ti-25Ta-70Zr Alloy	80
Edriely de Oliveira Saraiva, Pedro Akira Bazaglia Kuroda, Carlos Roberto Grandini	
Preparation and characterization of Ti-10mo-5mn-1ag	82
Melissa Daniela de Almeida Nespeque, Mariana Luna Lourenço, Carlos Roberto Grandini	
Development of Ti-, Mo- and Zr-based alloy for biomedical applications	84
Israel Ramos Rodrigues, Renan Eduardo de Lima Lopes, Carlos Roberto Grandini	
Structural and microstructural characterization of the Ti-10Mo-40Zr alloy	86
Renan Eduardo de Lima Lopes, Israel Ramos Rodrigues, Carlos Roberto Grandini	
Failure analysis of stiffened composite panels obtained by different adhesively bonding techniques and submitted to axial compression tests	88
Rita de Cássia Mendonça Sales, Geraldo Maurício Cândido, Maurício Vicente Donadon	
Physical-chemical characterization of poly(methyloctadecylsiloxane) immobilized on titanized silica as a sorbent for solid-phase extraction	90
José Matheus Cardoso Santa Brígida, Carla Grazieli Azevedo da Silva	
AGRADECIMENTOS	92



APRESENTAÇÃO

A Sociedade Brasileira de Vácuo (SBV), a Universidade Federal da Integração Latino-Americana (UNILA) e o Comitê Organizador da XLI Congresso Brasileiro de Aplicações de Vácuo na Indústria e na Ciência (CBrAVIC) convidaram a comunidade mundial de ciências, tecnologia e inovação a participar do CBrAVIC 2020, que ocorreu *online* no período de 09 a 11 de dezembro de 2020.

Desde 1979, pesquisadores e instituições que atuam na área de Ciência, Tecnologia e Engenharia vêm organizando, anualmente, o Congresso Brasileiro de Aplicações de Vácuo na Indústria e na Ciência. Esse importante e tradicional evento conta com o apoio de universidades e instituições de pesquisa que congregam os principais segmentos da comunidade científica.

Em busca de complementar as capacidades nacionais por meio de atividades e projetos de cooperação, colaborações internacionais foram associadas ao evento através da *“International Union for Vacuum Science, Technique and Applications (IUVSTA)”*, e da *“Nanosmat Society”*.

A IUVSTA (União Internacional para Ciência, Técnica e Aplicações do Vácuo) é uma união de 33 sociedades internacionais de ciência e tecnologia cujo papel é estimular a colaboração internacional nos campos da ciência, técnica e aplicações do vácuo, e tópicos multidisciplinares relacionados. Através desta colaboração, o CBrAVIC aproximou ciência e tecnologia para satisfazer interesses acadêmicos e industriais.

Dra. Nazir Monteiro dos Santos
Coordenadora do evento

Dr. Álvaro Damião
Presidente da SBV



PATROCÍNIO



Agilent

Trusted Answers

APOIO



REALIZAÇÃO





ORGANIZAÇÃO

COORDENADORA DO EVENTO (Chair)

Profa. Dra. Nazir Monteiro dos Santos
UNILA/PR

PROMOVEDOR DO EVENTO

Sociedade Brasileira de Vácuo (SBV)
Diretoria Executiva - Biênio 2019-2021

Presidente

Prof. Dr. Alvaro José Damião
IEAv

1ª Vice Presidente

Prof.ª Dra. Maria Lucia Pereira da Silva
USP/FATEC

2º Vice Presidente

Prof. Dr. Francisco Tadeu Degasperi
FATEC

1º Secretário

Profa. Dra. Deborah C. R. Santos
UNESP

2º Secretário

Luciano Rugério Silva
Inertsolutions

1º Tesoureiro

Prof.ª Dra. Nazir Monteiro dos Santos
UNILA

2º Tesoureiro

Prof. Marcos Massi
Universidade Mackenzie

Diretor Científico

Prof. Dr. Luis Cesar Fontana
UDESC

Diretor Cultural

Prof. Dr. Carlos Roberto Grandini
UNESP

COMITÊ LOCAL (UNILA, Foz do Iguaçu/PR)

Dra. Nazir Monteiro dos Santos (Chair)

Dr. Eduardo Goncalves Reimbrecht

Dr. Gustavo George Verdieri Nuernberg

Dr. Jose Ferreira da Silva Junior

Dr. Rafael Drumond Mancosu

Dra. Gislaíne Bezerra Pinto Ferreira

Dra. Liliane Cristina Battirola

Dra. Priscila Lemes Rachadel

COMITÊ CONSULTIVO

Dr. Álvaro José Damião
IEAV/CTA

São José dos Campos/SP

Dr. Carlos Roberto Grandini
UNESP – Bauru/SP

Dr. Clodomiro Alves Júnior
UFERSA
Mossoró/RN

Dr. Evaldo José Corat
INPE
São José dos Campos/SP

Dr. João Moro
IFSP
Bragança Paulista/SP

Dr. Konstantin G. Kostov
UNESP
Guaratinguetá/SP

Dr. Leonardo Contijo
IFES
Vitória/ES

Dr. Luís César Fontana
UDESC
Joinville/SC

Dr. Pedro Augusto de Paula Nascente
UFSCar
São Carlos/SP

Dr. Rogério Moraes de Oliveira
INPE
São José dos Campos/SP

Dr. Rogério Pinto Mota
UNESP
Guaratinguetá/SP

COMITÊ CIENTÍFICO

Dra. Adriana Silva
INPE
São José dos Campos/SP

Dr. Adriano Gonçalves dos Reis
UNESP
São José dos Campos/SP

Dra. Ana Neilde R Silva
USP
São Paulo/SP

Dr. André Ricardo Marcondes
INPE
São José dos Campos/SP

Ms. Ângelo Luiz Gobbi
LNNano
Campinas/SP

Dr. Antônio Renato Bigansolli
UFRRJ
Seropédica/RJ

Dr. Carlos Roberto Grandini
UNESP
Bauru/SP

Dr. Cícero Rafael Cena da Silva
UFMS
Campo Grande/MS

Dr. Clodomiro Alves Júnior
UFERSA
Mossoró/RN

Dra. Cristiane Costa Wachesk
UNIFESP
São Paulos/SP

Dra. Danieli Aparecida P. Reis
UNIFESP
São José dos Campos/SP

Dra. Deborah Cristina Ribeiro dos Santos
SBV
Guaratinguetá/SP

Dra. Elidiane Cipriano Rangel
UNESP
Sorocaba/SP

Dra. Érica Freire Antunes
INPE
São José dos Campos/SP

Dr. Evaldo José Corat
INPE
São José dos Campos/SP

Dr. Fernando Luiz de C. Carvalho
UNESP
São José dos Campos/SP

Dr. Francisco Tadeu Degasperi
CEETEPS
FATEC SP

Dr. Gelson B. de Souza
UEPG
Ponta Grossa/PR

Dr. Gilberto Petraconi Filho
ITA/CTA
São José dos Campos/SP

Dra. Graziela da Silva Savonov
INPE
São José dos Campos/SP

Dr. João Moro
IFSP
Bragança Paulista/SP

Dr. Konstantin G. Kostov
UNESP
Guaratinguetá/SP

Dr. Luís César Fontana
UDESC
Joinville/SC

Dra. Maria Lúcia Pereira da Silva
USP
São Paulo/SP

Dra. Maria Margareth da Silva
ITA/CTA
São José dos Campos/SP

Dra. Marina Fuser Pillis
IPEN/CNEN
São Paulo/SP

Dr. Mario Ueda
INPE
São José dos Campos/SP

Dr. Mauricio Antônio Algatti
UNESP
Guaratinguetá/SP

Dr. Michel Felipe Lima de Araújo
UDC
Foz do Iguaçu/PR

Dr. Milton Eiji Kayama
UNESP
Guaratinguetá/SP

Dr. Mostafa Dadashbaba
Yeditepe University
Istambul/Turquia

Dra. Nazir Monteiro dos Santos
UNILA
Foz do Iguaçu/PR

Dr. Nilson Cristino Cruz
UNESP
Sorocaba/SP

Dra. Neidenei Gomes Ferreira
INPE
São José dos Campos/SP

Dr. Pedro Augusto de Paula Nascente –
UFSCar
São Carlos/SP

Dr. Péricles L. Sant'Ana
UNESP
Sorocaba/SP

Dra. Renata Antoun Simao
UFRJ
Rio de Janeiro/RG

Dr. Rodrigo Sávio Pessoa
ITA/CTA
São José dos Campos/SP

Dr. Rogério de Almeida Vieira
UNIFESP
São Paulo/SP

Dr. Rogério Pinto Mota
UNESP
Guaratinguetá/SP

Dra. Samantha de F. M. Mariano
INPE
São José dos Campos/SP

Dr. Steven Frederick Durrant
UNESP
Sorocaba/SP

Dra. Gabriela Araújo Ranieri
UNIFEI
Itajubá/MG

Dr. Rafael Toledo
UNILA
Foz do Iguaçu/PR

Hudson Marques da Silva
Discente
UNILA

João Victor Ribeiro
Discente
UNILA

Júlia Karnoop
Mestranda
IFSC

COMITÊ ACADÊMICO

Alexandre Moreira
Discente
UNILA

BeatrizAssis Kalb
Discente
UNILA

Beiker Martínez Rueda
Discente
UNILA

Diego Ferreira Gonçalves da Silva
Discente
UNILA

Fernando Vieira dos Santos
Discente
UNILA

Kananda Pereira Fernando
Discente
UNILA

Mario Augusto Albertini Regatieri
Discente
UNILA

Rodolfo Javier Talavera
Discente
UNILA

Vinicius Candido Padilha Furtado
Discente
UNILA

Willian Alves Mello
Discente
UNILA



TEMAS E PUBLICAÇÃO

TEMAS

- Biomateriais: Ciência e Tecnologia (BCT)
- Ciência e Tecnologia de Plasmas (CTP)
- Ciência e Tecnologia de Sensores e Dispositivos (CTSD)
- Ciência e Tecnologia de Vácuo (CTV)
- Ciência e Tecnologia dos Materiais (CTM)
- Ciência, Tecnologia e Inovação de Materiais (CT& I Mat)
- Energia: Fontes Renováveis e Tecnologia (EFRT)
- Materiais Metálicos e Metalurgia (MMM)
- Superfícies, Interfaces e Filmes Finos (SIFF)
- Tratamento e Modificação de Superfície (TMS)
- Vácuo na Indústria (VA)

PUBLICAÇÃO

Os trabalhos completos devem ser submetidos a Revista Brasileira de Aplicações de Vácuo (RBAV), através do link:

<http://www.sbvacu.org.br/rbav/index.php/rbav>

Fontes de Indexação:

<http://www.sbvacu.org.br/rbav/index.php/rbav/about/editorialPolicies#custom-0>

Os artigos publicados na Revista Brasileira de Aplicações de Vácuo (RBAV) são indexados por:

CAS – Chemical Abstracts; LATINDEX; CSA – Materials Research Database e METADEX; CSA - Technology Research Database; Periódica - Índice de Revistas Latinoamericanas en Ciencias.

A Revista é qualificada pela Capes como:

- B3 nas áreas de Engenharias II e Interdisciplinar,
- B4 nas áreas Engenharias III e Materiais, e
- B5 nas áreas de Medicina II e Engenharias IV.

Contato

Dra. Maria Lúcia Pereira da Silva - USP/EP | E-mail: malu@lsi.usp.br



PROGRAMAÇÃO GERAL

PROGRAMAÇÃO GERAL - CBrAVIC 2020		
Quarta-feira 09/12/2020	Quinta-feira 10/12/2020	Sexta-feira 11/12/2020
<p>Abertura do evento Dr. Álvaro Damiano (Presidente da SBV)</p> <p>8h30 Dr. Gleisson Alisson P. Brito (Reitor/UNILA) Dr. Jian Pires Frigo (Diretor/UNILA/ILATIT) Dr. César Winter de Mello (CITI/UNILA)</p>	<p>Chair Prof. Dr. Rogério Pinto Mota (FEG-UNESP)</p> <p>Palestra online "Perspectives of Modified PECVD Technique of DLC Growth for New R&D&I Demands"</p> <p>Prof. Dr. Vladimir Trava-Airold (INPE-SJC)</p>	<p>Chair Prof. Dra. Rita de Cássia Mendonça Sales Contini (FATEC SJC)</p> <p>Palestra online "Missão do 1º Nanosatélite Científico Brasileiro (Nanosat C-BR1) e Empreendedorismo"</p> <p>Marcelo Essado (Presidente da Aliança das Startups Espaciais Brasileiras-ASB)</p>
<p>9h00 Abertura das apresentações dos trabalhos Profa. Dra. Nazir M. dos Santos (UNILA/ILATIT) Coordenador do evento</p>		
9h10 T238		
9h15 T204		
9h20 T255		
9h40 T254	T249	
9h45 T245	T220	
9h50 T198	T248	
9h55 T208	T233	
10h00 T231	T253	
10h20 T215	T199	
10h25 T203	T232	
10h35 Intervalo	Intervalo	
11h00 T193	Palestra online	<p>Minicurso (2h00): "Introdução aos Nanosatélites"</p> <p>Prof. Lázaro A. P. Camargo Coordenadoria de Ciências Espaciais (CEA-INPE SJC)</p>
11h05 T229	"Asymmetric Bipolar Pulsed Plasma: a new approach for cold plasma densification and process control"	
11h10 T197		
11h15 T217		
11h20 T242		
11h40 T243		
11h50 T228	Prof. Dr. Luis César Fontana (UDESC/Joinville-SC)	
12h00 Almoço	Almoço	Almoço
13h30	T250	
13h35	T251	
13h40	T212	
13h45	T236	
13h50	T247	
14h00	T192	
14h05	T194	
14h10	T244	
14h20		
14h40 Intervalo	Intervalo	Intervalo
15h00		
15h40	Chair: Prof. Dra. Luciana Sgarbi Rossino (FATEC Sorocaba)	Chair: Prof. Dr. Gustavo George Verdieri Nuernberg (UNILA)
15h50	Chair: Prof. Dra. Liliane Cristina Battirola (UNILA)	
<p>Palestra online "Ligas de Ti-Nb para aplicações biomédicas: passado, presente e futuro"</p> <p>Prof. Dr. Carlos Roberto Grandini (UNESP Bauru)</p>	<p>Palestra online "Atmospheric pressure jets for surface modification and biomedical applications"</p> <p>Prof. Dr. George Konstantin Kostov (FEG/UNESP)</p>	<p>Palestra online "Nanostructural Characterization of B-Ti-Nb-Zr Ternary Alloy Coatings Produced By Magnetron Co-Sputtering"</p> <p>Prof. Dr. Pedro A. P. Nascente (UFSCar São Carlos)</p>
16h00	T227	<p>Premiação dos melhores trabalhos</p>
16h20	T230	
16h35	T235	
16h40	T224	
16h45	T222	
16h50	T202	
17h00		<p>Assembleia Geral da SBV</p>
<p>Minicurso (2h00): "Vácuo para iniciantes"</p> <p>Prof. Dr. Álvaro Damiano (DCTA-IEAv)</p>	<p>Palestra online "How Vacuum Sub-System Development Drives Innovation in Instrumentation"</p> <p>John Screech (Agilent) Link for Registration: Event Registration (on24.com)</p>	
17h30		
18h00	Encerramento	



PROGRAMAÇÃO

09/12/20

Dia 9/12/2020 – 8h30
Local: <https://meet.google.com/qbh-zuha-dbo>

8h30 – 9h00

Abertura do evento
 Dr. Álvaro Damião (Presidente da SBV), Prof. Dr. Luís Evélio Garcia Azevedo (Vice-Reitor/UNILA), Prof. Dr. Jian Pires Frigo (Diretor/UNILA/ILATIT) e Prof. Dr. César Winter de Mello (CITI/UNILA)

9h00

Abertura das apresentações dos trabalhos
 Profa. Dra. Nazir Monteiro dos Santos (UNILA/ILATIT)
 Coordenadora do evento

APRESENTAÇÃO ORAL DOS TRABALHOS

Horário	N.	Título	Autor
9h10	T238	ON THE POLYMERIZATION PROCESSES OF 2-METIL-2-OXAZOLINE PLASMA POLYMER (pp-OXAZOLINE)	Rogério pinto Mota (FEG/UNESP)
9h15	T204	SYNTHESIS OF GRAPHENE ON NICKEL OXIDE BY PECVD	Larissa Solano De Almeida (UFSCar)
9h20	T255	A GLOBAL MODEL STUDY OF ARGON PLASMA CHEMISTRY USED AS PROPELLANT OF A GRIDDED ION THRUSTER	Bernardo Vieira Magaldi (DCTA-ITA)
9h40	T254	FAILURE ANALYSIS OF STIFFENED COMPOSITE PANELS OBTAINED BY DIFFERENT ADHESIVELY BONDING TECHNIQUES AND SUBMITTED TO AXIAL COMPRESSION TESTS	Rita De Cássia Mendonça Sales Contini (FATEC SJC)
9h45	T245	COLD ATMOSPHERIC PLASMA INHIBIT ESCHERICHIA COLI BIOFILMS FORMED ON PVC SPECIMENS	Mariana Raquel Da Cruz Vegian (ICT-UNESP)
9h50	T198	EFFECTS OF OXYGEN ADDITION ON ATMOSPHERIC PRESSURE PLASMA JET PARAMETERS	Fellype Do Nascimento (FEG-UNESP)
9h55	T208	STUDY OF THE ADDED NITROGEN EFFECT ON THE DLC FILM IN THE FILM ELETRIC CHARACTERISTIC	Mateus Da Silva Pereira (FATEC-Sorocaba)
10h00	T231	STUDY OF THE CORROSION RESISTANCE OF DLC FILM WITH MULTILAYERS OF ORGANOSILICONE AND SILICON OXIDE	Cesar Augusto Antonio Junior (FATEC-Sorocaba)
10h20	T215	EFFECT OF THE INTERLAYER ON DUPLEX TREATMENTS PROPERTIES	Miguel Rubira Danelon (FATEC -Sorocaba)
10h25	T203	PROCESSING AND PROPERTIES OF Ti-15Zr-15Mo-(1-3)Ag ALLOYS FOR APPLICATIONS AS BIOFUNCTIONAL MATERIALS	Jhuliene Elen Torrento (UNESP Bauru)
10h35	Intervalo		
11h00	T193	CARBON NANOTUBES FUNCTIONALIZATION THROUGH ELECTRICAL DISCHARGE ACROSS A MIXED OF NANOTUBES WITH SOLID CHEMICAL COMPOUNDS	Teresa Tromm Steffen (UDESC Joinville)
11h05	T229	GLOBAL MODEL OF ARGON ICP DISCHARGE: EFFECTS OF REACTION SET ON COLLISIONAL ENERGY	Julia Karnopp (DCTA-ITA)
11h10	T197	A GLOBAL MODEL FOR DC MAGNETRON SPUTTERING	Julia Karnopp (DCTA-ITA)
11h15	T217	ASSOCIATION OF ATMOSPHERIC PRESSURE COLD PLASMA AND NYSTATIN ON CANDIDA ALBICANS BIOFILMS	Lady Daiane Pereira Leite (ICT-UNESP)
11h20	T242	EFFECTS OF VACUUM EXPOSURE ON MECHANICAL PROPERTIES OF THERMOPLASTICS MATERIALS	Tiago Rodrigues Dos Santos (UnB)
11h40	T243	DEVELOPMENT OF A METHODOLOGY FOR MEASURING THE EVOLUTION OF DUPLEX STAINLESS STEEL LOW-TEMPERATURE PLASMA NITRIDED PHASES EXPANTION USING CONFOCAL LASER SCANNING MICROSCOPY	Carlos Eduardo Alves Feitosa (UFPR)
11h50	T228	DURABILITY OF FUNCTIONALIZATION USING PLASMA IN POLYAMIDE 6.6 TREATMENTS IN OPERATION CYCLES	Larissa Maciel Do Nascimento (DCTA-ITA)

12h00

Almoço

13h30 – 18h00

Chairs: Prof. Dr. Mário Ueda (INPE - SJC)
 Profa. Dra. Luciana Sgarbi Rossino (FATEC Sorocaba)

13h30 – 14h20

Palestra online
 “Calibração de Câmeras para Busca e Resgate”
 Prof. Dr. Álvaro Damião (DCTA-IEAv)

14h40

Intervalo

15h00 – 15h50

Palestra online
 “Ligas de Ti-Nb para aplicações biomédicas: passado, presente e futuro”
 Prof. Dr. Carlos Roberto Grandini (UNESP Bauru)

16h00 – 18h00

Minicurso (2h00)
 “Vácuo para iniciantes”
 Prof. Dr. Álvaro Damião (DCTA-IEAv)



PROGRAMAÇÃO

10/12/20

Dia 10/12/2020

Local: <https://meet.google.com/iaf-zkey-xeb>

Abertura das apresentações dos trabalhos
 Profa. Dra. Nazir Monteiro dos Santos (UNILA/ILATIT)
 Coordenadora do evento

Chairs: Prof. Dr. Rogério Pinto Mota (FEG-UNESP)
 Dr. André Ricardo Marcondes (INPE-SJC)

8h30 - 9h20 **Palestra online**
 "Perspectives of Modified PECVD Technique of DLC Growth for New R&D&I Demands"
 Prof. Dr. Vladimir Trava-Airold (INPE-SJC)

Horário	N.	Título	Autor
9h40	T249	Preparation and characterization of Ti-10Mo-5Mn-1Ag	Melissa Daniela de A. Nespeque (UNESP Bauru)
9h45	T220	NITRIDED AUSTENITIC STAINLESS STEEL: THE IMPORTANCE OF CHARACTERIZING THE SUB MICROMETRICAL REGION	Danilo Olzon Dionysio De Souza (UFVJM)
9h50	T237	STRUCTURE PROPOSED TO LEAD WITH DATA SENSOR BASED	Leandro Colevati Dos Santos (USP)
9h55	T233	MECHANICAL SPECTROSCOPY OF HOT-ROLLED TI-ZR-MO-AG ALLOYS	Renata Carolina Araujo De Camargo (IFSP)
10h00	T253	SHAPE MEMORY ALLOYS IN SCRAMJET ENGINES APPLICATIONS	Alana Aires Da Rocha Brito (DCTA-ITA)
10h20	T199	AVALIAÇÃO DA AGREGAÇÃO DE RESÍDUO DE BAGAÇO DA CANA- DEACÚCAR PARA FABRICAÇÃO DE TIJOLOS SOLO-CIMENTO	Samyra De Oliveira Figueira Da Silva (UFRJ)
10h25	T232	MICROESTRUTURA DE FILMES Ti(1-X)AL(X)N OBTIDOS NO MODO METÁLICO E MODO COMPOSTO VIA MAGNETRON SPUTTERING	Marcio Luiz Moretti (UFSC)

10h35 **Intervalo**

11h00 - 11h50 **Palestra online**
 "Asymmetric Bipolar Pulsed Plasma: a new approach for cold plasma densification and process control"
 Prof. Dr. Luis César Fontana (UDESC/Joinville)

12h00 **Almoço**

Chairs: Prof. Dr. Gustavo George Verdieri Nuernberg (UNILA)
 Prof. Dr. Álvaro Damião (DCTA-IEAv)

13h30	T250	STRUCTURAL AND MICROSTRUCTURAL CHARACTERIZATION OF THE Ti-10Mo-40Zr ALLOY	Renan Eduardo De Lima Lopes (UNESP Bauru)
13h35	T251	DEVELOPMENT OF Ti, Mo AND Zr BASED ALLOY FOR BIOMEDICAL APPLICATIONS	Israel Ramos Rodrigues (UNESP)
13h40	T212	COLD PLASMA JET IMPROVE TISSUE REPAIR IN WOUNDS INFECTED BY MULTISPECIES BIOFILMS	Maria Alcioneia Carvalho de Oliveira (ICT-UNESP)
13h45	T236	ASTM CA6NM MARTENSITIC STAINLESS STEEL PLASMA ASSISTED HYBRID HEAT-THERMOCHEMICAL TREATMENT: FIRST RESULTS FOR CARBON-EXPANDED AUSTENITE SURFACES	Felipe Gonçalves Jedyn (UNESP)
13h50	T247	Caracterização química e mecânica da liga Ti-25Ta-70Zr visando aplicações biológicas.	Edriely De Oliveira Saraiva (UNESP)
14h00	T192	ESTIMATION OF LAYER THICKNESS OF PLASMA NITRIDED MARTENSITIC STAINLESS STEELS WITH MACHINE LEARNING TECHNIQUES	Giovanni Corsetti Silva (UFPR)
14h05	T194	DEVELOPMENT AND TEST IN PILOT-SCALE OF A THERMAL PLASMA REACTOR FOR THE PRODUCTION OF CARBONACEOUS MATERIALS FROM COAL TAR PITCH	Eduardo Sant'Ana Petraconi Prado (INPE)
14h10	T244	CARIOGENIC MULTISPECIES BIOFILMS WERE INHIBITED BY COLD ATMOSPHERIC PLASMA	Leandro Wagner Figueira (ICT-UNESP)
14h15	T241	BIFUNCTIONALIZATION OF CARBON FIBER FABRICS USING ALD TiO ₂ THIN FILMS AND THERMAL PLASMA AS AN ALTERNATIVE TO DRY COLORING	Vanessa Dias (ITA)

14h40 **Intervalo**

15h00 - 15h50 **Palestra online**
 "Atmospheric Pressure Jets for Surface Modification and Biomedical Applications"
 Prof. Dr. Konstantin G. Kostov (FEG/UNESP)

16h00	T227	STRUCTURE PROPOSED TO DEAL WITH SENSOR BASED DATA	Leandro Colevati Dos Santos (USP)
16h20	T230	COMPOSITIONAL LIBRARY OF Ti-Nb-Zr BETA ALLOYS COATINGS APPLIED TO BIOMEDICAL PROSTHESIS	Ana Luiza De Castro (UFSCar)
16h35	T235	Hallow Cathode Effect Caused by Sample-Support Arrangement on Plasma Immersion Ion Implantation of Nickel Aluminum Bronze AMPCO M4	João Miguel De Oliveira Alves Da Silva (UFPR)
16h40	T224	ANALYSIS OF EPOXY / GRANITE COMPOSITES USING FTIR	Jorge Luiz Siqueira Da Costa Neto (UFRRJ)
16h45	T222	EFFECTS OF COLD ATMOSPHERIC PLASMA ON THE HEALING PROCESS OF DERMAL ULCERS INFECTED BY MULTISPECIES BIOFILMS	Aline Da Graça Sampaio (ICT-UNESP)
16h50	T202	DEVELOPMENT OF ALGORITHM TO STUDY TROPOSPHERE AND LOW STRATOSPHERE INSTABILITIES FROM RADIOSONDE OBSERVATIONS	Marisa Roberto (ITA)

Palestra online
 "How Vacuum Sub-System Development Drives Innovation in Instrumentation"

17h00 - 17h30

John Screech
 Senior Vacuum Applications Engineer
 (Agilent Technologies, Inc.)

Link for Registration:
[Event Registration \(on24.com\)](https://on24.com)





PROGRAMAÇÃO

II/I2/20

Dia 11/12/2020 Local: https://meet.google.com/kru-dpxk-rfo			
Abertura das apresentações dos trabalhos Profa. Dra. Nazir Monteiro dos Santos (UNILA/ILATIT) Coordenadora do evento			
Chairs Profa. Dra. Rita de Cássia Mendonça Sales Contini (FATEC SJC) Prof. Júlio Cesar Sagas (UDESC-Joinville)			
Palestra online “Missão do 1º Nanosatélite Científico Brasileiro (Nanosat C-BR1) e Empreendedorismo”			
8h30 - 9h20		Marcelo Essado (Presidente da ASB - Aliança das Startups Espaciais Brasileiras) Local: https://meet.google.com/kru-dpxk-rfo	
9h25	T248	EFFECT OF MANGANESE ON THE MECHANICAL PROPERTIES OF Ti-15Mo-Mn ALLOYS	Giovana Collombaro Cardoso (UNESP)
9h30	T259	PHYSICAL-CHEMICAL CHARACTERIZATION OF POLY(METHYLOCTADECYLSILOXANE) IMMOBILIZED ON TITANIZED SILICA AS A SORBENT FOR SOLID-PHASE EXTRACTION	Carla Grazieli Azevedo Da Silva (UFMT)
Minicurso (2h00) “Introdução aos Nanosatélites” Prof. Lázaro A. P. Camargo Coordenadoria de Ciências Espaciais (CEA-INPE SJC)			
9h40 – 11h40			
Almoço			
Chairs Prof. Dr. Giuseppe Pintaude (UTFPR) Profa. Dra. Liliane Cristina Battirola (UNILA)			
Palestra online “Tratamento Termoquímico de Aços Inoxidáveis” Prof. Dr. Rodrigo Perito Cardoso (UFSC-Florianópolis)			
13h30 – 14h20			
Intervalo			
Palestra online “Nanostructural Characterization of β -Ti-Nb-Zr Ternary Alloy Coatings Produced By Magnetron Co-Sputtering” Prof. Dr. Pedro A. P. Nascente (UFSCar São Carlos)			
15h00 – 15h50			
16h00	T239	MORPHOLOGICAL CHANGES INDUCED BY COLD ATMOSPHERIC PLASMA IN CANDIDA ALBICANS	Sabrina de Moura Rovetta (ICT-UNESP)
16h05	T206	EXPERIMENTAL SETUP FOR GRAPHITE EXFOLIATION VIA PULSED UNDERWATER DISCHARGE	Marco Aurelio Nespolo Vomstein (UDESC)
Premiação dos melhores trabalhos			
Assembleia Geral da SBV			
ENCERRAMENTO DO EVENTO			
18H00		Profa. Dra. Nazir Monteiro dos Santos (UNILA/ILATIT) Coordenadora do evento	



PALESTRAS E MINICURSO

CBraVIC – XLI Congresso Brasileiro de Aplicações de Vácuo na Indústria e na Ciência
09 – 11 de dezembro de 2020 – Foz do Iguaçu-PR

Palestra online
"Calibração de Câmeras para Busca e Resgate"
Prof. Dr. Álvaro Damião (DCTA-IEAv)

09/12/2020 – 13h30

CBraVIC – XLI Congresso Brasileiro de Aplicações de Vácuo na Indústria e na Ciência
09 – 11 de dezembro de 2020 – Foz do Iguaçu-PR

Palestra online
"Ligas de Ti-Nb para aplicações biomédicas: passado, presente e futuro"
Prof. Dr. Carlos Roberto Grandini (UNESP Bauru)

09/12/2020 – 15h00

CBraVIC – XLI Congresso Brasileiro de Aplicações de Vácuo na Indústria e na Ciência
09 – 11 de dezembro de 2020 – Foz do Iguaçu-PR

Palestra online: "Perspectives of Modified PECVD Technique of DLC Growth for New R&D&I Demands"
Prof. Dr. Vladimir Trava-Airold (INPE-SJC)

10/12/2020 – 8h30

CBraVIC – XLI Congresso Brasileiro de Aplicações de Vácuo na Indústria e na Ciência
09 – 11 de dezembro de 2020 – Foz do Iguaçu-PR

Palestra online
"Asymmetric Bipolar Pulsed Plasma: a new approach for cold plasma densification and process control"
Prof. Dr. Luis César Fontana (UESC/Joinville)

10/12/2020 – 11h00

CBraVIC – XLI Congresso Brasileiro de Aplicações de Vácuo na Indústria e na Ciência
09 – 11 de dezembro de 2020 – Foz do Iguaçu-PR

Palestra online
"Atmospheric Pressure Jets for Surface Modification and Biomedical Applications"
Prof. Dr. Konstantin G. Kostov (FEG/UNESP)

10/12/2020 – 15h00

CBraVIC – XLI Congresso Brasileiro de Aplicações de Vácuo na Indústria e na Ciência
09 – 11 de dezembro de 2020 – Foz do Iguaçu-PR

Webinar - 10/12/2020 – 17h00
"How Vacuum Sub-System Development Drives Innovation in Instrumentation"
John Screech (Agilent Technologies, Inc.)
Link for Registration:
[Event Registration \(on24.com\)](https://www.on24.com)

CBraVIC – XLI Congresso Brasileiro de Aplicações de Vácuo na Indústria e na Ciência
09 – 11 de dezembro de 2020 – Foz do Iguaçu-PR

Palestra online - 11/12/2020 às 8h30
"Missão do 1º Nanosatélite Científico Brasileiro (Nanosat C-BR1) e Empreendedorismo"
Marcelo H. Essado de Moraes
CEO of EMSISTI Space Systems & Technology Ltda.
Presidente da Aliança das Startups Espaciais Brasileiras (ASB)
Local: <https://meet.google.com/kru-dpxk-rfo>

CBraVIC – XLI Congresso Brasileiro de Aplicações de Vácuo na Indústria e na Ciência
09 – 11 de dezembro de 2020 – Foz do Iguaçu-PR

Palestra online - 11/12/2020 às 13h30
"Tratamento Termoquímico de Aços Inoxidáveis"
Prof. Dr. Rodrigo Perito Cardoso (UFSC-Florianópolis)
Local: <https://meet.google.com/kru-dpxk-rfo>

CBraVIC – XLI Congresso Brasileiro de Aplicações de Vácuo na Indústria e na Ciência
09 – 11 de dezembro de 2020 – Foz do Iguaçu-PR

Palestra online - 11/12/2020 às 15h00
"Nanostructural Characterization of β -Ti-Nb-Zr Ternary Alloy Coatings Produced by Magnetron Co-Sputtering"
Prof. Dr. Pedro A. P. Nascente (UFSCar São Carlos)
Local: <https://meet.google.com/kru-dpxk-rfo>

CBraVIC – XLI Congresso Brasileiro de Aplicações de Vácuo na Indústria e na Ciência
09 – 11 de dezembro de 2020 – Foz do Iguaçu-PR

Minicurso - 11/12/2020 às 9h40
"Introdução aos Nanosatélites"
Prof. Lázaro A. P. Camargo
Coordenadoria de Ciências Espaciais (CEA-INPE SJC)
Local: <https://meet.google.com/kru-dpxk-rfo>



RESUMOS DAS PALESTRAS

Perspectives of modified PECVD technique of DLC growth for new R&D&I demands

Vladimir Jesus Trava-Airoldi¹ 

1. Instituto de Ciência e Tecnologia – São José dos Campos (SP), Brazil.

*Correspondence author: vladimir.airoldi@inpe.br

ABSTRACT

Diamond-like carbon (DLC) films (a-C:H) have been a choice of protective coatings for many years, for many applications, due to their set of superior mechanical, chemical, tribological and biological properties such as: high hardness, high-wear resistance, low coefficient of friction, high chemical inertness, good biocompatibility, and bactericide. However, in order to improve the adhesion between the DLC and the different metals substrates, a huge modification of a pulsed DC plasma-enhanced chemical vapor deposition (PECVD) technique has been obtained introducing, at the first time, an additional cathode working as electron and ion confinement. With these modifications, pressure as low as 10^{-3} mbar allows operating in collisionless regime improving not only the adhesion, but also a set of DLC properties already cited. In this work, we present studies concerning more improvement properties of the DLC films as a function of ions confinement parameters in a plasma discharge by using argon as an ignitor gas for the interlayer precursor and keeping it during all the process of DLC deposition. In this case, the best condition of collisionless operation was reached at pressure as low as $3 \cdot 10^{-4}$ mbar. Basically, due to the condition of operating in very low pressure, this technique allows to grow the DLC film with very good uniformity and higher hardness, higher adhesion, lower coefficient of friction, less porosity and, also, provides to be able to get a DLC deposition in the form of multilayer like thicker films, promoting less residual stress. More specifically, studies of the DLC film properties as a function of the argon buffer gas density and as a function of bias voltage will be presented. Raman scattering spectroscopy, Rockwell indentation, nanoindentation, FEG, and tribological analyses are discussed. Also, the operating parameters as a scaling up studies will be presented as an important part of this work.

KEYWORDS: a-C:H films, PECVD, Ion confinement, Adhesion, Mechanical and tribological properties, Argon ignitor.



Asymmetric bipolar pulsed plasma: a new approach for cold plasma densification and process control

Luis César Fontana¹

1. Universidade do Estado de Santa Catarina – Santa Catarina, Brazil

*Correspondence author: luis.fontana@udesc.br

ABSTRACT

The waveform voltage has played a crucial role to generate and to control cold plasma processes. Different configurations of waveform voltage as direct current (DC), pulsed, and radio frequency (RF) have been developed over a wide range of frequencies and power. The influence of voltage waveform on the plasma generation is a well-known issue, so different power suppliers have been developed over time. The present paper shows the results of an asymmetric pulsed bipolar power supply named ABiPPS, developed at Universidade do Estado de Santa Catarina (UDESC), Santa Catarina, Brazil. The ABiPPS supply can be adjusted according to the following parameters: frequency, amplitude, pulse width, and number of pulses. Results show that, when the voltage waveform presents short period positive pulses (nanosecond scale) between longer negative pulses, it can increase greatly the secondary electron emission from the electrodes and, consequently, the plasma ionization rate. The kind of plasma generated in this way is free of electric arc and can be kept stable within a broader range of operating parameters, mainly the voltage and the working gas pressure. This paper presents the plasma ABiPPS working principles and some promising application results, such as: graphene production, nanoparticles deposition on fabric through underwater discharge, plasma oxidation, and plasma nitriding.

KEYWORDS: Plasma density, Secondary electrons, Voltage waveform, Plasma source.



Thermochemical treatments of stainless steels

Rodrigo P. Cardoso^{1,2*}, Cristiano J. Scheuer², Fernando I. Zanetti², Igor G. Zanella², Leonardo L. Santos², Lauro M. Ferreira², Adriano D. dos Anjos², Carlos E. A. Feitosa², Aécio F. Mendes², Laércio Malfatti², João F. F. Lima², Tarciana D. Toscano², Silvio F. Brunatto²

1. Universidade Federal de Santa Catarina - Laboratório de Materiais - Departamento de Engenharia Mecânica – Florianópolis (SC), Brazil.

2. Universidade Federal do Paraná - Departamento de Engenharia Mecânica - Grupo de Tecnologia de Fabricação Assistida por Plasma e Metalurgia do Pó – Curitiba (PR), Brazil.

*Correspondence author: rodrigo.perito@labmat.ufsc.br

INTRODUCTION

Stainless steels (SSs) are mainly applied in situations in which high corrosion resistance is required. Sometimes in such applications, SSs components are also subjected to wear. Being the wear resistance of SSs relatively low, thermochemical treatments can be applied to enhance the component wear performance.

THEORY

Thermochemical treatments have the objective of modifying the chemical composition and, consequently, the properties of components surface. But, thinking about the thermochemical treatment of SSs, special attention must be paid to the fact that the treatment must not reduce the component corrosion resistance. This limitation makes thermochemical treatments of SSs considerably different in terms of the treatment design.

Contrarily from other steels, in which nitrides can contribute to the surface hardening and are desired, in SSs, since the most thermodynamically favorable nitrides to precipitate are chromium nitrides, when these nitrides precipitate, reduction in the Cr-content of the steel matrix's solid solution is observed, decreasing the material corrosion resistance. So, to overcome this problem, thermochemical treatments of SSs are conducted at low temperature, in paraequilibrium, being the treated surface mainly interstitially hardened. As SSs present different subclasses, the treatment parameters are strongly related to the steel type. Treatment parameters also depend on the thermochemical treatment type. More details about these treatments can be found in Cardoso et al.¹

RESULTS AND DISCUSSION

Most studies in SSs thermochemical treatments are related to nitriding and carburizing of austenitic SSs. In such steels, nitriding is typically carried out below 430°C for about 20 h, and the treated layer, composed of N-expanded austenite, presents hardness around 1,200 HV. On the other hand, carburizing is usually carried out below 540°C for about 20 h, and the treated layer, composed of C-expanded austenite, presents hardness around 1,000 HV.

In the case of martensitic SSs, due to its different structures, treatments are carried out in relatively lower temperatures and shorter times. Nitriding is typically carried out below 400°C for about 12 h, and the treated layer, composed of N-expanded martensite and complex nitrides, presents hardness around 1,500 HV. Carburizing is

carried out below 450°C for about 12 h, and the treated layer, composed of C-expanded martensite and complex carbides, presents hardness around 1,000 HV. Other SSs classes have also been studied, but information is limited if compared to that of the austenite and martensitic SSs classes.

Concerning the performance of SSs thermochemically treated surfaces, in most cases, and for all SSs types, they present significant improvements in sliding wear, abrasive wear, and cavitation erosion wear resistances. Additionally, in most studied cases, reduction in the friction coefficient is also observed. Concerning corrosion resistance, if the treatment parameters are accordingly set, it is not significantly altered. However, some studies have reported significant improvements of corrosion resistance of SSs treated surfaces, including generalized, pitting and crevice corrosion resistance.

Despite the well established processes, new treatment strategies are in development, as for example a novel kind of thermochemical treatment that can be applied for some martensitic SSs, as presented in Toscano et al.².

ACKNOWLEDGMENTS


Coordenação de Aperfeiçoamento de Pessoal de Nível Superior, Conselho Nacional de Desenvolvimento Científico e Tecnológico and Fundação Araucária are acknowledged.

REFERENCES

1. Cardoso RP, Mafra M, Brunatto SF. Low-temperature thermochemical treatments of stainless steels – an introduction. In: Mieno T (Ed.). Plasma science and technology: progress in physical states and chemical reactions. IntechOpen; 2016. p. 135-158. <https://doi.org/10.5772/61989>
2. Toscano TD, Cardoso RP, Brunatto SF. A novel concept of hybrid treatment for high-hardenability steels: concomitant hardening and paraequilibrium thermochemical treatment to produce interstitially hardened/stabilized austenite surfaces. *Steel Res Int.* 2020;91(10):2000189. <https://doi.org/10.1002/srin.202000189>



Nanostructural characterization of β -Ti-Nb-Zr ternary alloy coatings produced by magnetron co-sputtering

E. David Gonzalez¹, Angelo Luiz Gobbi², Conrado R. M. Afonso¹ , Pedro Augusto de Paula Nascente^{1,*} 

1. Universidade Federal de São Carlos - Department of Materials Engineering - Graduation Program in Materials Science and Engineering – São Carlos (SP), Brazil.

2. Brazilian Center for Research in Energy and Materials - Brazilian Nanotechnology National Laboratory – Campinas (SP), Brazil.

*Correspondence author: nascente@ufscar.br

INTRODUCTION

Titanium and its alloys have been the most studied metallic materials for their use in the production of biomedical implants due to their mechanical properties, low density, biocompatibility, and wear and corrosion resistance in biological environment¹. The Ti-Nb-Zr system is one of the most promising metallic biomaterials since Nb and Zr are non-toxic and non-allergenic elements, and their addition to Ti helps to stabilize the β (body centered cubic – BCC) phase and causes decrease in the elastic modulus, a shape memory effect, and superelastic characteristic, favoring the mechanical compatibility between the bone and the material². Magnetron sputtering has been successfully employed for depositing Ti-Nb alloy coatings³⁻⁵.

EXPERIMENTAL

The Ti-Nb-Zr coatings were deposited on AISI 316L stainless steel substrate at 200°C by an AJA Orion 8 Phase II J magnetron sputtering system. Five compositions were produced: Ti80Nb20, Ti75Nb20Zr5, Ti60Nb20Zr20, Ti50Nb20Zr30, and Ti40Nb20Zr40 (at.%). X-ray diffraction (XRD) data were acquired by a Bruker diffractometer, model D8 Advance ECO, in Bragg-Brentano grazing incidence mode (GIXRD). The transmission electron microscopy (TEM) and scanning transmission electron microscopy (STEM) analyses were conducted using a FEI Tecnai G2 F20 200 kV microscope equipped with a field emission gun (FEG), an energy-dispersive detector (EDS), and an ASTARTM NanoMegas automatic crystallography orientation mapping (ACOM) system.

RESULTS AND DISCUSSION

The XRD analysis identified only the β phase with lattice parameters ranging from 3.2945 Å, for the coating without Zr, to 3.3628 Å, for 40 at.% of Zr. ACOM is a technique that provides information of ultrafine features due to its very high spatial resolution (approximately 2 nm), and it showed that the coating with no Zr presents a characteristic growth of the zone II of the SZD with a {111} texture for the β phase. In this case, the growth processes are mainly dominated by the Nb species, favoring the growth in the most compact directions and on the most strained planes for this type of alloy³⁻⁵. With the increase in the Zr content, the coating texture changes from a growth on the {111} plane orientation to a preferential growth on the densest {101} plane. TEM micrograph for the Ti75Nb20Zr5 coating

obtained with the dark field (DF) mode revealed nanometric precipitates of the **w** phase. Magnetron sputtering is a non-equilibrium process that leads to the formation of metastable phases due to abrupt changes in the energetic conditions of the system. These phenomena are correlated to the film morphology changes during growth that influences the coating structural evolution.

The addition of Zr in Ti-Nb-based alloy coatings influenced the phase formation, morphology, texture, and film growth. For low Zr content (5 at.%), two phases were formed: predominantly the β phase and, in a lesser degree, the nanoscale metastable **w** phase. For higher Zr content (20, 30, and 40 at.%), only the β phase was stabilized. The coating morphology was affected by the increasing addition of Zr, from a growth characteristic of the zone I to a growth characteristic of the zone T of the SZD diagram. The increase in the Zr amount directly influenced the texture, going from {111} to {101} for the direction of the film growth, due to the increase in the strain energy and the total mass of the species in the plasma.

ACKNOWLEDGMENTS

This work received financial support from Fundação de Amparo à Pesquisa do Estado de São Paulo (proposal 2017/25983-9), Conselho Nacional de Desenvolvimento Científico e Tecnológico (proposal 302450/2017- 3), Coordenação de Aperfeiçoamento de Pessoal de Nível Superior (fellowship granted to EDG), and Laboratório Nacional de Nanotecnologia/Centro Nacional de Pesquisa em Energia e Materiais (proposals LMF-23110 and TEM-23498).

REFERENCES

1. Niinomi M. Biologically and mechanically biocompatible titanium alloys. *Mater Trans.* 2008;49(10):2170-8.
2. Chang C, Wang YD, Ren Y. In-situ investigation of stress-induced martensitic transformation in Ti-Nb binary alloys with low Young's modulus. *Mater Sci Eng A.* 2016;651:442-8. <https://doi.org/10.1016/j.msea.2015.11.005>
3. Gonzalez ED, Niemeyer TC, Afonso CRM, Nascente PAP. Ti-Nb thin films deposited by magnetron sputtering on stainless steel. *J Vac Sci Technol A.* 2016;34(2):021511. <https://doi.org/10.1116/1.4940753>
4. Gonzalez ED, Afonso CRM, Nascente PAP. Influence of Nb content on the structure, morphology, nanostructure, and properties of titanium-niobium magnetron sputter deposited coatings for biomedical applications. *Surf Coat Technol.* 2017;326(Part B):424-8. <https://doi.org/10.1016/j.surfcoat.2017.03.015>
5. Gonzalez ED, Afonso CRM, Nascente PAP. Nanostructural characterization of sputter deposited Ti-Nb coatings by automated crystallographic orientation mapping. *Thin Solid Films.* 2018;661:92-7. <https://doi.org/10.1016/j.tsf.2018.06.051>



RESUMOS DOS TRABALHOS PREMIADOS



A global model study of argon plasma chemistry used as propellant of a gridded ion thruster

Bernardo Vieira Magaldi¹ , Rodrigo Sávio Pessoa^{1,*}, Argemiro Soares da Silva Sobrinho¹ 

1. Instituto Tecnológico de Aeronáutica - Plasma and Processes Laboratory – São José dos Campos (SP), Brazil.

*Correspondence author: rpessoa@ita.br

INTRODUCTION

The growing demand for data transmission with greater speed and capacity has proved to be a major challenge facing humanity today. Many of these obstacles can be solved by space systems composed of an infrastructure of small constellations of nanosatellites in low orbits. Frequent orbit adjustments are necessary for the disposition of these satellites, which results in increased propellant consumption and, consequently, the need for a small propulsion system. Electric propulsion systems feature ion exhaustion at high speed, reducing the mass of the propellant and allowing long mission times. Electric thrusters can be classified according to the method used to accelerate and produce the respective thrust. Electrostatic thrusters use the stationary electric field to accelerate ions, and gridded ion thrusters (GIT) have been widely used since the 1960s^{1,2}.

The physics associated with electrostatic thrusters is better defined than that of other types of engines, enabling a more in-depth initial study to optimize the efficiency of these thrusters. Global model, or zero-dimensional modeling, was developed based on fluid theory, used in the transport equations obtained from the Boltzmann equation, in order to request a low computational resource, but it can be applied for chemically complex discharges of the types of propellants used^{2,3}.

This study aimed to evaluate the zero-dimensional modeling of argon plasma chemistry for a cylindrical ion propellant based on inductively coupled plasma (ICP) whose output has a polarized grid system. The neutral propellant (argon gas) is injected at a fixed gas flow into the thruster chamber, and an ICP is generated by circulating a radio frequency current in an inductive coil that surrounds the cylinder. Neutral and excited species are ejected out of the chamber by drift, while ionized species are accelerated due to the electric field generated by the pair of polarized grids in direct current.

The global model developed is based on the particle and energy balance equations, in which the latter considers both charged species and neutral species. Thus, the model allows the determination of the temperature of the neutral gas. Finally, the model considers the effect of single and multi-stage ionization, as well as the effect of the electron energy distribution function (EEDF)^{3,4}.

The option for the use of argon is due to the fact that it is economically more interesting, since its commercial and maintenance cost is very low compared to other inert gases with greater atomic mass.

However, this study also aimed to evaluate the chemical properties of argon plasma, due to the generation of excited species in several metastable states. These metastables significantly affect the EEDF and, consequently, all reaction rates that involve electrons, thus reducing the energy cost to sustain the ion density in the thruster³.

THEORY

For this study, a plasma composed of three interactions of mutual fluids was considered: neutral atoms, positive ion with a single charge, and electrons. Particle balance differential equation takes into account species production and loss through many processes: reactions between electrons and gas species, reactions between two-gas species, recombination of neutral species on chamber walls, ion neutralization positive in the chamber walls, extinction of metastable states in the chamber walls, and the pumping of gas species into and out of the chamber all neutral and positive ions⁴.

For each species, there is a particle balance equation, given by Eq. 1.

$$\frac{dn_{(X)}}{dt} = \sum_i R_{(X) production,i} - \sum_i R_{(X) loss,i} \quad (1)$$

In which:

$\sum_i R_{(X) production,i}$: the sum of all reaction rates that contribute to the production of X species;

$\sum_i R_{(X) loss,i}$: the sum of all reaction rates that contribute to the loss of X species.

Electron density is obtained through charge neutrality (Eq. 2)⁵.

$$n_e = n^+, \quad (2)$$

Since collisions among charged and neutral particles lead to significant gas heating, the neutral energy balance equation to calculate the gas temperature (T_g) is given by the collision terms (Eq. 3)⁶.

$$\frac{d}{dt}(W_g) = G_{el} + G_{in} - L_p - L_i - L_{in}, \quad (3)$$

The neutral energy density (in J/m³) is given by $W_g = (3/2)n_g k_B T_g$, the gains are associated to gas heating due to electron-neutral elastic collisions, $G_{el} = 3(m_e/M)k_B(T_e - T_g)n_e n_g K_{el}$, and to ion-neutral collision heating, $G_{in} = (1/4)M^{-2}n_e n_g K_{in}$. With the losses given by the heat flow to the walls, $L_p = \kappa(T_g - T_{g0}/\Lambda_0)A/V$ by the heat conduction by thermal diffusion to the walls, which are at a fixed temperature, T_{g0} , by the thermal loss due to ionization collisions, , and finally by the thermal loss due to the collisions ion-neutral, $L_{in} = (3/4)k_B(T_g - T_i)n_e n_g K_{in}$. The electron neutral moment transfer rate and neutral ion are given by $K_x = \sigma_x \bar{v}_x$ with $\bar{v}_x = (8k_B T_x / \pi m_x)^{0.5}$.^{6,7}

The electron power balance closes the set of differential equations. It can be written as Eq. 4⁸.

$$\frac{d}{dt}(W_e) = \frac{(P_{abs} - P_{loss})}{V}, \quad (4)$$

In which:

$W_e = (3/2)n_e T_e$ the electron energy density (in J/m³);

P_{abs} : the power absorbed by the plasma;

P_{loss} : the loss power;

V : the volume of the discharge chamber.

The most general form to the power loss equation is given by Eq. 5⁹.

$$P_{loss} = P_{iw} + P_{ew} + P_{ev}, \quad (5)$$

With the power lost by the positive ions on the walls given by $P_{iw} = eA\epsilon_{iw}n_{+s}u_B$, in which n_{+s} is the ion density in plasma sheath region and u_B is the average Bohm velocity and assuming a Maxwellian distribution for the electron energy, $\epsilon_{iw} = (T_e/2) + V_s$ is the average kinetic energy lost by the ions to the walls, for which $T_e/2$ is the energy gained by the ion

on entering the plasma sheath, and $V_s = (T_e/2)/n (M_i/2\pi m_e)$ is the potential drop in the sheath formed on the walls of the reactor¹⁰; $P_{ew} = eA\varepsilon_{ew}n_{es}u_B$ is the power lost by electrons on the chamber walls, in which A is the chamber's internal area, $\varepsilon_{ew} = 2T_e$ is the mean kinetic energy per electron lost, and n_{es} is the electron density at the sheath edge; and, $P_{ev} = en_eV\sum k_{i2}n_{(x)}\varepsilon_{c(x)}$ is the power lost due to electron-particle reactions.

From the four main variables of the model: the density of the plasma n , the density of the neutral gas (atom) n_g , the electron's temperature T_e and the temperature of the neutral gas T_g . These four variables are calculated by numerically integrating the four first order nonlinear differential equations (1-4, until the steady state is reached.

RESULTS AND DISCUSSION

A special region near the walls of the propellant chamber due to the electrical properties of the particles that advance to the grids creates the so-called Child-Langmuir sheath, changing the balance of the particles, their density in the plasma, and their potential¹. The most common form of Child-Langmuir's law is given by Eq. 6.

$$J_i = \frac{4}{9}\varepsilon_0 \left(\frac{2e}{M}\right)^{0.5} \frac{V_{grid}^{1.5}}{s^2} \quad (6)$$

In which:

J_i : the current density;

ε_0 : the permittiveness of the free space;

s : the distance between the grids, also known as Child-Langmuir's length³.

The Child-Langmuir's sheath that accelerates the ions to high energy and reflects the electrons varies in proportion to the mass of the ions, needing to be adjusted the distance between the grids according to each propellant used. For the setting of $V_{grid} = 1,000$ V and $s = 1$ mm, the maximum ion current density extracted by the grids is given when J_i is equal to the Child-Langmuir's limit⁴. Child-Langmuir's limit for the current density of extracted ions was $J_{CL} = 273.4$ A/m², which is obtained at $P_{RF} = 665.5$ W, as Fig. 1, corresponding to $I_{coil} = 5.23$ A. However, the thruster parameters can be adapted, in order to achieve a better result for specific chosen propellant and the demand that the mission will present, therefore the same parameters used by Chabert et al.⁴ will be adopted in order to analyze the plasma chemistry of argon and from these results analyze the other parameters in future studies.

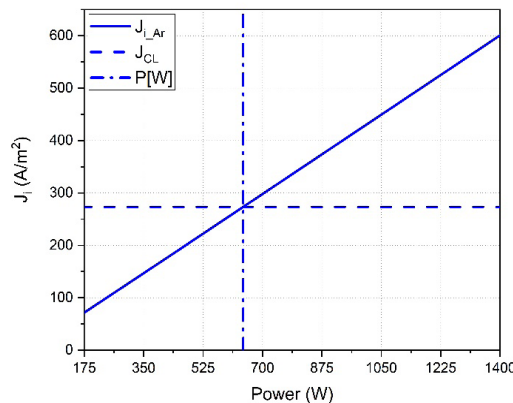


Figure 1: Current density in the thruster chamber as a function of the radio frequency power.

The gas chemistry model used in this article includes six species: argon in the fundamental state (Ar), positive argon ion (Ar^+), metastable argon atoms (Ar_m), resonant argon atoms (Ar_r), atoms in the state $4p$ (Ar_p), and electrons (e). Ar_m includes the two metastable states 3P_0 and 3P_2 , and Ar_r includes two resonant states 1P_1 and 3P_1 . The excited state $4p$ has 10 energy levels in the range of 12.9–13.5 eV. The two metastable levels are combined in the calculations: the radioactive and $4p$ levels.

Figure 2 shows the densities of the argon plasma species (Ar , Ar^+ , Ar_m , Ar_r , Ar_p , and electrons) as a function of the radio frequency power. Argon produces an electropositive plasma, i.e., it has no negative ions, and low pressure has only one ionized species. The ionization energy grows as the atomic mass of the noble gases decreases, giving argon a high ionization energy. However, the high concentration of metastable species facilitates multiple steps ionization, thus reducing the energy cost to sustain the discharge, increasing the electron density, and consequently reducing the electron temperature, as in Fig. 3. Despite having considered the limit of the ionic density current, it is possible to perceive that for slightly higher powers the temperature of the electrons tends to increase in order to stabilize the formation of ions despite the tendency to deplete the densities of neutral species.

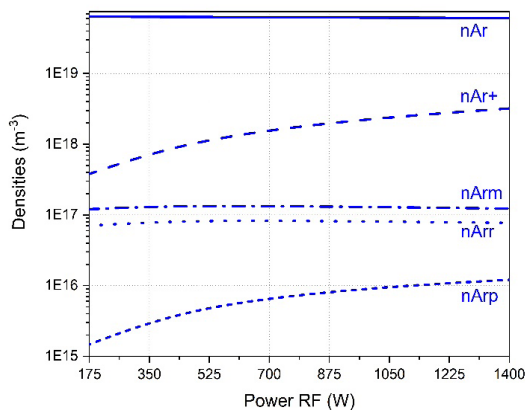


Figure 2: Densities of neutral and charged species inside the thruster as a function of radio frequency (RF) power.

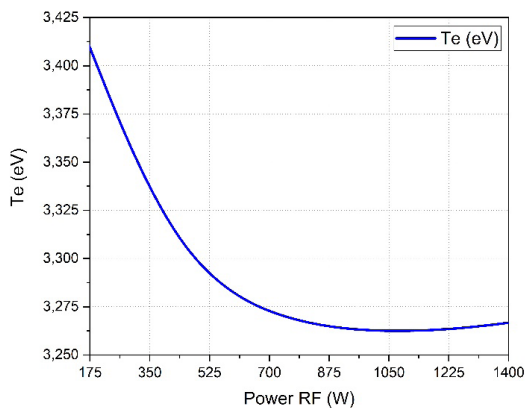


Figure 3: Electron temperature as a function of the radio frequency (RF) power.

In Fig. 4, the neutral gas heating increases with the discharge power, maintaining this growth because the drop in the density of the neutral gas is too small to change the heating rate. The gas pressure is a function of the gas flow entering the chamber, so that the density of neutral gas is not varying as a function of pressure, but rather as a function of the reaction rate that varies with the radio frequency power. A deeper analysis of the influence of the collisional loss terms given in the Eq. 3 shows that the thermal loss terms due to ionization collisions (L_i) and the thermal loss due to ion-neutral (L_{in}) collisions have a great influence on the gas temperature, since the presence of both terms shows how the gas loses much of its temperature through these collisions, even reaching 40 K above the temperature in Fig. 4. The gas temperature is extremely mattering for a thermal study of the propellant, since the propellant and many of its components have low efficiency, or even loss of certain properties required for the application in a real mission, like the propeller coils, which are made of copper, which has a melting point of 1,085°C.

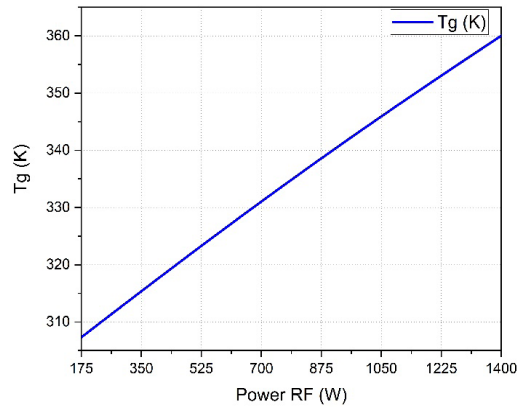


Figure 4: Neutral gas temperature as a function of the radio frequency (RF) power.

Further study of the chemistry of argon plasma has already allowed factors such as gas temperature to be influenced by the terms of heat exchange and electron temperature to interfere with species densities, so that the number of species closest to reality has a direct influence in the ionization rate. Although it does not interfere much in the density of ions, it ends up leaving a higher rate of ion replacement, which is extremely important for a propellant that uses the acceleration of ions to gain thrust and specific impulse.

From this significant study of the plasma parameters, it is possible to determine a series of factors that will assist in a more realistic analysis of the numerical development of the GIT model ICP. When developing a more detailed study of the collisional terms in the neutral gas energy balance, in view of a deepening in the quantity of metastable species, it was comprehended that the greater number of reactions and species close to physical reality better approximates the characteristic properties to that of models experimental, making argon a viable propellant, even though it is a noble gas with atomic mass three times smaller than that of xenon, and with high ionization potential.

Another perception is that the variation in the geometry of the propellant has a direct influence on the yield of the plasma chemistry output parameters, and it can be better evaluated in a second moment, after the predefined plasma parameters depending on the type of propellant used. This geometry control can be a solution to the demands of new specific space missions and conditions.

ACKNOWLEDGMENTS

The authors acknowledge the financial support given by Coordenação de Aperfeiçoamento de Pessoal de Nível Superior (CAPES) – Finance Code 001.

REFERENCES

1. Goebel DM, Katz I. Fundamentals of electric propulsion: ion and hall thrusters. New Jersey: John Wiley & Sons; 2008.
2. Mazouffre S. Electric propulsion for satellites and spacecraft: established technologies and novel approaches. *Plasma Sources Sci Technol.* 2016;25(3):033002. <https://doi.org/10.1088/0963-0252/25/3/033002>
3. Liberman MA, Lichtenberg AJ. Principles of plasma discharges and materials processing. 2^a ed. New York: Wiley; 2005. 757 p.
4. Chabert P, Monreal JA, Bredin J, Popelier L, Aanesland A. Global model of a gridded-ion thruster powered by a radiofrequency inductive coil. *Phys Plasmas.* 2012;19(7):073512. <https://doi.org/10.1063/1.4737114>
5. Monahan DD, Turner MM. Global models of electronegative discharges: critical evaluation and practical recommendations. *Plasma Sources Sci Technol.* 2008;17(4):045003. <https://doi.org/10.1088/0963-0252/17/4/045003>

6. Liard L, Raimbault JL, Rax J-M, Chabert P. Plasma transport under neutral gas depletion conditions. *J Phys D Appl Phys*. 2007;40(17):5192. <https://doi.org/10.1088/0022-3727/40/17/026>
7. Golant V, Zhilinsky AP, Sakharov IE, Brown SC. *Fundamentals of plasma physics*. New York: Wiley; 1980.
8. Almeida GRC. *Modelo global aplicado a uma descarga de oxigênio a baixa pressão [dissertation]*. São José dos Campos: Instituto Tecnológico de Aeronáutica; 2006.
9. Grondein P, Lafleur T, Chabert P, Aanesland A. Global model of an iodine gridded plasma thruster. *Phys Plasmas*. 2016;23(3):033514. <https://doi.org/10.1063/1.4944882>
10. Takegahara H, Nakayama Y. C60 feasibility study on application to ion thruster. In: *AIAA/ASME/SAE/ASEE, 31., Joint Propulsion Conference and Exhibit, July 10-12, 1995. Proceeding*. San Diego; 1995.



Development of a methodology for measuring the evolution of duplex stainless steel low-temperature plasma nitrided phases expansion using confocal laser scanning microscopy

Carlos Eduardo Alves Feitosa^{1*} , Rodrigo Perito Cardoso¹ , Silvio Francisco Brunatto^{1,2} 

1. Universidade Federal do Paraná - Graduate Program of Mechanical Engineering - Plasma Assisted Manufacturing Technology & Powder Metallurgy Group – Curitiba (PR), Brazil.

2. Universidade Federal do Paraná - Department of Mechanical Engineering – Curitiba (PR), Brazil.

*Correspondence author: carlos.feitosa@ufpr.br

INTRODUCTION

The low-temperature plasma nitriding is a technology used for modifying the properties of stainless steels surfaces, frequently resulting in an increase of both hardness¹ and corrosion resistance² without necessarily modifying these properties in the substrate bulk. The low-temperature plasma nitriding technology is applied to stainless steels aiming to avoid that the chromium solved in the matrix solid solution leaves this condition to form stable nitride precipitates.

It has been seen in the literature that such phases are deleterious³, and they appear under very specific conditions, such as high temperature or high exposure time to relatively low temperatures⁴. However, in the technical-scientific literature, two competing factors, influencing the surface topology modification, take place during plasma nitriding: the sputtering⁵; and the matrix phases expansion by the action of nitrogen⁶.

Sputtering is the ejection of atoms into the glow region by the high-energy ions' bombardment. Then, it is expected that, due to this effect, the surface of the samples exposed to the plasma tends to be eroded along nitriding, similar to the verified from a wear effect. On the other hand, the expansion of phases by the surface enrichment from nitrogen atoms is expected to occur by increasing the lattice parameter, thus implying in the elevation of the sample surface.

Some recently published works have shown the growth of the nitrided layer as a function of the nitriding temperature or time⁷⁻⁹, but the quantitative techniques available to measure such a layer are almost always destructive. It is worth mentioning that, at least from the authors knowledge, no study has been developed up to the moment aiming to characterize if the real nitrided layer evolution leads the sample geometry to be swelled (as a result of the net layer growth to the plasma direction), or, differently, to be shrunk (as a result of the net layer growth into the substrate bulk). In the specific case of duplex stainless steel, which presents ferrite and austenite phases' balanced microstructure, one has the advantage of studying the action of nitriding on both phases simultaneously. However, due to the lack of an efficient and reliable method of measuring the sample height, before and after nitriding, reports available in the literature are mostly qualitative.

Thus, a methodology was developed to follow grains before and after nitriding, as well as to monitor the height of the nitride phases to clearly determine which of these effects prevails, in net way, in the present treatment. The main characteristic of this method is that it is non-invasive, but also quantitative.

EXPERIMENTAL

Duplex stainless steel $20 \times 20 \times 3 \text{ mm}^3$ samples presenting chemical composition of Fe-25.5Cr-6.6Ni-4.1Mo, in wt.%, were ground with sandpaper and polished to $0.020 \pm 0.004 \text{ }\mu\text{m Sa}$ roughness. Vickers indentation marks were then made on the polished surface to make easier to locate the grains under the confocal laser scanning microscope (CLSM) observation. For this purpose, an Olympus OLS4100® equipment was used. One indentation of 1 kg load was made in the center of the sample to make ease the marks location afterwards, by using an optical microscope. The whole procedure was constituted of making eight other smaller indentations (with 0.1 kg load), arranged in three different squares from which the vertices were separated $500 \text{ }\mu\text{m}$ one each other, as shown schematically in Fig. 1. In the sequence, a stainless-steel plate of $\approx 100 \text{ }\mu\text{m}$ thickness was welded to a region of the polished surface in such a way to prevent the area below it to be thermochemically treated. This procedure was necessary to determine a zero-level reference for the height measurements to be carried out after the nitriding treatment. The plate was welded by the point welding process, in which a $10,000\text{-}\mu\text{F}$ electrolytic capacitor was charged with a 20-V power supply, being discharged into the stainless steel plate already positioned to partially cover the indentation marks, as shown in the schematic Fig. 2.

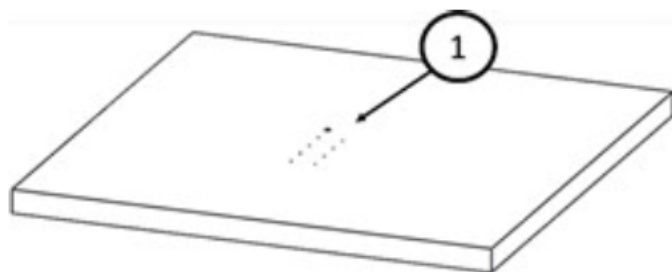


Figure 1: Schematic of the duplex stainless-steel sample with Vickers indentations on the polished surfaces.

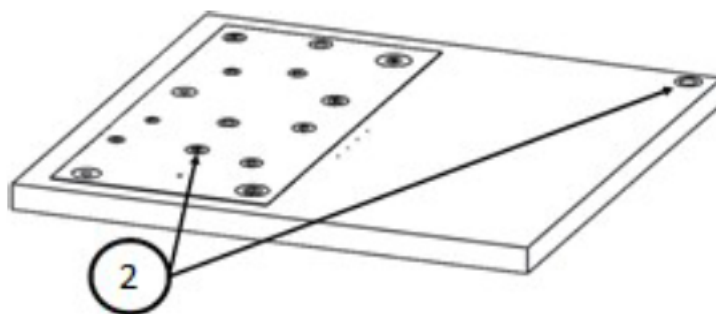




Figure 2: Schematic showing the spot welding of the stainless-steel blade on the sample surface to partially cover the Vickers indentations.



Effect of manganese on the mechanical properties of Ti-15Mo-Mn alloys

Giovana Collombaro Cardoso^{1*} , Mariana Luna Lourenço¹ , Carlos Roberto Grandini¹ 

1. Universidade Estadual Paulista "Júlio de Mesquita Filho" - Laboratório de Anelasticidade e Biomateriais – Bauru (SP), Brazil.

*Correspondence author: giovana.collombaro@unesp.br

INTRODUCTION

Nowadays, the requirement for new hard tissue replacement instruments, such as the femur and hip prostheses, is growing because of the increase of accidents and the growth of the elderly population as the increase in life expectancy¹. Due to its excellent properties, such as high mechanical strength and good biocompatibility, Ti and its alloys are widely used for making implants². Mo and Mn are two β -stabilizing alloy elements that improve Ti's mechanical properties and corrosion resistance and are not cytotoxic³. Hence, they are two elements studied in the development of new Ti alloys with low elastic modulus. This study's objective was to analyze the influence of substitutional elements on the mechanical properties of the Ti-15Mo-xMn ($x = 2.5$ and 5.0 wt%) alloys.

EXPERIMENTAL

The ingots were prepared by arc-melting in an inert argon atmosphere to avoid contamination. Later, a homogenization heat treatment was made for 24 h at $1,000^{\circ}\text{C}$ in a vacuum of 10^{-6} Torr and cooled at a rate of $10^{\circ}\text{C}/\text{min}$ to relieve the stresses from the melting process. Then, the ingots were hot-rolled at $1,000^{\circ}\text{C}$ to obtain a regular format for future analysis. The samples were subject to a chemical analysis of elements by inductively coupled plasma optical emission spectrometry (ICP-OES), and the density measurements using the Archimedes' method. The alloys' structure and microstructure were analyzed using X-ray diffraction measurements, optical and scanning electron microscopy. Mechanical properties were study by microhardness and Young's modulus tests.

RESULTS AND DISCUSSION

Results showed that the alloys have low density and gradual increase, according to the increase in manganese concentration. It is important to keep Ti alloy density low because high-density implants can cause pain and discomfort. The microstructure presented only the Ti β phase. The alloys hardness remained above, and Young's modulus remained below the cp-Ti, as shown in Figs. 1 and 2. A significant difference between the bone and the implant elasticity modulus can cause bone density loss due to the lack of mechanical stress applied to the bone. Then, the studied alloys have some excellent properties to be used as a biomaterial.

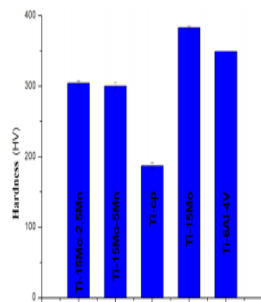


Fig. 1. Studied alloys hardness compared to cp-Ti and other alloys.

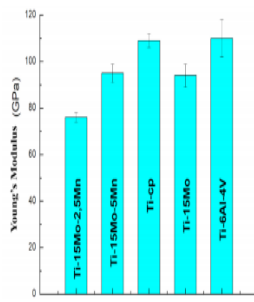


Fig. 2. Studied alloys Young's modulus compared to cp-Ti and other alloys.

Figure 1: Studied alloys hardness compared to cp-Ti and other alloys.

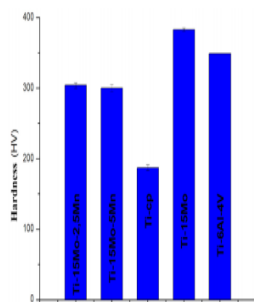


Fig. 1. Studied alloys hardness compared to cp-Ti and other alloys.

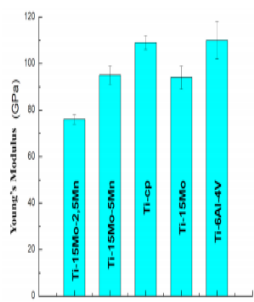


Fig. 2. Studied alloys Young's modulus compared to cp-Ti and other alloys.

Figure 2: Studied alloys Young's modulus compared to cp-Ti and other alloys.

ACKNOWLEDGMENTS

The authors thank Coordenação de Aperfeiçoamento de Pessoal de Nível Superior (CAPES), Conselho Nacional de Desenvolvimento Científico e Tecnológico (CNPq), and Fundação de Amparo à Pesquisa do Estado de São Paulo (FAPESP) for financial support, PosMat, and the laboratory's colleagues who collaborate with the research.

REFERENCES

1. Li P, Ma X, Tong T, Wang Y. Microstructural and mechanical properties of β -type Ti-Mo-Nb biomedical alloys with low elastic modulus. *J Alloys Compd.* 2020;815:152412. <https://doi.org/10.1016/j.jallcom.2019.152412>
2. Ehtemam-Haghighi S, Attar H, Dargusch MS, Kent D. Microstructure, phase composition and mechanical properties of new, low cost Ti-Mn-Nb alloys for biomedical applications. *J Alloys Compd.* 2019;787:570-7. <https://doi.org/10.1016/j.jallcom.2019.02.116>
3. Ho WF, Ju CP, Lin JH. Structure and properties of cast binary Ti-Mo alloys. *Biomaterials.* 1999;20(22):2115-22. [https://doi.org/10.1016/s0142-9612\(99\)00114-3](https://doi.org/10.1016/s0142-9612(99)00114-3)

Estimation of layer thickness of plasma nitrided martensitic stainless steels with machine learning techniques

Giovanni Corsetti Silva^{1,*} 

1. Universidade Federal do Paraná - Undergraduate Department of Mechanical Engineering – Curitiba (PR), Brazil.

Correspondence author: corsetti@ufpr.br

INTRODUCTION

The estimation of layer thickness in plasma nitriding processes of martensitic stainless steels has vital importance in several industrial applications. However, due to the considerable complexity associated with the layer parameters, which affect the thickness, few models were developed to estimate it, typically relying solely on a limited set of parameters¹. The author proposed to employ machine learning techniques to develop a more robust and reliable model for layer thickness prediction of plasma nitrided martensitic stainless steels.

THEORY

A survey on the scientific literature was carried out in order to gather points of plasma nitrided martensitic stainless steels at different treatment conditions. The total number of points collected was equal to 70. Since the treatment temperature, time, gas mixture and pressure are virtually the most relevant parameters², they were considered as the only inputs of the model, although for future works more parameters will be taken into account.

A regression gradient boosting algorithm was built using the *sklearn* python library, in which the only parameter changed to 1,000 was the number of boosting stages, mainly because gradient boosting algorithms are sufficiently robust against overfitting, but not to underfit. All the other parameters were left as default. To assess the model's performance, a leave-one-out cross-validation (LOOCV) was carried out, and the predicted values were compared to the real ones.

RESULTS AND DISCUSSION

Figure 1 illustrates the model predictive power on the given data. As expected, up to 40 μm the model tends to perform with superior accuracy, mainly because more available points in the mentioned range enable the algorithm to comprehend how the layer thickness behaves for low treatment temperature or time, for instance. The significant R^2 value obtained (83.8%) suggests that machine learning approaches can be successfully employed for plasma nitriding processes with great accuracy for ordinary treatment conditions and may be useful to obtain an estimative of treatments performed under extraordinary treatment conditions.

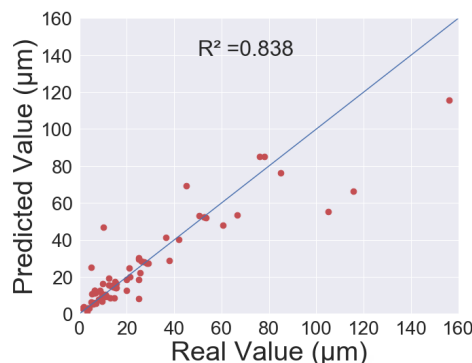


Figure 1: Comparison between predicted and real values.

ACKNOWLEDGMENTS

The author would like to acknowledge the faculty members of Universidade Federal do Paraná for all the provided help.

REFERENCES

1. Triwiyanto A, Zainuddin A, Abidin KAZ, Billah MA, Hussain P. Mathematical modelling of nitride layer growth of low temperature gas and plasma nitriding of AISI 316L. MATEC Web Conf. 2014;13. <https://doi.org/10.1051/mateconf/20141304022>
2. Scheuer CJ, Gralak AC, Zanetti FI, Amaral TF, Pereira R, Brunatto SF, et al. Effect of plasma nitriding parameters on surface properties of low-temperature nitride AISI 420 martensitic stainless steel. ABM Int Cong. 2013;68. <https://doi.org/10.5151/2594-5327-23492>



Carbon nanotubes functionalization through electrical discharge across a mixed of nanotubes with solid chemical compounds

Teresa Tromm Steffen^{1,*} , Daniela Becker, Luis César Fontana, Peter Hammer² 

1. Universidade do Estado de Santa Catarina - Center for Technological Sciences – Joinville (SC), Brazil.

2. Universidade Estadual Paulista “Júlio de Mesquita Filho” - Institute of Chemistry – Araraquara (SP), Brazil.

*Correspondence author: teretromm@hotmail.com

INTRODUCTION

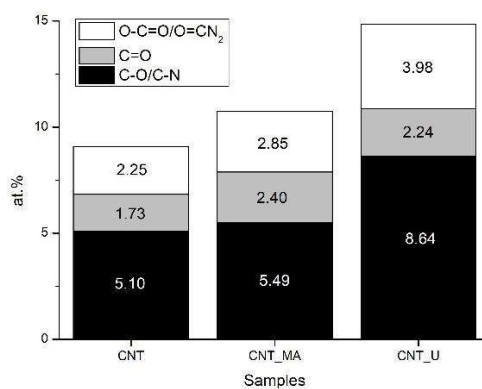
Modification of carbon nanotubes (CNT) has been subject of several researches, once their properties and interaction with other materials are considerably improved after chemical modifications, i.e., functionalization. It can be achieved through plasma treatment, which involves parameters as voltage pulses waveform, reactor geometry and even the way the functionalization agents are inserted in the chamber¹. Regarding to this last parameter, we proposed an insertion of chemical compounds as solid, mixed with CNT.

EXPERIMENTAL

Two chemical compounds, maleic anhydride (MA) and urea (U), were mixed in solid form with CNT, following the procedure described in our previous work². Samples were treated in a plasma homemade reactor, configured as capacitively coupled plasma (CCP). The electrical discharge through the mixed powder was provided by an ABBiPS power supply³, and the treatment time lasted 30 minutes. After plasma treatment, the samples were washed with methanol, as described previously², aiming to remove the non-reacted chemical groups. Samples were named as CNT (CNT pristine sample), CNT MA (sample mixed with MA and treated by plasma) and CNT U (sample mixed with urea and treated by plasma).

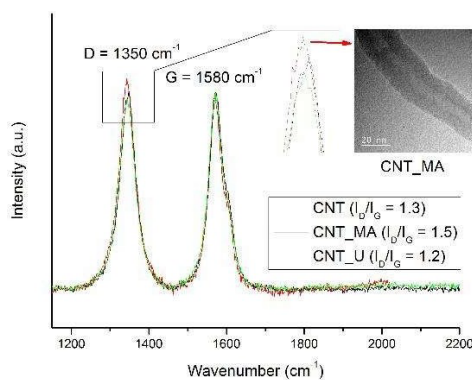
RESULTS AND DISCUSSION

XPS results enabled to evaluate atomic percent contribution of chemical groups in each sample. Figure 1 presents these results, indicating CNT functionalization by the increase of oxygen and nitrogen groups (in urea case). Total chemical groups contribution increases more than 50% for CNT_U sample, regarding to CNT sample. Plasma treatment was more effective for CNT U sample, which can be associated to the urea lower ionization energy (eV), regarding to MA. Important to conserve CNT properties, nanoparticles integrity was preserved after plasma treatment, as ID/IG ratio indicates, provided from Raman results (Fig. 2). Even for CNT MA sample, to which I_n/I_c was the highest, CNT walls were preserved, as corroborates transmission electron microscopy (TEM) image (Fig. 2). Results indicated plasma functionalization of CNT from chemical compounds in solid form.



CNT: carbon nanotubes; CNT_MA: sample mixed with MA and treated by plasma; CNT_U: sample mixed with urea and treated by plasma.

Figure 1: Atomic percent contribution of oxygen and nitrogen groups in samples composition. Data provided from C 1s XPS spectra.



CNT: carbon nanotubes; CNT_MA: sample mixed with MA and treated by plasma; CNT_U: sample mixed with urea and treated by plasma.

Figure 2: Raman spectra indicating CNT integrity. Transmission electron microscopy image corroborates pointing regular walls to CNT MA sample, the one with the highest I_D/I_G value.

ACKNOWLEDGMENTS

The authors are thankful for the multi-user facility infrastructure from the Technological Sciences Center of the Universidade do Estado de Santa Catarina.

FUNDING

This work was supported in part by Coordenação de Aperfeiçoamento de Pessoal de Nível Superior - Brasil (CAPES) [Finance Code 001] and Conselho Nacional de Desenvolvimento Científico e Tecnológico (CNPq) [project Universal/445242/2014-0].

REFERENCES

1. Vandenabeele CR, Stéphane L. Technological challenges and progress in nanomaterials plasma surface modification: a review. *Materials Science and Engineering: R*, 2020;139:100521. <https://doi.org/10.1016/j.mser.2019.100521>
2. Steffen TT, Fontana LC, Hammer P, Becker D. carbon nanotube plasma functionalization: the role of carbon nanotube/ maleic anhydride solid premix. *Applied Surface Science*. 2019;491:405-10. <https://doi.org/10.1016/j.apsusc.2019.06.176>
3. Scholtz JS, et al. *IEEE Transactions on Plasma Science*. 2018;46:2999-3007.



Development and test in pilot-scale of a thermal plasma reactor for the production of carbonaceous materials from coal tar pitch

Eduardo Petraconi Prado^{1,2*} , Felipe De Souza Miranda^{1,2} , Gisele Amaral Labat¹ , Gilberto Petraconi² , Maurício Ribeiro Baldan¹ 

1. Instituto Nacional de Pesquisas Espaciais – São José dos Campos (SP), Brazil.

2. Instituto Tecnológico de Aeronáutica – São José dos Campos (SP), Brazil.

*Corresponding author: edu.petraconi@gmail.com

INTRODUCTION

Coal tar pitch (CTP) is a waste with high carbon content produced on large scale in the steel industries¹. Thermal plasma processing of waste with high carbon content has been promising for its potential of energy generation (combustible gases) and products of high added value (advanced carbonaceous materials)².

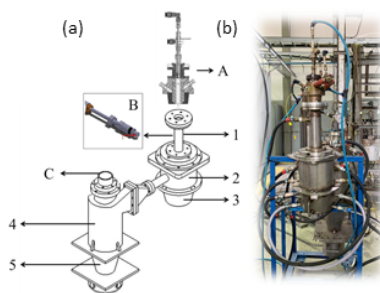
In this scenario, the present work shows the schematic design and real system of the thermal plasma reactor and a preliminary result of the initial experiment. The process of feasibility and technical feature were verified, which are very beneficial to guide the further design of this process and scale it up.

EXPERIMENTAL SETUP

The CTP sample adopted in this study was a from coking plant in National Steel Company (Brazil). The thermal plasma reactor pilot plant has the treating capacity of 2 liters/h for CTP, which operates at atmospheric pressure. As shown in Fig. 1, it consists of a non-transferred arc plasma torch coupled to the process reactor, a feeding system of the CTP, a particulate separator (cyclone), and a gas cleaning system.

RESULTS AND DISCUSSION

The process reactor has cylindrical geometry and double walls made of water-cooled stainless steel. It contains several flanges, through which the plasma torch is coupled, CTP injector, exhaust gases, and chambers for collecting carbonaceous solid material. The power of the plasma torch, working gas flow rate and CTP feed rate, is more complex, largely influencing the distribution of temperature and pressure, and product property. So, examining the effect of operating conditions on reaction behavior in the pilot plant is necessary and essential for the research and development of the production of carbonaceous materials process. Tests of the new CTP processing pilot plant were performed using air as working gas, and the Raman spectrum (Fig. 2) of the product obtained with the proportion of peak intensities $I_D / I_G = 0.85$ indicates a high potential of thermal plasma technology in obtaining carbonaceous material with high added value.



A: plasma torch; B: injector nozzle; C: gas treatment system; 1 to 5: material collection chambers.

Figure 1: (a) Schematic design; (b) real system.

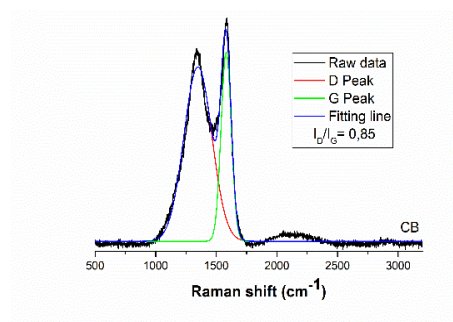


Figure 2: Raman spectra of carbon black.

ACKNOWLEDGMENTS

The authors acknowledge the Plasma and Process Laboratory (LPP-ITA) and Associated Laboratory of Sensors and Materials (LABAS-INPE).

REFERENCES

1. Zhang Y, Yan Q, Wang J, Han S, He R, Zhao Q, et al. Emission characteristics and potential toxicity of polycyclic aromatic hydrocarbons in particulate matter from the prebaked anode industry. *Sci Total Environ.* 2020;722:137546. <https://doi.org/10.1016/j.scitotenv.2020.137546>
2. Mohsenian S, Esmaili MS, Fathi J, Shokri B. Hydrogen and carbon black nano-spheres production via thermal plasma pyrolysis of polymers. *Int J Hydrog Energy.* 2016;41(38):16656-63. <https://doi.org/10.1016/j.ijhydene.2016.05.150>



A global model for DC magnetron sputtering

Júlia Karnopp^{1,2,*} , Julio César Sagás¹ 

1. Universidade do Estado de Santa Catarina - Laboratório de Plasmas, Filmes e Superfícies – Joinville (SC), Brazil.

2. Instituto Tecnológico de Aeronáutica – São José dos Campos (SP), Brazil.

*Corresponding author: julia_karnopp@outlook.com

INTRODUCTION

Magnetron sputtering is one of the most used methods for thin film deposition. In this process, atoms are removed from a target due to ion bombardment. The ions are generated in a magnetically confined plasma in front of the target. A high slope of the current-voltage curves characterizes the magnetron discharge¹.

The modelling of this discharge is essential to understand parameters that are hard to measure, simplifying the search for the best deposition conditions. However, the presence of a non-homogeneous magnetic field becomes modeling a difficult task. Recently, papers have proposed a global model for magnetron discharges^{2,3}.

METHODOLOGY

A global model was developed for argon plasma and titanium target. Two electron populations – electrons and hot electrons (secondary electrons emitted from the cathode) –, three populations of argon in ground state (cold, warm, and hot), argon ions, metastable argon atoms, titanium atoms in the ground state, singly ionized metal ions and doubly ionized metal ions were considered. The Maxwell-Boltzmann distribution was used for cold electrons. Experimental current-voltage curves for different gas pressures were reproduced in the simulations.

RESULTS AND DISCUSSION

Increasing the current, the electron density grows up. Consequently, more ionizations of the argon and the metal atoms occur, as it can be seen in Fig. 1. With the increase in the ion density, there is also increase in metal production (by sputtering) and in the generation of hot electrons.

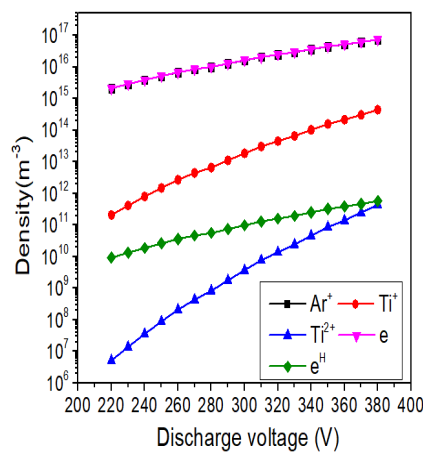


Figure 1: Density of charged particles at pressure 0,40 Pa.

For the same voltage, electron density increases with the pressure (Fig. 2). The constant rates are functions of electron temperature. With the increase in plasma density, smaller constant rates are necessary to maintain the electron rate production. Therefore, the electron temperature decreases with pressure (Fig. 2).

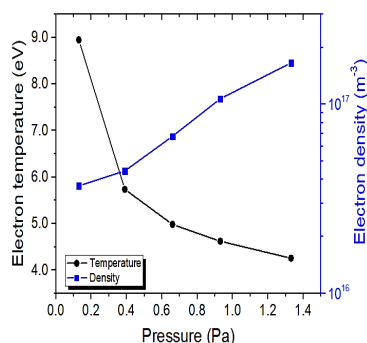


Figure 2: Electron temperature and density for different pressures and voltage 350 V.

ACKNOWLEDGMENTS

This project has been funded by Fundação de Amparo à Pesquisa do Estado de Santa Catarina through the Programa de Apoio à Pesquisa, in association with Universidade do Estado de Santa Catarina, under contract PAP-TR 655. Júlia Karnopp also thanks Fapesc and Coordenação de Aperfeiçoamento de Pessoal de Nível Superior for the scholarship.

REFERENCES

1. Rossnagel SM, Kaufman HR. Current-voltage relations in magnetrons. *J Vac Sci Technol.* 1988;6(2):223-9. <https://doi.org/10.1116/1.574985>
2. Huo C, Lundin D, Gudmundsson JT, Raadu MA, Bradley JW, Brenning N. Particle-balance models for pulsed sputtering magnetrons. *J Phys D Appl Phys.* 2017;50(35):354003. <https://doi.org/10.1088/1361-6463/aa7d35>
3. Gudmundsson JT, Lundin D, Brenning N, Raadu MA, Huo C, Minea TM, et al. An ionization region model of the reactive Ar/O₂ high power impulse magnetron sputtering discharge. *Plasma Sources Sci Technol.* 2016;25(6):065004. <https://doi.org/10.1088/0963-0252/25/6/065004>



Effects of oxygen addition on atmospheric pressure plasma jet parameters

Fellype do Nascimento^{1,*} , Kleber Petroski¹, Ananias Alves Barbosa¹ , Konstantin Kostov¹ 

1. Universidade Estadual Paulista “Júlio de Mesquita Filho” - Faculty of Engineering in Guaratinguetá – Guaratinguetá (SP), Brazil.

Correspondence author: fellype@gmail.com

INTRODUCTION

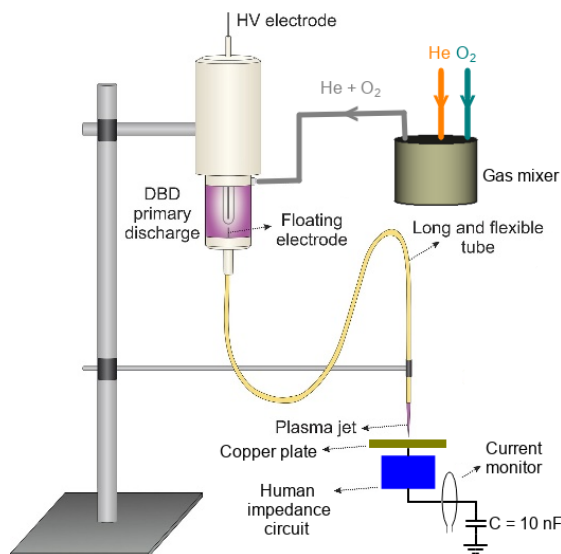
Atmospheric pressure plasma jets (APPJs) produced in open environments have received a lot of attention in recent years, mainly due to their versatility, ease to use and low-cost implementation when compared to low-pressure plasmas¹. Special attention has been given to medical and biological applications of APPJs, whose positive effects have been attributed to the presence of reactive oxygen and nitrogen species produced by the plasma jets. Recent studies have indicated that the admixture of oxygen (O₂) to the gas employed to produce plasma, usually argon (Ar) or helium (He), can increase the amount of reactive oxygen species induced by the plasma. Thus, this work aimed to evaluate the possible changes in the parameters of helium plasma jets when a small amount of oxygen gas is added to the working gas.

EXPERIMENTAL

Figure 1 shows the experimental setup used in this work. A small plasma jet is ignited at the end of a long and flexible plastic tube when the primary discharge inside a dielectric barrier discharge (DBD) type reactor polarizes a conducting wire placed inside the tube. The plasma jet was directed towards a copper plate connected to an impedance circuit that follows an international standard aimed to simulate the electrical properties of the human body². Electrical measurements were performed in order to obtain discharge power and root-mean-square (RMS) current. Optical emission spectroscopy was used to determine rotational and vibrational temperatures and to estimate the production of atomic oxygen as a function of the O₂ percentage added to the He flow rate fixed at 1.5 L/min.

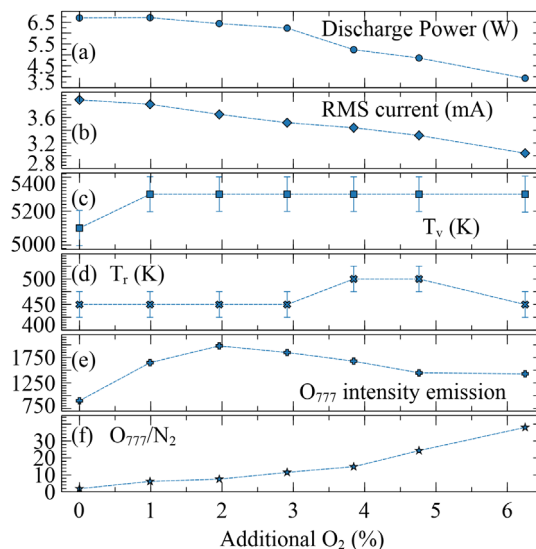
RESULTS AND DISCUSSION

The variations in the values of plasma parameters as a function of the percentage of O₂ in the total gas flow rate are shown in Fig. 2. The increment in O₂ percentage reduces both discharge power and RMS current, while the vibrational and rotational temperatures (T_v and T_r , respectively) remain almost constant. The total intensity emission of atomic oxygen at 777 nm (O₇₇₇) starts to increase with the O₂ increment, reaching a peak value when the additional amount of O₂ is ~2% of the gas flow rate. Then, within the evaluated range, it gradually decreases until reaches an almost constant level. On the other hand, the relative intensity of atomic oxygen, when compared with the intensity of emissions from N₂, grows monotonically with O₂ increment. These results indicate that the addition of O₂ to the He flow rate must be limited below 3% (best around 2%), in order to take full advantage of higher discharge power combined with the maximum atomic oxygen production.



HV: high voltage; DBD: dielectric barrier discharge.

Figure 1: Scheme of experimental setup.



RMS: root-mean-square

Figure 2: Plasma parameters *versus* O₂ added.

ACKNOWLEDGMENTS


This work was supported by Coordenação de Aperfeiçoamento de Pessoal de Nível Superior (CAPES) and Fundação de Amparo à Pesquisa do Estado de São Paulo (FAPESP) [grants #2019/05856-7 and #2020/09481-5].

REFERENCES

1. Brandenburg R. Dielectric barrier discharges: progress on plasma sources and on the understanding of regimes and single filaments. *Plasma Sources Sci Technol.* 2017;26(5):053001. <https://doi.org/10.1088/1361-6595/aa6426>
2. Stancampiano A, Chung T-H, Dozias S, Pouvesie J-M, Mir LM, Robert E. Mimicking of human body electrical characteristic for easier translation of plasma biomedical studies to clinical applications. *IEEE Trans Rad Plasma Med Sci.* 2020;4(3):335-42. <https://doi.org/10.1109/TRPMS.2019.2936667>



Evaluation of the aggregation of sugarcane bagasse residue in the manufacture of soil-cement bricks

Samyra De Oliveira Figueira Da Silva¹, F. M. T. Sampaio¹, Antônio Renato Bigansolli^{1,*} 

¹. Universidade Federal Rural do Rio de Janeiro – Seropédica, (RJ), Brazil.

*Correspondence author: bigansolli.arb@gmail.com

INTRODUCTION

The soil-cement brick, consisting of soil, cement, and water, is an outlet to minimize production costs and excessive consumption of resources, and a portion of cement can be replaced by waste generated by industries, further reducing the costs involved in its manufacture¹. This work aimed to analyze the effect of the incorporation of sugarcane bagasse in the properties of cement soil blocks with potential for the manufacture of ecological brick.

EXPERIMENTAL

Samples were analyzed with different percentages of incorporation of residues in their composition: 0, 100 and 150 grams of bagasse residue. The analyses were performed with different days of curing the bricks, seven and 28 days. The brick blocks were pressed in a manual press with rectangular shape in the size of 21 × 10 × 5 cm. After the time limit for water absorption tests (with kiln drying performed at 110°C until mass constancy), and after a period of 24 hours, the samples were submerged in water to obtain the wet mass, according to the NBR 10834 standard (2013). For the compressive strength assay, samples were used at seven and 28 days of cure, according to the NBR 8492 standard (1984), comparing the results obtained with a reference sample, without adding any percentage of residue to the mass, which should be greater than 2.0 MPa.

RESULTS AND DISCUSSION

Figures 1 and 2 show the behavior of compressive strength, as a function of the residue content of sugarcane bagasse incorporated in the tested bricks at seven and 28 days of cure.

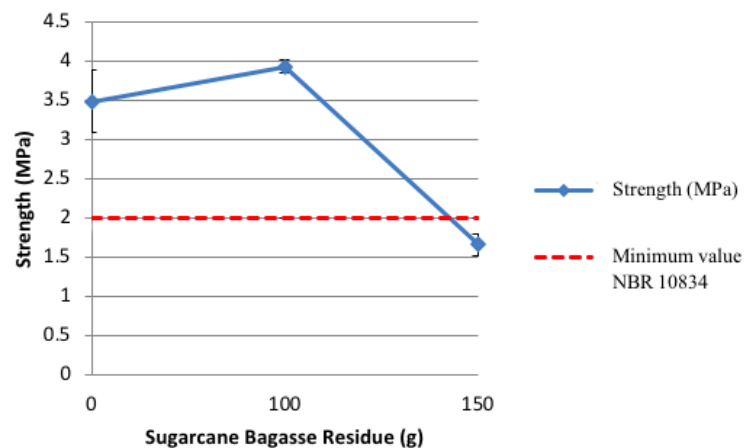


Figure 1: Compression test at seven days.

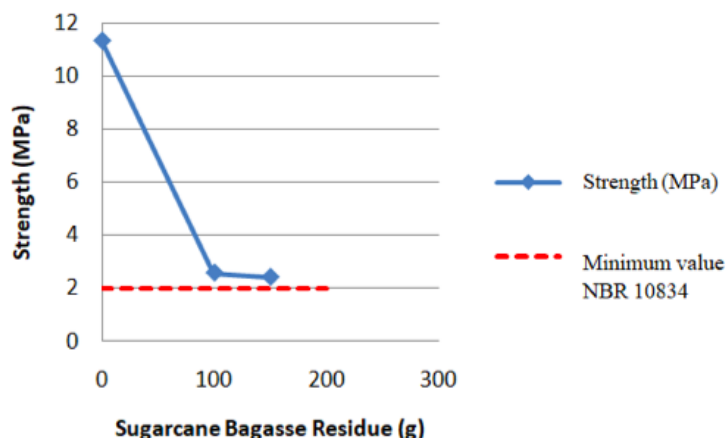


Figure 2: Compression test at 28 days.

Figure 1 shows that, out of the three traits analyzed in this trial, only one, containing 150 g of sugarcane bagasse residue, did not meet the value recommended by the standard. Cement is one of the components that confers hardness and mechanical resistance to the bricks, and the time established for its curing process to be considered complete is 28 days. So, for the test performed at seven days of age, there was not enough time for all reactions to happen in the place of Portland cement. There was a significant decrease in the mechanical strength of the brick, due to a reduction in the amount of cement in the trace, because this is the agent that promotes the increase of resistance of the mixture.

ACKNOWLEDGMENTS




The authors would like to thank the Chemical Engineering Department of Universidade Federal Rural do Rio de Janeiro (UFRRJ) and the Architecture and Urbanism Department of UFRRJ, for the support.

REFERENCES

1. Lucas D, Bernatti CT. Utilização de resíduos industriais para a produção de artefatos cimentícios e argilosos empregados na construção civil. *Rev Agronegócios Meio Ambiente*. 2008;1(3):405-418. <https://doi.org/10.17765/2176-9168.2008v1n3p405-418>
2. Associação Brasileira de Normas Técnicas. NBR 10833: Fabricação de tijolo e bloco e solo-cimento com utilização de prensa manual ou hidráulica – procedimento. Rio de Janeiro: Associação Brasileira de Normas Técnicas; 2013.



Development of algorithm to study troposphere and low stratosphere instabilities from radiosonde observations

Elson de Campos¹, Marco Antonio Ridenti¹ , Marisa Roberto^{1,*} , Alysson Brhian de Souza Muniz Silva¹ , José Ricardo Abalde Guedes¹, Alessandro José de Abreu^{1,2}

1. Instituto Tecnológico de Aeronáutica – São José dos Campos (SP), Brazil.

2. Instituto Nacional de Pesquisas Espaciais – São José dos Campos (SP), Brazil.

*Correspondence author: r.marisa@gmail.com

INTRODUCTION

The atmosphere behaves like a fluid allowing the propagation of several types of waves, such as atmospheric tides, planetary waves, and gravity waves (GW). While the density of the atmosphere decreases with altitude, the amplitude of the GW increases exponentially and becomes maximum in the region of the ionospheric F layer¹. Numerical simulations have shown how important is the presence of GW for the generation of plasma bubbles². There are several techniques for observing these waves. However, using data from weather stations allows a wide analysis of the country.

This work presents the development of an algorithm for reading and analysis capable of distinguishing and identifying the typical behavior of the formation of GW, and/or instabilities, in the troposphere and lower stratosphere (TLS).

EXPERIMENT

Data from the years 2009 and 2014 obtained by the Altitude Meteorological Station of Brasília (SBBR) were used. The radiosonde performed measurements at 0 and 12 UTC. A balloon inflated with helium gas takes the radiosonde to altitudes of the order of 30 km. The displacement of the probe was recorded by a global positioning system (GPS) antenna, and the observed data was sent by radio to the receiving station. The algorithm was developed based on previous articles^{3,4}. The curve fitting was made from the input values to determine the wind or background temperature.

Figure 1 shows curves that fit wind direction and temperature as a function of altitude, respectively. After this step, the experimental data were subtracted from the reference value, then the fast Fourier transform (FFT) was calculated from the residuals. Therefore, the quadratic sum of the FFT components was calculated for each acquisition.

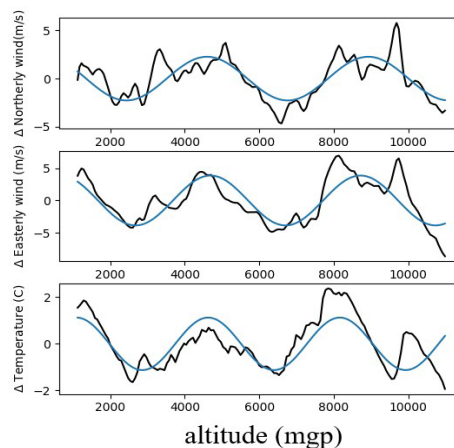


Figure 1: Fitted curves to read wind and temperature data.

RESULTS AND DISCUSSION

The temperature (Fig. 2a) and pressure (Fig. 2b) agreed with the expected values and confirmed the reliability of the algorithm. The behavior of the temperature was well defined for the values in the troposphere and tropopause. For a condition of hydrostatic equilibrium, the behavior of the pressure approached an exponential decay. The results of kinetic energy (Fig. 2c) and potential energy (Fig. 2d) showed that there are high values (e.g., above $5 \text{ m}^2/\text{s}^2$ for kinetic energy) indicating the possibility of instabilities in the TLS or conditions for possible gravity wave formation.

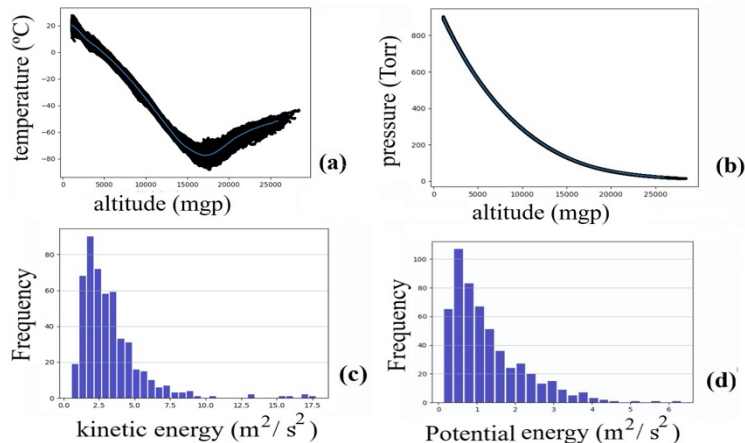


Figure 2: Measurements of temperature, pressure, and kinetic energy (SBBR 2009).

ACKNOWLEDGMENTS



Divisão de Pesquisa, Seção de Meteorologia Aeronáutica (Departamento de Controle do Espaço Aéreo).
Fundação de Amparo à Pesquisa do Estado de São Paulo (Fapesp), Process no. 2018/14,435-2.

REFERENCES

1. Abdu MA, Kherani EA, Batista IS, Paula ER, Fritts DC, Sobral JHA. Gravity wave initiation of equatorial spread F/plasma bubble irregularities based on observational data from the SpreadFEx campaign. *Ann Geophys.* 2009;27(7):2607-22. <https://doi.org/10.5194/angeo-27-2607-2009>
2. Kherani EA, Abdu MA, Paula ER, Fritts DC, Sobral JHA, Meneses Jr. FC. The impact of gravity waves rising from convection in the lower atmosphere on the generation and nonlinear evolution of equatorial bubble. *Ann Geophys.* 2009;27(4):1657-68. <https://doi.org/10.5194/angeo-27-1657-2009>
3. Yoshiki M, Sato K. A statistical study of gravity waves in the polar regions based on operational radiosonde data. *J Geophys Res.* 2000;105(D14):17995-8011. <https://doi.org/10.1029/2000JD900204>
4. Zhang SD, Yi F. A statistical study of gravity waves from radiosonde observations at Wuhan (30° N, 114° E) China. *Ann Geophys.* 2005;23(3):665-73.



Synthesis of graphene on nickel oxide by PECVD

Larissa Solano de Almeida^{1,*} , Andressa L. O. Pinto², Marcos D. Manfrinato^{1,2} , Luciana Sgarbi Rossino^{1,2}

1. Universidade Federal de São Carlos – Sorocaba (SP), Brazil.

2. Faculdade de Tecnologia José Crespo Gonzales – Sorocaba (SP), Brazil.

*Corresponding author: solano.larissa@gmail.com

INTRODUCTION

Graphene is formed by a one-atom thin carbon layer with a hexagonal structure which arouses research interest due to its unique structure, presenting excellent chemical and physical properties, like high thermal conductivity and high young's modulus. It can be applied in many fields¹. The sensing materials for aqueous and gaseous species are promising applications by the graphene and its derivatives. The conventional methods for synthesis of the graphene require a very high temperature. However, the plasma-enhanced chemical vapor deposition method (PECVD) has been explored to produce this crystalline structure of carbon due to its relatively large-scale and low-temperature production². The objectives of this work were to synthesize and characterize the graphene carried out by PECVD.

EXPERIMENTAL

For the development of this work, nickel (Ni) was used as a substrate, which was oxidized with a gas mixture of argon (Ar) and oxygen (O₂) at the total gas pressure of 0.42 torr, with 600V, for 30 minutes. Immediately after oxidation, the carbon nanostructure was synthesized with the precursor gases methane (CH₄), hydrogen (H₂) and argon (Ar) at the total pressure of the gases at 1.50 torr, with 700V and 30 minutes. The effect of argon on the carbon nanostructure synthesis was investigated. The oxidized substrate (catalyst) was characterized by scanning electron microscopy (SEM) / energy dispersive x-ray spectroscopy (EDS). The carbon nanostructures obtained were characterized by Raman spectra.

RESULTS AND DISCUSSION

The SEM / EDS analysis pointed out that the surface submitted to plasma oxidation showed the formation of a uniform oxide layer throughout the substrate, as seen in Fig. 1. The results present the positive influence of argon on the formation and crystallinity of the sintered materials, providing the narrowing of D and G peaks and the distinguishing of the 2D peaks. The Raman spectra showed the presence of D, G and 2D peaks characterizing

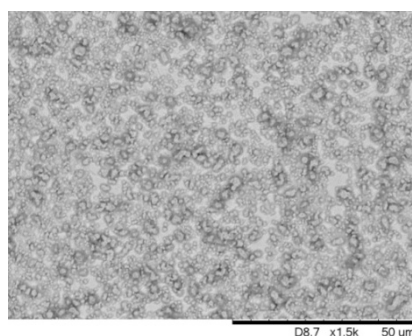


Figure 1: The image 1,500X of oxidized nickel surface.

the formed structure as graphene with the addition of 0.39 torr argon, as verified in Fig 2. The parameters obtained for Raman spectra were $I_D/I_G = 1,10$, cluster size $L_a = 8.9$ nm, point defects $L_D = 10.3$ nm, and defect density $ND = 300 \times 10^{10} \text{cm}^{-2}$. It can be concluded that the structure formed has a crystalline character, with spectra of graphene nanostructures, but with defects.

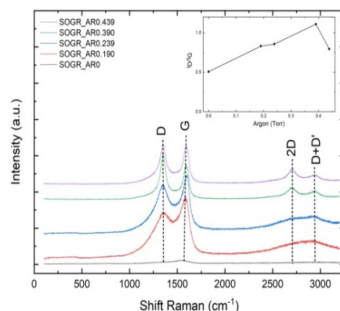


Figure 2: Raman spectra and ratio I_D/I_G by Ar pressure.

ACKNOWLEDGMENTS

The authors acknowledge Faculdade de Tecnologia José Crespo Gonzales, in Sorocaba, Universidade Estadual de Campinas, Conselho Nacional de Desenvolvimento Científico e Tecnológico and Coordenação de Aperfeiçoamento de Pessoal de Nível Superior for the financial support.

REFERENCES

1. Peng K-J, Wu C-L, Lin Y-H, Liu Y-J, Tsai D-P, Pai Y-H, et al. Hydrogen-free PECVD growth of few-layer graphene on an ultra-thin nickel film at the threshold dissolution temperature. *J Mater Chem C*. 2013;1(24):3862. <http://doi.org/10.1039/c3tc30332b>
2. Liu Y, Chen Y. Synthesis of large scale graphene oxide using plasma enhanced chemical vapor deposition method and its application in humidity sensing. *J Appl Phys*. 2016;119(10):103301. <http://doi.org/10.1063/1.4942999>



Study of the added nitrogen effect on the diamond-like carbon film in the film electric characteristic

Mateus da Silva Pereira^{1,*}, Larissa Solano de Almeida² , Marcos Dorigão Manfrinato^{1,2} , Luciana Sgarbi Rossino^{1,2} 

1. Faculdade de Teologia e Ciências – Sorocaba (SP), Brazil.
 2. Universidade Federal de São Carlos – Sorocaba (SP), Brazil.
- * **Corresponding author:** mapereirasilva1999@gmail.com

INTRODUCTION

Diamond-like carbon (DLC) films present excellent performance, such as high wear resistance, high hardness, low friction coefficient, chemical inertness, and high electrical resistivity. The DLC films are applied in many areas, among which we can highlight the anti-wear and anti-corrosion protection¹. The nitrogen, added to the DLC film, considerably improves the adhesion of the DLC film to metallic substrates. However, there are no studies in literature that show the effect of adding this element in relation to the electrical impedance of DLC films².

EXPERIMENTAL

For this work, samples of 321 stainless steel were polished and cleaned to perform the surface treatments of the DLC and DLCN films by plasma-enhanced chemical vapor deposition (PECVD). The treatment started with cleaning by plasma ablation for 30 minutes with 2-torr pressure and gas proportions of 80% Ar + 20% H₂. Afterwards, the deposition of an interlayer of silicon was carried out using hexamethyldisiloxane (HMDSO) as a precursor. Then, the DLC film was deposited using CH₄ and Ar as precursors. For DLCN, CH₄ and N₂ were used, modifying the nitrogen percentage in the treatment, varied from 10 to 50%. The samples were subjected to the electrical impedance test using the ModuLab XM MTS equipment configured for dielectric elements.

RESULTS AND DISCUSSION

The DLC film features high electrical resistivity. The nitrogen added to the DLC not only improves the adhesion of the film to the substrate, but also acts as a facilitator of the electrical passage by decreasing the resistivity of the DLC film. It was observed that the treatment that obtained the highest electrical impedance was DLC without adding nitrogen, with a similar result found for the DLCN treatment performed with 30% N₂ in the treatment. It has been shown that the increase in nitrogen in the structure considerably decreases the impedance of the formed film. The DLCN film formed with 50% of N₂ in the treatment presented the lowest electrical impedance, what turns this film more conductive.

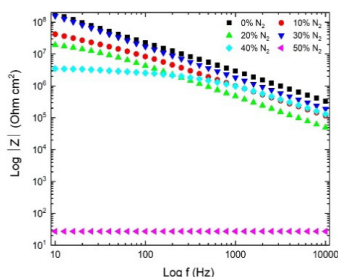


Figure 1: Electrical impedance by frequency.

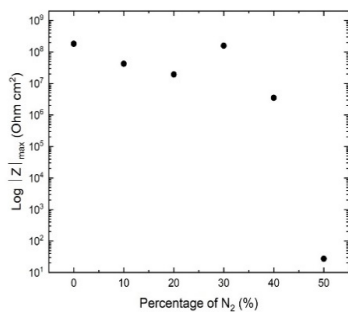


Figure 2: Maximum electrical impedance by %N₂.

ACKNOWLEDGMENTS

The authors acknowledge Faculdade de Teologia e Ciências of Sorocaba and Universidade Estadual Paulista “Júlio de Mesquita Filho”, Campus Sorocaba, for the support.

REFERENCES

1. Robertson J. Diamond-like amorphous carbon. *Mater Sci Eng.* 2002;37(4-6):129-281. [https://doi.org/10.1016/S0927-796X\(02\)00005-0](https://doi.org/10.1016/S0927-796X(02)00005-0)
2. Morona MT. Ensaio eletroquímico e influência da nitretação à plasma na resistência a corrosão do aço inoxidável ISO 5832-1 [dissertation]. Curitiba: Universidade Tecnológica Federal do Paraná; 2007.



Cold plasma jet improve tissue repair in wounds infected by multispecies biofilms

Maria Alcioneia Carvalho de Oliveira^{1,*} , Aline da Graça Sampaio¹ , Thalita Mayumi Castadelli Nishime² , Kostantin Georgiev Kostov³ , Cristiane Yumi Koga-Ito¹ 

1. Universidade Estadual Paulista “Júlio de Mesquita Filho” - Institute of Science and Technology - Department of Environmental Engineering/Oral Biopathology Graduate Program – São José dos Campos (SP), Brazil.

2. Leibniz Institute of Plasma Science and Technology – Greifswald, Germany.

3. Universidade Estadual Paulista “Júlio de Mesquita Filho” - Guaratinguetá Faculty of Engineering - Department of Physics – Guaratinguetá (SP), Brazil.

*Correspondence author: macoliveira12@gmail.com

INTRODUCTION

Previous studies reported that treatment with helium cold plasma accelerates the rate of wound repair in diabetic mice¹ and patients². However, little is known about its effect on infected wounds. The purpose of this study was to test the applicability of cold plasma jet as a novel therapy for infected wounds.

EXPERIMENTAL

The protocol of the experiment was approved by the Ethical Committee. The murine model of chronic wound reported by Dalton et al.³ was used. After anesthesia, the animals were trichotomized, and, after asepsis, a 6-mm wound was produced with the aid of surgical instruments (Fig 1).

Groups treated with cold atmospheric plasma (CAP) and non-treated group were compared at two different periods of follow up (n = 10/group). The wounds were inoculated with multispecies biofilms formed by methicillin-resistant *Staphylococcus aureus* (ATCC 33591), *Pseudomonas aeruginosa* (ATCC 27853) and *Enterococcus faecalis* (ATCC 29212), and treated with cold plasma jet once a day during 5 min for three consecutive days. Helium (99.5% purity) was used as working gas (flow rate 2 SLM), and the adopted treatment parameters were 32 kHz signal frequency and discharge power of 1 W. The distance between the wound surface and the plasma jet was 1.5 cm.

The wounds were observed and evaluated daily at day 0, day 4 and day 8 to check the repair process. Wounds were photographed with a digital camera, and wound surface area was calculated using ImageJ 1.49 v image analysis software. The wound closure rate was calculated by Eq. 1:

$$[1 - (\text{wound area } T_r) / (\text{wound area } T_0)] \times 100^4 \quad (1)$$

Data was compared statistically by Kruskal-Wallis/Dunn's test (level of significance of 5%).

RESULTS AND DISCUSSION

Wound size reduction was significantly lower in plasma-treated group when compared to controls from day 8 (p < 0.05). The wound area and the percentage decrease in wound size are shown in Fig. 2. Although previous studies reported the positive effect of cold plasma on wound repair^{3,4}, this effect was not studied in infected wounds.

The results of this study indicated that cold plasma can improve wound healing, even in the presence of a mature multispecies biofilm. In conclusion, this research demonstrates that cold plasma jet accelerates the tissue repair of wounds infected by multispecies biofilm.



Figure 1: Murine model wounds.

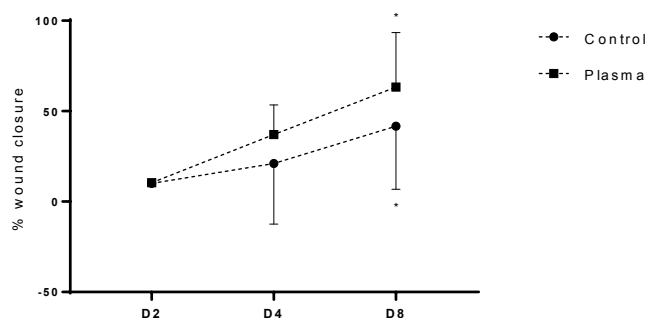


Figure 2: Percentage decrease of wound surface area.

ACKNOWLEDGMENTS




Funding by National Council for Scientific and Technological Development (CNPq), 405653/2016-6 and 308127/2018-8).

REFERENCES

1. Jacofsky MC, Lubahn C, McDonnell C, Seepersad Y, Fridman G, Fridman FA, et al. Spatially resolved optical emission spectroscopy of a helium plasma jet and its effects on wound healing rate in a diabetic murine model. *Plasma Med.* 2014;4:177-91. <https://doi.org/10.1615/PlasmaMed.2015012190>
2. Brehmer F, Haenssle HA, Daeschlein G, Ahmed R, Pfeiffer S, Görlitz A, et al. Alleviation of chronic venous leg ulcers with a hand-held dielectric barrier discharge plasma generator (PlasmaDerm®) VU-2010): results of a monocentric, two-armed, open, prospective, randomized and controlled trial (NCT01415622). *J Eur Acad Dermatol Venereol.* 2015;29(1):148-55. <https://doi.org/10.1111/jdv.12490>
3. Dalton T, Dowd SE, Wolcott RD, Sun Y, Watters C, Griswold JA, et al. An in vivo polymicrobial biofilm wound infection model to study interspecies interactions. *PLoS One.* 2011;6(11):e27317. <https://doi.org/10.1371/journal.pone.0027317>
4. Chatraie M, Torkaman G, Khani M, Salehi H, Shokri B. In vivo study of non-invasive effects of non-thermal plasma in pressure ulcer treatment. *Sci Rep.* 2018;8:5621. <https://doi.org/10.1038/s41598-018-24049-z>



Effect of the interlayer on duplex treatments properties

Miguel Rubira Danelon^{1,*} , Marcos Dorigão Manfrinato^{1,2} , Luciana Sgarbi Rossino^{1,2} 

1.Faculdade de Tecnologia de São Paulo – Sorocaba (SP), Brazil.

2.Universidade Federal de São Carlos – Sorocaba (SP), Brazil.

*Correspondence author: miguelrubida@gmail.com

INTRODUCTION

Duplex treatments are alternative to combine high hardness and low friction coefficient of the diamond-like carbon (DLC) with wear, fatigue, and corrosion resistance from nitriding treatments, wherein the main objective in the duplex treatment of DLC and nitriding is to improve the adhesion of the DLC film in metallic substrate due to the reduction of the tensions between the substrate and the DLC film using a silicon interlayer or a thermochemical treatment¹.

The objective of this work was to study the formation of a DLC deposition in a nitriding surface of 4,340 steel using a carbon and nitrogen gradient keeping the adhesion of the film on substrate without interlayer.

EXPERIMENTAL

The treatments were carried out using a pulsed-direct current (DC) power supply. The conventional duplex treatment was carried out by a nitriding treatment at 80% N₂-20% H₂ gas mixture for 5 h, 500 sscm at 450°C, followed by an interlayer deposition with a hexamethyldisiloxane (HMDSO) as a precursor using 70% HMDSO-30%Ar, for 15 min at 300°C, and DLC film deposition with 90% CH₄-10Ar, 30 sccm for 2 h. The duplex without interlayer was carried out by a nitriding and DLC film deposition at the same parameters of conventional duplex treatment, but without interlayer formation.

A duplex treatment was performed without interlayer which was carried out at the same nitriding parameters previously cited, with nitrocarburizing treatment with 75% N₂-20% H₂-5% CH₄, for 1 h, 500 sccm at 450°C. After it, a DLC film with 90% CH₄-10%Ar, 30 sccm, for 2 h, with a gradient of CH₄, increasing 20% every 30 min, without N₂, was deposited. Also, another duplex treatment was made, but with a DLC deposition with 70% CH₄-30% N₂, increasing the gradient of CH₄ propellant by the same amount, with N₂.

The samples were characterized by micro-abrasive wear test by fixed ball with 8 N load for 600 s, corrosion cyclic polarization test in a NaCl (w/w 3,5%) solution and VDI 3,189 adhesion test.

RESULTS AND DISCUSSION

It was possible to verify that the duplex treatment with CH₄ gradient presented lower wear volume, justified by the combination of high hardness and low friction coefficient of the DLC film and the hardness in depth due the thermochemical treatments. The duplex treatment with CH₄ and N₂ gradient presented high wear volume due to the lower hardness surface despite the good adhesion of the DLC film in the substrate. The duplex treatment without interlayer and without gradient obtained higher volume due to the lower film adhesion.

It was observed that the conventional duplex showed high wear and corrosion resistance, once the interlayer presented good corrosion resistance and influence in adhesion of the DLC film in the substrate. The duplex treatments with CH₄ gradient presented good corrosion resistance, due to the combination of the DLC film and thermochemical treatments, improving the properties of the base material.

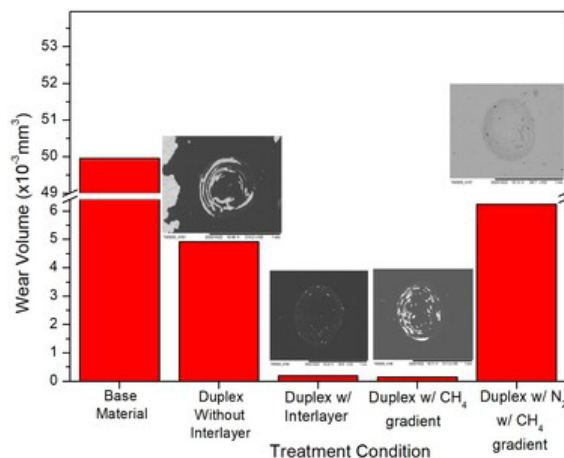


Figure 1: Micro-abrasive wear and adhesion test.

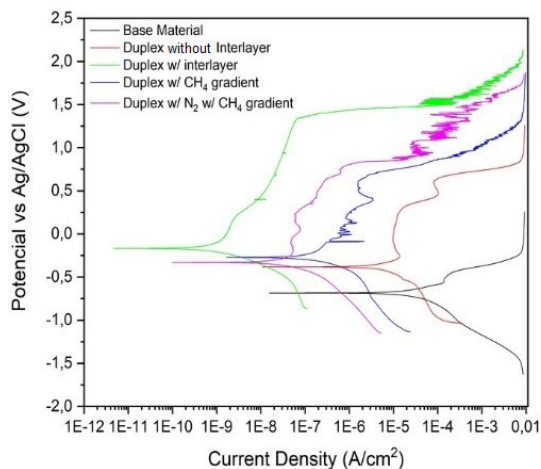


Figure 2: Potentiodynamic polarization curve.

ACKNOWLEDGMENTS






The authors acknowledge Fundação de Amparo à Pesquisa do Estado de São Paulo (Fapesp) (2019/13041-3), Universidade Estadual Paulista “Júlio de Mesquita Filho” (Unesp), Campus Sorocaba, and Faculdade de Tecnologia de São Paulo (Fatec) Sorocaba.

REFERENCES

Dalibón E, Guitar MA, Trava-Airoldi V, Mücklich F, Brühl SP. Plasma nitriding and DLC coatings for corrosion protection of precipitation hardening stainless steel. *Adv Eng Mater.* 2015;18(5):826-32. <https://doi.org/10.1002/adem.201500411>



Association of atmospheric pressure cold plasma and nystatin on *Candida albicans* biofilms

Lady Daiane Pereira Leite¹ , Maria Alcioneia Carvalho de Oliveira¹ , Thalita Mayumi Castaldelli Nishime² , Konstantin Georgiev Kostov³ , Cristiane Yumi Koga-Ito¹ 

1. Universidade Estadual Paulista "Júlio de Mesquita Filho" - Institute of Science and Technology - Department of Environmental Engineering/Oral Biopathology Graduate Program – São José dos Campos (SP), Brazil.
2. Leibniz Institute of Plasma Science and Technology – Greifswald, Germany.
3. Universidade Estadual Paulista "Júlio de Mesquita Filho" - Faculdade de Engenharia de Guaratinguetá - Department of Physics – Guaratinguetá (SP), Brazil.

*Correspondence author: cristiane.koga-ito@unesp.br

INTRODUCTION

The increasing incidence of antifungal resistance represents a great challenge in the medical areas. For this reason, the search for new alternative methods is urgently necessary. The aim of this project was to study the effects of the association of cold atmospheric plasma (CAP) and nystatin on *Candida albicans* biofilms.

EXPERIMENTAL

Candida albicans SC 5314 (wide type reference strain) standardized suspension were obtained. Then, 24 h *C. albicans* biofilms were formed in 96 wells microplates using RPMI broth + 2% glucose. After initial adherence for 90 min under shaking, plates were incubated for 24 h at 37°C, for biofilm formation. After incubation, biofilms were exposed to the treatments. The associations between CAP and the nystatin were done according to the following experimental groups: nystatin followed by CAP (nystatin/CAP), and CAP followed by the nystatin (CAP/nystatin). Treatments with CAP and nystatin separately were also tested for comparative purposes. The exposure time to CAP and nystatin was 2.5 min. For nystatin, reductions of 75% (60 µg/mL) and 50% (40 µg/mL) minimal inhibitory concentration were used. Helium plasma jet (99.5% purity, 2.0 slm) was excited by using a low-frequency high-voltage signal with 32 kHz frequency and power of 1 W. The distance between nozzle and biofilm surface was kept fixed at 1.5 cm. The number of colony-forming units was determined by plating method. Non-exposed control was included. The experiments were performed in triplicate in three separate occasions. Data was compared by one-way analysis of variance (ANOVA) and post-hoc Tukey (5%).

RESULTS AND DISCUSSION

Both CAP and nystatin (40 and 60 µg/mL) reduced significantly the viability of *C. albicans* biofilms. When CAP was associated to nystatin at 40 µg/mL, no synergic effect was observed. In fact, CAP by itself was more effective than when associated with nystatin. Similarly, no synergic effect of nystatin at 60 µg/mL and CAP was detected. It could be concluded that no synergic effect between cold plasma and nystatin was detected.

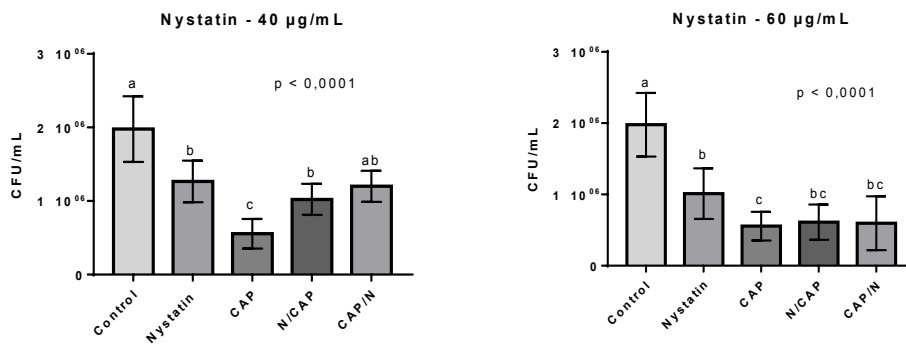




Figure 1: Viability of *Candida albicans* SC 5314 24 h expressed in values of colony forming units per mL (cfu/mL, mean and standard deviation), treated with cold atmospheric plasma (CAP) (2.5 min), nystatin (40 and 60 µg/mL), CAP followed by nystatin (CAP/nystatin), nystatin followed by CAP (nystatin/CAP), and untreated negative control group.

ACKNOWLEDGMENTS

Funding by Fundação de Amparo à Pesquisa do Estado de São Paulo (Fapesp) 2019/05856-7 and Conselho Nacional de Desenvolvimento Científico e Tecnológico (CNPq) (308127/2018-8). This study was financed in part by the Coordenação de Aperfeiçoamento de Pessoal de Nível Superior – Brasil (Capes) – Finance Code 001.



Nitrided austenitic stainless steel: the importance of characterizing the submicrometrical region

Danilo Olzon-Dionysio^{1,*} , Solange de Souza¹, Sylvio D. de Souza¹, Maristela Olzon-Dionysio¹ 

1. Universidade Federal dos Vales do Jequitinhonha e Mucuri - Institute of Science and Technology – Diamantina (MG), Brazil.

*Correspondence author: dolzon@gmail.com

INTRODUCTION

Plasma nitriding of austenitic stainless steel (ASS) is a very sensitive process to its parameters. Depending on these parameters, a myriad of physically and chemically distinguishable layers on the ASS matrix may be produced and the layer formed¹. The diffusion of the nitrogen into the ASS matrix forms a gradient of nitrogen concentration and gives rise, mainly, to a non-stoichiometric metastable phase, called expanded austenite (EA) (also known as γ_N or S phase). Sometimes, the formation of nitrides is also mentioned, notably when a thick layer is formed. However, it is common to find in the literature the functional properties of the layer related to EA.

The combination of the EA non-stoichiometry with the nitrogen gradient of the layer makes the characterization of this layer very challenging, boosted by the fact that the EA crystallographic structure is not established. In this context, the presence of nitrides in a submicrometric region of the nitrided layer may easily be masked, due characterizations techniques limitation (or inappropriate choice of parameters) or/and misinterpretation of the results.

EXPERIMENTAL

Disk-shaped ASS samples, nitrided at 673 K, for 4 h, in 80% H₂-20% N₂ gas. Energy dispersive X-ray (EDX) cross sectional line scans were used to determine the nitrogen composition-depth profiles. X-ray diffraction (XRD) was also used, with a synchrotron radiation source (LNLS) of 7.5 keV beam energy in a grazing-incidence geometry diffraction and incident angle fixed in 21°, in which 99% of the absorption was set to reach a probing depth of 3.8 μm . Atomic force microscope was used with CoCr coating tip for imaging the magnetic domains on the disk-sample surface and on the cross-sectioned sub-samples. Mössbauer spectra for the samples were obtained in the backscattering geometry at room temperature, using a 50 mCi-⁵⁷Co source for both CXMS and CEMS setups.

RESULTS AND DISCUSSION

The nitrogen concentration and thickness of the nitrided layer was found to be 7 at.% and 2 μm for the 4 Torr-sample; for those at 6 and 10 Torr, the concentration was 16 and 24 at.%, with nearly the same thickness, namely 7 μm . These values are well correlated with the framework of an expanded austenite, as pointed by the XRD data. The magnetic force microscopy data are well correlated with the observed nitrogen concentration, evidencing the absence of any magnetic domain for the 4 Torr-sample; the magnetic patterns for the 6 Torr and 10 Torr-samples are quite similar, despite of the great difference in their nitrogen concentrations. The ⁵⁷Fe hyperfine parameters at two different sample depths were assessed by Mössbauer spectroscopy, by collecting data with two distinct backscattering setup geometries.

Fitting the corresponding spectra with model-independent hyperfine field distributions, starting from very low hyperfine field values, allowed correlating the magnetic force microscopy data to find out that the transition from paramagnetic to magnetic for the expanded austenite occurs at smaller hyperfine magnetic fields than it is usually

reported in the scientific literature. Such correlations point to the formation of a submicrometer layer occurring on the outermost surface of the sample. Despite the complexity and difficulties in differentiating the nitrides on the surface of the samples obtained at 6 and 10 Torr pressures, the results obtained in this work strongly indicate the existence of them in the submicrometer surface layer.

ACKNOWLEDGMENTS

Fundação de Amparo à Pesquisa do Estado de Minas Gerais (FAPEMIG), Fundação de Amparo à Pesquisa do Estado de São Paulo (FAPESP), LNLS (XDR2/20170261) and LNNano (SEM-C1_25050)

REFERENCE

Olzon-Dionysio D, Fabris JD, Martins MD, Tavares MAB, Ardisson JD. Magnetic and ^{57}Fe hyperfine structural features of nitrided austenitic stainless steel. *Surf Coat Tech.* 2020;388:125544. <https://doi.org/10.1016/j.surfcoat.2020.125544>



Effects of cold atmospheric plasma on the healing process of dermal ulcers infected by multispecies biofilms

Maria Alcioneia Carvalho de Oliveira¹ , Aline da Graça Sampaio¹ , Thalita Mayumi Castaldelli Nishime² , Konstantin Georgiev Kostov³ , Cristiane Yumi Koga-Ito^{1,*} 

1.Universidade Estadual Paulista “Júlio de Mesquita Filho” - Institute of Science and Technology - Department of Environmental Engineering/Oral Biopathology Graduate Program – São José dos Campos (SP), Brazil.

2.Leibniz Institute of Plasma Science and Technology – Greifswald, Germany.

3.Universidade Estadual Paulista “Júlio de Mesquita Filho” - Faculdade de Engenharia de Guaratinguetá - Department of Physics – Guaratinguetá (SP), Brazil.

*Correspondence author: cristiane.koga-ito@unesp.br

INTRODUCTION

The prevalence of ulcerative wounds in patients in intensive care units is high, affecting the individual's quality of life and leading to high financial costs. Atmospheric pressure cold plasma (CAP) shows promising antimicrobial and anti-inflammatory actions. The purpose of this study was to evaluate the effect of the plasma jet as a new therapy for the treatment of dermal ulcers in an *in-vivo* model.

EXPERIMENTAL

The study was conducted to evaluate the effect of CAP as a therapy in dermal ulcer wounds (Fig 1) *in vivo* in rabbits, according to the methodology of Gurjala et al.¹. Ventral region of the ears of 10 female New Zealand rabbits, from 3 to 6 months old, were trichotomized and cleaned with 70% alcohol. Afterwards, two wounds were confectioned up to the perichondrium with the aid of a 6-mm punch. The wounds were infected with multispecies biofilm formed by methicillin-resistant *Staphylococcus aureus* (ATCC 33591), *Pseudomonas aeruginosa* (ATCC 27853), and *Enterococcus faecalis* (ATCC 29212). Wounds were protected with dressings. Wounds were treated with CAP for four and eight days (n = 5). Plasma was applied at a distance of 1.5 cm, once a day, for three consecutive days, for 5 minutes. Plasma jet was produced by electric discharge in helium (99.5% purity) with 2 SLM gas flow rate. The adopted treatment parameters were 32 kHz signal frequency and 1 W of power. Wounds were followed up daily. The wounds were photographed (day 0, 2, 4 and 8), the area of the wound surface was calculated using the ImageJ 1.49 software, and the healing rate was calculated, according to the methodology of Chatraie et al.². Wounds exposed to non-ionized gas were included as controls. The percentage of wound closure were compared by Kruskal-Wallis test with Dunn's post hoc test, with a 5% significance level.

RESULTS AND DISCUSSION

Percentages of wound closure were significantly higher in CAP groups in relation to control at day 4 ($p < 0.05$) (Fig. 2). At day 8, although the group treated with plasma showed a more evident wound closure (up to 60%), significant differences were not detected ($p > 0.05$). In conclusion, CAP can enhance the closure of dermal ulcers infected by multispecies biofilms, with a more significative effect on the first days of the healing process.

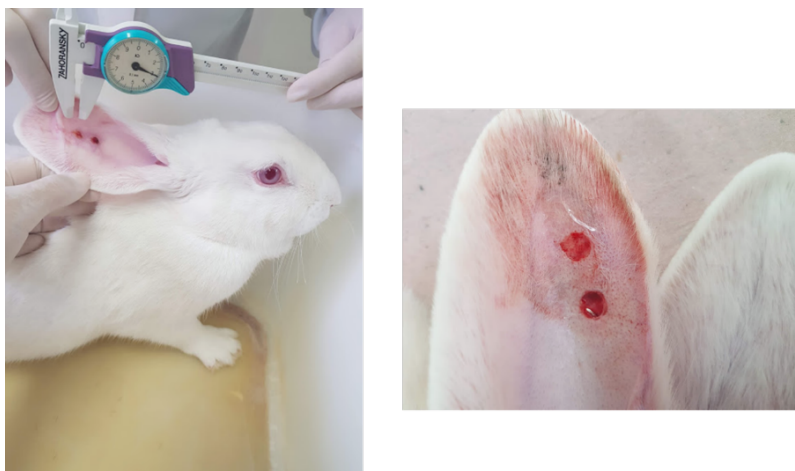


Figure 1: Dermal ulcer.

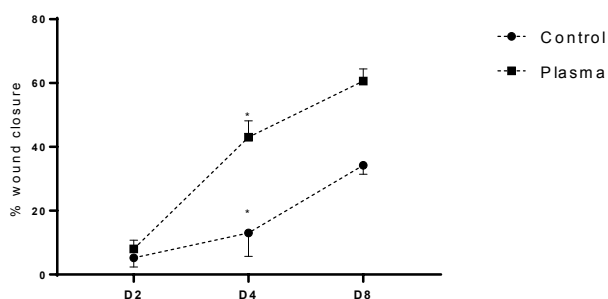


Figure 2: Percentage of wound closure at day 4 and day 8.

ACKNOWLEDGMENTS

Funding by Conselho Nacional de Desenvolvimento Científico e Tecnológico
Grants No: 405653/2016-6 and 308127/2018-8.

REFERENCES

1. Gurjala AN, Geringer MR, Seth AK, Hong SJ, Smeltzer MS, Galiano RD, et al. Development of a novel, highly quantitative in vivo model for the study of biofilm-impaired cutaneous wound healing. *Wound Repair Regen.* 2011;19(3):400-10. <https://doi.org/10.1111/j.1524-475x.2011.00690.x>
2. Chatraie M, Torkaman G, Khani M, Salehi H, Shokri B. In vivo study of non-invasive effects of non-thermal plasma in pressure ulcer treatment. *Sci Rep.* 2018;8:5621. <https://doi.org/10.1038/s41598-018-24049-z>

Analysis of epoxy/granite composites using FTIR

Jorge Luiz Siqueira-Costa-Neto¹, Guilherme Soares Damasceno¹, Antônio Renato Bigansolli¹ , Belmira Benedita de Lima-Kühn^{1,*}

¹.Universidade Federal Rural do Rio de Janeiro – Seropédica (RJ), Brazil.

*Correspondence author: belmira@ufrj.br

INTRODUCTION

The main use of ornamental stone, such as granite and marble, is as a covering material, especially in the construction sector. The exploration and processing of these rocks generate a high amount of particulate material that can cause numerous environmental impacts¹. Thus, the management of this material has motivated the study of possible applications of it, and one of these applications is the incorporation of the material as reinforcement fillers in polymer². The aim of this work was to study the chemical reactions suspected of occurring during the modification of the epoxy resin with granite powder filler using Fourier-transform infrared (FTIR) spectroscopy.

EXPERIMENTAL

Initially, the granite stone was fragmented to obtain pieces of reduced size. Then, it was grinded using the hammer and then comminuted in a porcelain mortar, and all material sieved to below 250 mesh screen. For the manufacture of the composite, silicone molds were used. The polymer bisphenol A diglycidyl ether epoxy resin (DGEBA) and the hardener, Aradur 2963, were used in the proportions indicated by the manufacturer. The powders were weighed and manually mixed with Aradur 2963 and Araldite GY 279 BR in a beaker for 10 min using a glass stirring rod to produce epoxies with 0, 3, 5 and 10 wt% granite powder concentrations. Finally, the mixture was poured into a silicone mold coated with a mold release agent and cured at room temperature for 48 h.

After curing, a small portion of fine powder from each sample was prepared. The composite powder was analyzed by FTIR spectroscopy. FTIR spectra was recording with a Bruker Vertex 70 spectrometer by applying the ATR Platinum. The recording of the samples was obtained for the 4,000-cm⁻¹ to 400-cm⁻¹ regions. The testing was used to identify the chemical bonds present in the samples based on the absorption bands that are shown in the infrared spectra. Finally, monitoring and evaluation of the chemical reactions suspected of occurring during the modification of the epoxy resin were achieved.

RESULTS AND DISCUSSION

The obtained infrared spectra of the granite-epoxy composites did not identify the existence of a chemical reaction between the granite and the epoxy resin (Fig. 1).

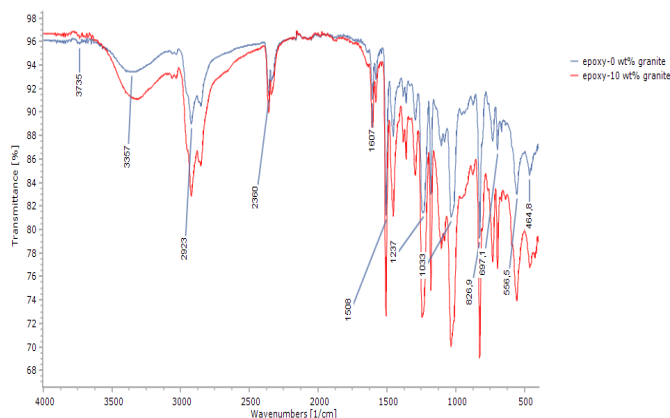


Figure 1: Spectrum of samples epoxy-0 wt% granite and epoxy-10 wt% granite.

ACKNOWLEDGMENTS

The authors gratefully acknowledge the financial support of Conselho Nacional de Desenvolvimento Científico e Tecnológico (CNPq), by Programa Institucional de Bolsas de Iniciação Científica (PIBIC) from Universidade Federal Rural do Rio de Janeiro (UFRRJ).

REFERENCES

1. Mofati LM, Vidal FWH, Silva REC, Correia JCG, Ribeiro RCC. Estudo do aproveitamento de Resíduos e Rejeitos na Cadeia Produtiva de Rochas Ornamentais. In: IV Congresso Brasileiro de Rochas Ornamentais & VIII Simpósio de Rochas Ornamentais do Nordeste. Proceedings. 2012.
2. Gonçalves JAV, Campos DAT, Oliveira GJ, Rosa MLS, Macedo MA. Mechanical properties of epoxy resin based on granite stone powder from the Sergipe fold-and-thrust belt composites. Mater Res. 2014;17(4):878-87. <http://doi.org/10.1590/S1516-14392014005000100>



Study of the corrosion resistance of DLC film with multilayers of organosilicone and silicon oxide

César A. A. Júnior^{1,*}, Marcos Dorigão Manfrinato^{1,2} , Luciana Sgarbi Rossino^{1,2} 

1. Faculdade de Tecnologia de Sorocaba – Sorocaba (SP), Brazil.

2. Universidade Federal de São Carlos – Sorocaba (SP), Brazil.

*Correspondence author: cesar.augustoantoniojr@hotmail.com

INTRODUCTION

Although the diamond like carbon (DLC) films present high hardness, low friction coefficient, high wear resistance and chemical inertness, they have defects that impair the corrosion behavior of the treated material¹. To minimize the effect of the DLC film defects in the corrosion properties of aluminum alloys, the application of interlayer and multilayer based on silicon was studied, in order to improve the adhesion of the film to the metallic substrate, to inhibit the formation of defects on the film surface and to slow down the corrosion process.

The objective of this work was to evaluate the deposition of DLC film by plasma enhanced chemical vapor deposition (PECVD) technique using direct current (DC)-pulsed source, studying the influence of multilayer deposition based on silicon and silicon oxide, modifying time parameters and quantity of deposition of the DLC layer.

EXPERIMENTAL

To perform the treatments, the Al7050-T7451 alloy was cleaned by plasma ablation using 50% Ar and 50% H₂ applying 230 V for 1,800 s. The organosilicon interlayer (C-Org) was deposited using 70% hexamethyldisiloxane (HMDSO) and 30% Ar at a total pressure of 9.75×10^{-2} Torr, 500 V and 450 s. The deposition of the SiOx interlayer (C-SiOx) was carried out using 70% HMDSO, 30% Ar and 15 sccm of O₂ with the total pressure of 4.5×10^{-1} Torr, 430 V and 450 s. The DLC film (DLC2h) was deposited with 90% CH₄ and 10% Ar, with 500 V and pressure of 3.5×10^{-1} torr at 7,200 s, while the same condition was used to perform the DLC (DLC4h) deposited for 14,000 s.

The deposition system employed was the production of C-Org+DLC2h and C-Org+DLC4h, deposition of DLC2h+C-Org and the deposition of interlayer of organosilicone and silicon oxide in the deposition of Triple-InterC+DLC4h. The morphology and chemical composition of the layers formed in the treatments were analyzed by scanning electron microscope (SEM), and the untreated and treated samples were characterized by cyclic polarization corrosion test applied to the treated samples.

RESULTS AND DISCUSSION

It was observed that the defects of the DLC film occurred due to the precipitates of the aluminum alloy. The chemical composition of the deposited layers, observed in Fig. 1, showing the multilayer deposition, demonstrated for C-Org+DLC2h, C-Org+DLC4h and Triple-InterC+DLC4h the presence of silicon in contact with the substrate, referring to the organosilicone films and silicon oxide. For the DLC2h+C-Org sample, the presence of silicon was verified on both sides of the DLC film, indicating the deposition of the C-Org layer covering the DLC film. In the corrosion test, showed in Fig. 2, the DLC2h film improved the corrosion resistance of the studied alloy. However, when applied the treatments C-Org+DLC4h, Triple-InterC+DLC4h and DLC2h+C-Org, the potential of corrosion of the film increased considerably, indicating that deposition with DLC film in longer times can cover the substrate precipitates, decreasing the defects of the film and providing better resistance to corrosion of the film in the studied material.

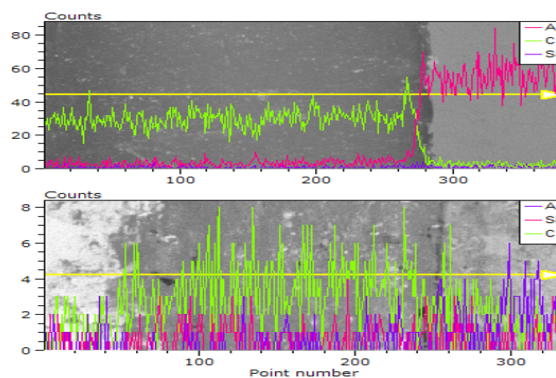


Figure 1: Chemical composition of layers.

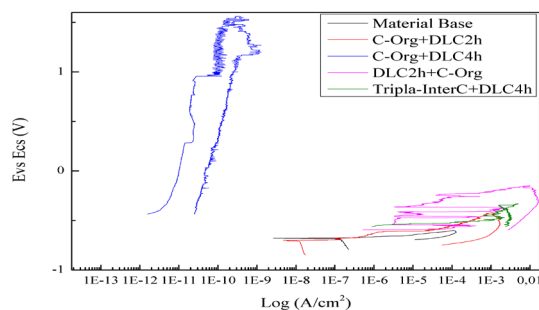


Figure 2: Cyclic polarization curve.

ACKNOWLEDGMENTS

The author thanks Fundação de Amparo à Pesquisa do Estado de São Paulo (FAPESP)(2019/12192-8), Universidade de São Paulo and Faculdade de Tecnologia de Sorocaba for providing the laboratory.

REFERENCES

1. Ilic E, Pardo A, Suter T, Mischler S, Schmutz P, Hauert R. A methodology for characterizing the electrochemical stability of DLC coated interlayers and interfaces. Surf Coat Tech. 2019;375:402-13. <https://doi.org/10.1016/j.surfcoat.2019.07.055>



Global model of argon ICP discharge: effects of reaction set on collisional energy

Júlia Karnopp^{1,*} , Rodrigo Sávio Pessoa¹ , Julio César Sagás² 

1. Instituto Tecnológico de Aeronáutica – São José dos Campos (SP), Brasil.

2. Universidade do Estado de Santa Catarina – Joinville (SC), Brasil.

*Correspondence author: julia_karnopp@outlook.com

INTRODUCTION

The interest in plasma modeling has been increased in the last few decades¹. Modeling and simulations of discharge are fundamental activities of research to complement and give further information of plasma chemistry and its dependence on process parameters. The zero-dimensional modeling of plasmas, also known as global model, requires chemical data namely cross sections and/or rate constants as input information, to describe the collisional process in gas/plasma phases².

In literature, there are several models of different gas discharges, and the most common models are developed for argon-based plasmas. Differences on chosen species, reactions, rate constants and/or cross sections affect the plasma chemistry and its parameters, such as electron temperature and density. This can be observed primarily in the collisional energy per pair electron ion created, that corresponds to the energy lost by electron between two consecutive ionizations. Therefore, it is interesting to investigate the most appropriate reaction set for a given plasma chemistry.

METHODOLOGY

In this work, two reaction sets for argon discharge occurring in inductive coupled plasma (ICP) were investigated. A survey of reaction sets, cross sections data and rate constants of Ar plasma was made. In the sets, the species argon in fundamental state, Ar , argon ion, Ar^+ , and three metastable argon atoms, Ar^m , Ar^r , Ar^p and electrons were considered. The sets include elastic scattering, ground state ionization, multistep ionizations, excitations, desexcitation and superelastic collisions, in a total of 17 reactions. The collisional energy was calculated for the two different reaction sets, one with the most common constant rates, and the other one is a new set. Commonly, the models consider only the metastable Ar^m . Then, the effect on collisional energy of the three metastable atoms was also studied.

RESULTS AND DISCUSSION

Differences were observed in the collisional energy with the change of some rate constants, reaching a few electron volts for the same electron temperature. It affects the energy balance in the model and, consequently, the plasma chemistry. The collisional energy also changes when multistep ionization is considered (Fig. 1).

With the inclusion of the metastable species and considering the multistep ionization, reduction in collisional energy was verified (Fig. 1). The ionization energy of this species was less than the one of argon in fundamental state. Therefore, the collisional energy necessary to create an electron-ion pair decreases due to multistep ionizations. The observed changes in collisional energy showed that it is necessary to consider the most complete reaction set.

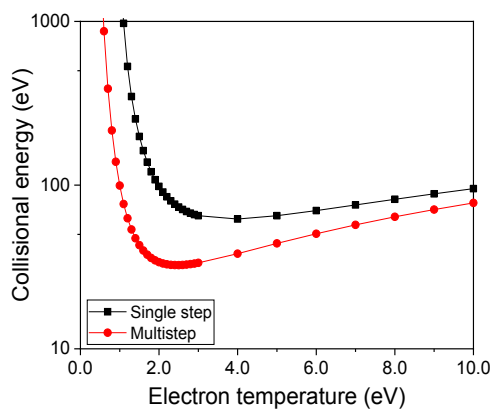


Figure 1: Collisional energy for single and multistep ionization.

ACKNOWLEDGMENTS

Júlia Karnopp thanks Coordenação de Aperfeiçoamento de Pessoal de Nível Superior (CAPES) for the scholarship.

REFERENCES

1. Samukawa S, Hori M, Rauf S, Tachibana K, Bruggeman P, Kroesen G, et al. The 2012 Plasma Roadmap. *Phys D Appl Phys.* 2012;45(25):253001. <https://doi.org/10.1088/0022-3727/45/25/253001>
2. Alves LL, Bogaerts A, Guerra V, Turner MM. Foundations of modelling of nonequilibrium low-temperature plasmas. *Plasma Sources Sci Technol.* 2018;27:023002. <https://doi.org/10.1088/1361-6595/aaa86d>



Microestrutura de filmes $Ti(1-x)Al(x)N$ obtidos no modo metálico e no modo composto via *magnetron sputtering*

Abel André Cândido Recco^{1,*} 




1. Universidade do Estado de Santa Catarina – cidade (SC), Brasil.

*Autor correspondente: abel.recco@udesc.br

O $Ti(1-x)Al(x)N$ corresponde a um sistema ternário, metaestável e policristalino. Entre as técnicas para obtenção desse composto, a deposição física a vapor via *magnetron sputtering* tem sido amplamente utilizada. Nessa técnica, os filmes podem ser obtidos por meio de dois modos de deposição bem definidos: metálico e composto. O presente trabalho propôs investigar a microestrutura formada nos filmes depositados nos modos metálico e composto de $Ti(1-x)Al(x)N$ depositados sobre silício. Observou-se que o crescimento do filme está diretamente relacionado às energias da superfície e de deformação, e a predominância de uma ou de outra energia é determinante na formação da microestrutura dos revestimentos e na orientação cristalográfica.



Mechanical spectroscopy of hot-rolled Ti-Zr-Mo-Ag alloys

Renata Carolina Araujo de Camargo^{1,*} , Diego R. N. Correa^{1,3} , Jhulienne Elen Torrento² , Carlos Roberto Grandini^{2,3} 

1. Instituto Federal de Educação, Ciência e Tecnologia de São Paulo - Research Group on Advanced Metallic Materials – Sorocaba (SP), Brazil.

2. Universidade Estadual Paulista “Júlio de Mesquita Filho” - Laboratory of Anelasticity and Biomaterials – Bauru (SP), Brazil.

3. Instituto Brasileiro de Terapia Neural - Institute of Biomaterials, Tribocorrosion, and Nanomedicine – Bauru (SP), Brazil.

*Correspondence author: renata.araujo@aluno.ifsp.edu.br

INTRODUCTION

The Ti-15Zr system alloys, with different amounts of Mo, have recently been developed for biomedical applications, combining low elastic modulus and non-toxic or allergenic composition^{1,2}. In this sense, its body-centered cubic (bcc) structure, combined with its solid solution with Zr and Mo atoms, may favor the occurrence of internal friction peaks associated with metallic matrix interactions with eventual punctual defects, such as oxygen and nitrogen. However, the addition of other alloying elements, such as Ag, can significantly impact the diffusion mechanisms of interstitials. Therefore, the aim of this study was to investigate the anelastic properties of the Ti-15Zr-Mo sample with small amounts of Ag by mechanical spectroscopy measurements.

EXPERIMENTAL

For the study, the Ti-15Zr-15Mo-(1,3)Ag (wt%) samples were obtained by argon arc-melting, and a stress relief treatment process was carried out, followed by a hot-rolling, at 1,273 K, with air cooling. The crystalline structure was analyzed by X-ray diffraction measurements (Rigaku equipment D/Max 2100PC, CuK α radiation). The measurements of mechanical spectroscopy were obtained in a dynamo-mechanical analyzer (DMA50 from Metravib), in the tensile mode, with oscillatory frequency around 1 and 40 Hz, heating rate of 1 K per min, from room temperature until 700 K. The internal friction results were analyzed through the OriginLab 8.0 software. Firstly, the curves were submitted to a smoothing process. Then, the background contribution was subtracted by using an exponential simulated curve. The peak fitting was performed from the simulation of multiple peaks following some previous studies in literature. The simulated peaks were later related with the corresponding relaxation processes of interstitial elements.

RESULTS AND DISCUSSION

The measurement of the internal friction and elastic modulus as a function of temperature at 1 Hz, between 300 and 700 K, for the Ti-15Zr-15Mo sample is shown in Fig. 1. The sample showed an asymmetric peak in the range of 450 and 600 K, which could be related to the stress-induced reordering of oxygen in the metallic matrix. The elastic modulus showed values below 100 GPa, evidencing its potential for use in the biomedical field. The decayment in the elastic modulus value as a function of temperature is related to the weakening of the metallic bonding in the sample. Similar results were obtained for the samples with the addition of 1Ag and 3Ag, but with distinct peak asymmetry, showing that the alloying elements acted in the anelastic relaxation processes.

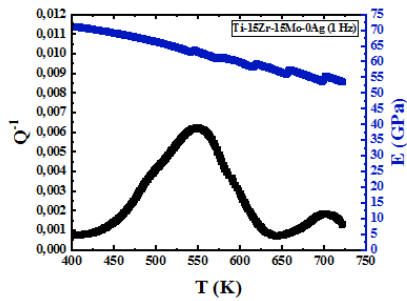


Figure 1: Internal friction and elastic modulus as a function of temperature for the Ti-15Zr-15Mo (% wt) sample, at 1 Hz, after the background removing.

ACKNOWLEDGMENTS

The study was funded by the National Council for Scientific and Technological Development (CNPq).

REFERENCES

1. Correa DRN, Rocha LA, Donato TAG, Sousa KSJ, Grandini CR, Afonso CRM, et al. On the mechanical biocompatibility of Ti-15Zr-based alloys for potential use as load-bearing implants. *J Mater Res Technol.* 2020;9(2):1241-50. <https://doi.org/10.1016/j.jmrt.2019.11.051>
2. Correa DRN, Rocha LA, Grandini CR. Mechanical Spectroscopy of Ti-15Zr-based Alloys with Mo Addition. *Mater Res.* 2017;20(Suppl. 2):688-93. <https://doi.org/10.1590/1980-5373-MR-2017-0060>



Hallow cathode effect caused by sample-support arrangement on plasma immersion ion implantation of nickel aluminum bronze AMPCO M4

Bruna C. E. S. Kurelo¹ , Gelson B. de Souza¹ , Silvio Francisco Brunatto^{2,*} 

1. Universidade Estadual de Ponta Grossa - Department of Physics – Ponta Grossa (PR) Brazil

2. Universidade Federal do Paraná - Department of Mechanical Engineering – Curitiba (PR), Brazil.

*Corresponding author: brunatto@ufpr.br

In nickel aluminum bronze (NAB) alloys Cu is the primary element, Al is present on the order of 6 to 12,5 wt.%, and Fe and Ni are both present up to 7 wt.% each. In these alloys, solution treatment followed by aging allows finely dispersed Ni and Fe-enriched intermetallic phases to precipitate in the matrix as the kappa phases group, enhancing hardness and corrosion resistance in marine environments. Thus, the efficiency of plasma immersion ion implantation (PIII) process working both as a heat source for aging and as a nitrogen source, aiming the N-enrichment of the surface by implantation and diffusion, was evaluated by means of surface hardness. In this work, emphasis was given to a hollow cathode effect, dependent on the sample-support arrangement, that occurred and its effect on the sample surface hardness distribution.

Keywords: Nickel aluminum bronze, Plasma immersion ion implantation, Nitriding, Age-hardening.



ASTM CA6NM martensitic stainless steel plasma assisted hybrid heat-thermochemical treatment: first results for carbon-expanded austenite surfaces

Felipe Jedyn^{1*} , Rodrigo Perito Cardoso¹ , Silvio Francisco Brunatto¹ 

1. Universidade Federal do Paraná - Graduate Program of Mechanical Engineering - Plasma Assisted Manufacturing Technology & Powder Metallurgy Group - Department of Mechanical Engineering – Curitiba (PR), Brazil.

*Correspondence author: felipejedyn@ufpr.br

Keywords: High-hardenability steels, Hybrid treatments, Metastable austenite, Thermochemical treatments, Carbon-expanded austenite.

INTRODUCTION

Recently, an innovative hybrid treatment for high-hardenability steels involving low-temperature plasma nitriding in the metastable austenite field was developed^{1,2}, allowing to obtain a N-expanded austenite layer over a martensitic substrate bulk. The present work proposed, then, to show the evaluation of the feasibility of obtaining a C-expanded austenite layer through the development of a hybrid heat-thermochemical treatment comprising hardening and low-temperature plasma carburizing carried out on the high-hardenability ASTM CA6NM martensitic stainless steel (MSS).

EXPERIMENTAL

A 620°C tempered ASTM CA6NM MSS sample, as previously described in Toscano et al.², was plasma austenitized at 1,050°C inside the glow discharge chamber. After 45 min soaking time at the austenitizing temperature, the sample was cooled, under Ar + H₂ plasma, to the carburizing temperature of 400°C (above the martensite start temperature M_i), when CH₄ gas was introduced in the plasma, being the sample kept at this temperature during 4 h. So, the sample was carburized in the metastable austenite field of the studied steel, during the partially interrupted hardening treatment step.

The sample was characterized by X-ray diffraction (XRD) before and after the plasma treatment, while the chemically etched cross-section was analyzed by scanning electron microscopy (SEM).

RESULTS AND DISCUSSION

Figure 1 shows XRD patterns obtained for a treated (by this new hybrid treatment) and untreated (as-tempered) sample, confirming that a C-expanded austenite layer (see γ -phase peaks) was successfully produced at the surface of the CA6NM MSS substrate presenting typically tempered-martensite microstructure (see α' -phase peaks).

This result indicating the formation of a C-expanded austenite layer on the surface of the carburized substrate martensitic bulk is in agreement with the cross-section micrograph shown in Fig. 2. Although more detailed studies are necessary, these preliminary results point out that it is possible to obtain a C-expanded austenite layer in high hardenability steels by this hybrid treatment.

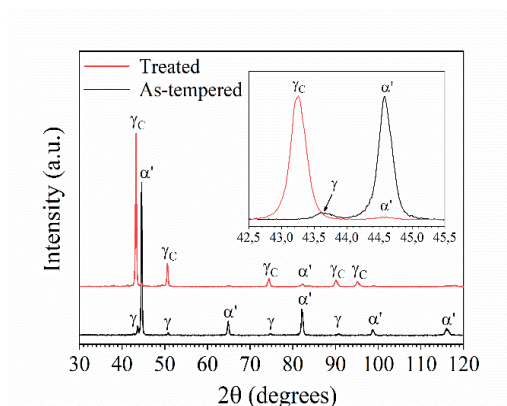


Figure 1: X-ray diffraction patterns for both as-tempered (untreated) and plasma carburized (treated) conditions.

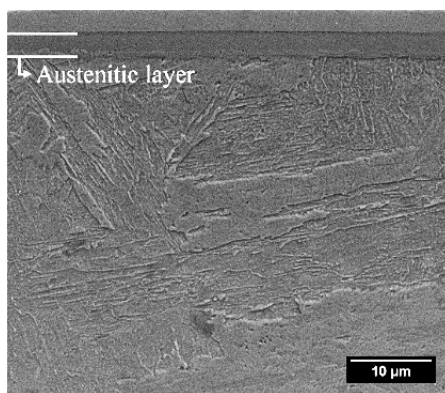


Figure 2: Cross-section scanning electron microscopy micrograph of the treated sample showing the austenitic layer and the substrate.

REFERENCES

1. Cardoso RP, Brunatto SF, Scheuer CJ, Zanetti FI, Zanella IG, Santos LL, et al. BR1020180150758 (INPI Patent Pending). Curitiba: UFPR; 2018.
2. Toscano TD, Cardoso RP, Brunatto SF. Steel Research Int. 2020;2000189.



Structure proposed to lead with data sensor based

Leandro Colevati dos Santos^{1,2,*} , Sebastião Gomes dos Santos Filho² , Maria Lúcia Pereira da Silva^{1,2} 

1. Faculdade de Tecnologia do Estado de São Paulo - Centro Paula Souza – São Paulo (SP), Brazil.

2. Universidade de São Paulo - School of Engineering – São Paulo (SP), Brazil.

*Correspondence author: leandro.colevati@usp.br

INTRODUCTION

The technology internet of things (IoT), in which elements such as sensor circuits or actuators are arranged as nodes in a large and interconnected network and exchanging data¹, is consolidated. In addition, intelligent and integrated devices, such as smartphones, offer a large number of sensor circuits. Natively, they are already nodes in a large network, since they are already designed connected in high-speed packet access (HSPA), long-term evolution (LTE) or wireless fidelity (WiFi) networks. Direct consequences of high availability of sensor devices are the high amount of data generated and the difficulties in storing, filtering, analyzing, and interpreting this data, besides the high latency established by conventional solutions². The objective of this work was to present a solution to the listed difficulties, establishing a low-cost computational structure and with reduced latency.

EXPERIMENTAL

This work presents a proof of concept of a thermal sensing system applied to a Fog computing structure. The objective was to monitor the temperature of an environment, the temperature of which cannot vary, to provide a structure in which connected computers or smartphones receive messages in case the temperature rises to undesirable levels. The experiment is a proof of concept in a Fog computing environment proposed in Santos et al.², including two new services in the structure.

RESULTS AND DISCUSSION

A matrix of thermal sensors was placed in a room whose temperature should be 18°C and cannot exceed 20°C. The matrix was connected to a WiFi network and had a unique identification.

The Fog computing structure offers a service that is directly connected to the sensor matrix, receiving its data, and storing it in the NoSQL database. The service provides a message if the temperature is above the established limit. The web scraping service, looking for a reliable source for the external temperature, is necessary because the average room temperature may need to be adjusted if the temperature outside is too high. The schematic representation is shown in Fig. 1. To validate that, the proposed environment is also efficient in this configuration, and an application connected to the Fog computing environment was developed to present the temperature variation in real time, as well as the external temperature. Figure 2 shows an application connected to the Fog computing environment. The proof of concept shows that the structure is consolidated, also to deal with a mass generating environment of data in real time, and provides a solution with quick response to immediate decision-making needs.

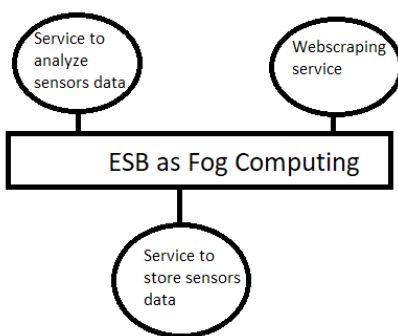


Figure 1: Fog computing structure.

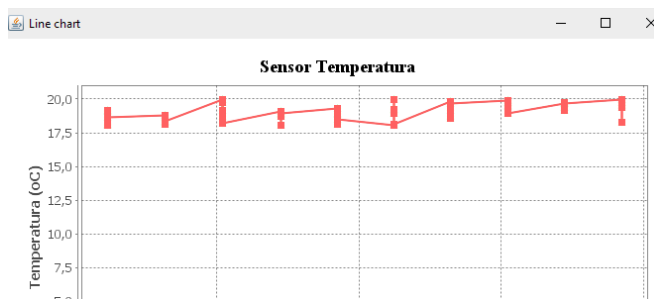


Figure 2: Third-party application consuming Fog computing service.

ACKNOWLEDGMENTS

Fundação de Amparo à Pesquisa do Estado de São Paulo (FAPESP) and Conselho Nacional de Desenvolvimento Científico e Tecnológico (CNPq) for financial support.

REFERENCES

1. Sehrawat D, Gill NS. Smart sensors: analysis of different types of IoT sensors. In: 3rd ICOEI. Proceedings. IEEE; 2019;523-8. <https://doi.org/10.1109/ICOEI.2019.8862778>
2. Soares RA, Santos LMF, Almeida TA, Medeiros JT. Características financeiras e emissão de gases de efeito estufa: uma análise das empresas brasileiras listadas na B3. In: XXI Engema. Proceedings. 2019;1-16.



On the polymerization processes of 2-metil-2-oxazoline plasma polymer (pp-oxazoline)

Pedro William Paiva Moreira Júnior^{1,*} , Felipe Vicente de Paula Kodaira¹ , Rogério Pinto Mota¹ 

1. Universidade Estadual Paulista “Júlio de Mesquita Filho” – Guaratinguetá (SP), Brazil.

*Correspondence author: pedro_kcond28@hotmail.com

INTRODUCTION

2-metil-2-oxazoline plasma polymers (pp-oxazoline) are known by its biocompatibility and functionalities, making them suitable for uses in the human body. As remarkable properties, they present non-fouling and pinhole-free surfaces that are friendly to appropriated proteins for human cells colonization¹. Furthermore, they are alternative polymers to polyethylene glycol (PEO) and polyethylene glycol (PEG). Besides holding the same biocompatibility of these materials, they are also more resistant to biological degradation². This new class of materials has been substantially investigated on the last decade, but the polymerization process is still poorly understood.

EXPERIMENTAL

In this work, pp-oxazoline films were deposited by plasma-enhanced chemical vapor deposition (PECVD) process under low pressure conditions in a standard stainless-steel reactor chamber with parallel plates electrode configuration. The discharges were performed at 80, 120, 160 and 200 mTorr of total pressure and excited by a radio frequency (RF) power supply operating at 13.56 MHz. The applied power ranged from 5 to 25 W.

In order to investigate the plasma polymerization process of pp-oxazoline, the 2-metil-2-oxazoline plasmas were monitored by optical emission spectroscopy by the actinometric method (A-OES), and the electrons temperature was acquired by a self-cleaning Langmuir probe. To analyze the plasma thin films, the techniques of water contact angle (WCA), atomic force microscopy (AFM), confocal microscopy (CM) and Fourier transformed infrared spectroscopy (FTIR) were employed.

RESULTS AND DISCUSSION

The electrons temperatures were observed between 0.2 and 0.4 eV. The electronic temperature behavior was analyzed as a function of operating pressure and applied power. This behavior was linked to production of CH, CN, CO, and NH in 2-methyl-2-oxazoline plasmas, as showed in Fig. 1. The mean roughness investigation, the bonds observed by FTIR technique, and the deposition rates revealed the role of these species on polymerization processes. There were no species in the plasma phase related to volatile compounds production. High deposition rates, decreasing of closed oxazoline rings amounts in plasma polymers and at least three kinds of oxygen bonds were observed, showing that the plasma polymerization process was able to perform the ring opening process and fragmentation of monomer molecules. These conclusions are also supported by integrated absorption calculus results, displayed in Fig. 2. The cross-link structures and number of polar groups on the plasma polymers surface were assigned to the thin films hydrophilic character. High concentrations of polar groups in 2-methyl-2-oxazoline plasma polymers were responsible to low contact angle values, around 10°.

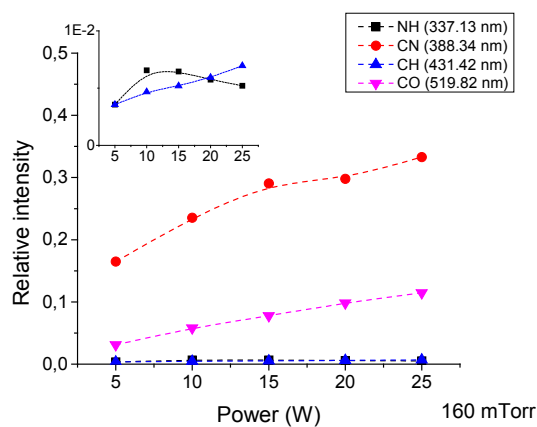


Figure 1: Actinometric method observed main plasma species evolution as a function of applied power.

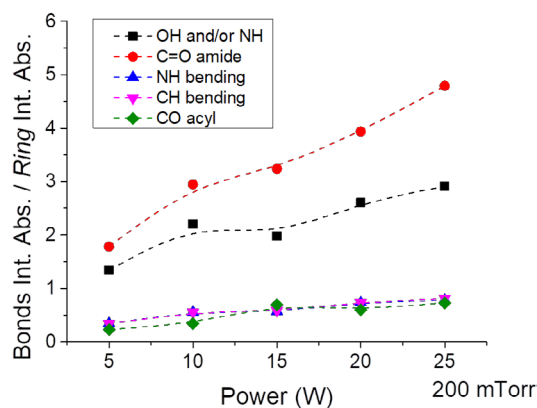


Figure 2: Main bounds integrated absorption (Fourier transformed infrared spectroscopy) divided by oxazoline ring skeletal vibration absorption.

REFERENCES

1. Xiang LN, Chen L-J, Tan L, Zhang C, Cao F-H, Liu S-T, et al. The preparation of a novel polydopamine-graft-poly(2-methyl-2-oxazoline) protein-resistant coating and its applications in protein separation. *Chin Chem Lett.* 2013;24(7):597-600. <https://doi.org/10.1016/j.ccllet.2013.04.001>
2. Ramiasa MN, Cavallaro AA, Mierczynska A, Christo SN, Gleadle JM, Hayball JD, et al. Plasma polymerised polyoxazoline thin films for biomedical applications. *Chem Commun.* 2015;51(20):4279-82. <https://doi.org/10.1039/C5CC00260E>



Cariogenic multispecies biofilms were inhibited by cold atmospheric plasma

Leandro Figueira¹, Maria Alcioneia Carvalho de Oliveira¹ , Marcia Hiromi Tanaka¹ , Thalita Mayumi Castadelli Nishime² , Konstantin Kostov³ , Cristiane Koga-Ito¹ 

1. Universidade Estadual Paulista “Júlio de Mesquita Filho” - Institute of Science and Technology - Department of Environmental Engineering/Oral Biopathology Graduate Program – São José dos Campos (SP), Brazil.

2. Leibniz Institute of Plasma Science and Technology – Greifswald, Germany.

3. Universidade Estadual Paulista “Júlio de Mesquita Filho” - Faculdade de Engenharia de Guaratinguetá - Department of Physics – Guaratinguetá (SP), Brazil.

*Correspondence author: cristiane.koga-ito@unesp.br

INTRODUCTION

Caries disease may lead to dental loss and might significantly affect the systemic health, impairing the quality of life¹. In this sense, less invasive methods for caries treatment have been studied to avoid unnecessary loss of dental tissue². Focusing on it, low temperature plasma at atmospheric pressure (LTAPP) has shown effective results for biological applications due to its characteristic of operating close to room temperature³. With this in mind, the hypothesis is that LTAPP might be an effective and non-invasive tool for the disinfection of carious cavities previous to restoration procedures⁴. However, the aim of this study was to evaluate the application of LTAPP in the control of multispecies cariogenic biofilms.

EXPERIMENTAL

The effective parameters of LTAPP against polymicrobial biofilms composed by *Streptococcus gordonii*, *Streptococcus mutans* and *Streptococcus sanguinis* were established. The microorganisms were activated in blood agar and incubated at 37°C for 48 h, 5% CO₂. Standardized suspensions were prepared (10⁷ cells/mL) using a spectrophotometer. These suspensions were diluted to 8 × 10⁶ cells/mL. Equal volumes of standardized suspensions were mixed up. Aliquots of 40 µL of the multi-species inoculum and 160 µL of tryptic soy broth (TSB) supplemented with 1% sucrose were added to the wells of microdilution plates. Plates were incubated (37°C, 5% CO₂, 48 h). After 24 h, the biofilm was washed with sterile saline, and the culture medium was refreshed. Subsequently, multispecies biofilms were exposed to LTAPP and chlorhexidine digluconate (0.12%) for 1, 3, 5 and 7 min. The number of viable cells was determined by plating method. LTAPP was generated in helium gas (99.5% purity, 2.0 SLM flow rate) using electric discharge (32 kHz signal frequency, 1.0 W mean power). Non-exposed control was included.

RESULTS AND DISCUSSION

Data of percentage of reduction was analyzed by variance analysis (ANOVA). Reductions (%) in total viable cells counts (86.0±20.0, 79.0±26.0, 87.0±21.0 and 82.0±19.0) were observed after exposure for 1, 3, 5 and 7 min with LTAPP. A previous study that treated a dual-species biofilm formed by *S. mutans* and *S. sanguinis* formed in polystyrene plates with atmospheric non-thermal argon/oxygen plasma for 120 seconds observed reduction of 99% in the quantity of viable cells when compared to the negative control⁵. This outcome corroborates with our results, that showed significant reduction in the viability of a multispecies biofilm formed by *S. mutans*, *S. gordonii* and *S. sanguinis* when treated with LTAPP. Additionally, treatment with chlorhexidine provided significant reductions

(94.0±15, 99.0±14, 99.0±13.0 and 99.0±14.0) after treatment for 1, 3, 5 and 7 min, respectively. Both LTAPP and chlorhexidine showed significant inhibitory effect on these cariogenic multispecies biofilms.

ACKNOWLEDGMENTS

Funding by Fundação de Amparo à Pesquisa do Estado de São Paulo (FAPESP) 2019/05856-7, 18/17707-3 and Conselho Nacional de Desenvolvimento Científico e Tecnológico (CNPq) (308127/2018-8). This study was financed in part by the Coordenação de Aperfeiçoamento de Pessoal de Nível Superior – Brasil (CAPES) – Finance Code 001.

REFERENCES

1. Marceles W, Kassebaum NJ, Bernabé E, Flaxman A, Naghavi M, Lopez A, et al. Global burden of oral conditions in 1990-2010: a systematic analysis. *J Dent Res.* 2013;92(7):592-7. <https://doi.org/10.1177/0022034513490168>
2. Mackenzie L, Banerjee A. Minimally invasive direct restorations: a practical guide. *Br Dent J.* 2017;223(3):163-71. <https://doi.org/10.1038/sj.bdj.2017.661>
3. McCombs GB, Darby ML. New discoveries and directions for medical, dental and dental hygiene research: low temperature atmospheric pressure plasma. *J Dent Hyg.* 2010;8(1):10-5. <https://doi.org/10.1111/j.1601-5037.2009.00386.x>
4. Sladek REJ, Stoffels E, Walraven R, Tiebeek PJA, Koolhoven RA. Plasma treatment of dental cavities: a feasibility study. *IEEE Trans Plasma Sci.* 2004;32(4):1540-3. <https://doi.org/10.1109/TPS.2004.832636>
5. Liu T, Wu L, Babu JP, Hottel TL, Garcia-Godoy F, Hong L. Effects of atmospheric non-thermal argon/oxygen plasma on biofilm viability and hydrophobicity of oral bacteria. *Am J Dent.* 2017;30(1):52-6.



Cold atmospheric plasma inhibits *Escherichia coli* biofilms formed on PVC specimens

Ellen Rodrigues de Souza Reis¹, Konstantin Georgiev Kostov² , Cristiane Yumi Koga Ito^{1,*} 

1. Universidade Estadual Paulista “Júlio de Mesquita Filho” - Instituto de Ciência e Tecnologia – São José dos Campos (SP), Brazil.

2. Universidade Estadual Paulista “Júlio de Mesquita Filho” - Faculdade de Física – Guaratinguetá (SP), Brazil.

*Correspondence author: cristiane.koga-ito@unesp.br

The ability of *Escherichia coli* to remain in biofilms allows bacteria to protect against environmental stresses and also to chemical agents. Such formation makes it difficult to contain these pathogens in water distribution systems. Studies linked to the use of cold atmospheric plasma (CAP) in the environmental area have shown many advantages. Its technology is considered green, as it does not produce residues toxic to the biotic factors of ecosystems, and its observed antimicrobial effects make plasma an interesting option in pipe and effluent treatments.

The aim of this study, therefore, was to evaluate the effects of CAP treatment on *E. coli* biofilms formed on polyvinyl chloride (PVC) in nutrient depleted medium. *E. coli* biofilms were then incubated for three days at 24°C, on PVC fragments, in a minimum medium of nutrients, and treated with CAP for 5 or 7.5 min. The effects of the treatments were evaluated by counting CFU/mL with statistical analysis performed by analysis of variance (ANOVA) and Dunnett’s tests, with the significance level of 5%. The results showed that *E. coli* was able to develop biofilms on PVC in conditions with nutrient depletion, during the incubation period, and that CAP had a significant effect ($p < 0.05$) on the reduction of biofilms at all times used for treatments.

In view of this, CAP technology has shown promising effects providing data for future investigations in the search for its use in disinfecting pipes, an important step for the distribution of quality water.

Keywords: *Escherichia coli*, Biofilms, Cold atmospheric plasma.

Chemical and mechanical characterization of Ti-25Ta-70Zr Alloy

Edriely de Oliveira Saraiva^{1,*} , Pedro Akira Bazaglia Kuroda¹ , Carlos Roberto Grandini¹

1. Universidade Estadual Paulista “Júlio de Mesquita Filho” - Laboratório de Anelasticidade e Biomateriais – Bauru (SP), Brazil.

*Corresponding author: edriely.oliveira@unesp.br

INTRODUCTION

Titanium is an element widely used in biomedical applications due to its reasonable physical, chemical, and biological properties¹. It has two crystalline structures. It is more stable in the compact hexagonal crystalline structure, phase known as α , for temperatures above 882°C, its turn to the body-centered cubic crystalline structure, phase β . With the addition of elements, it is possible to change the allotropic transformation temperature to modify the phases' volume fractions as desired. Tantalum added to titanium is excellent for biocompatibility and stabilizes the β phase. Zirconium assists in biocompatibility, and it is a β stabilizer in the presence of another β -stabilizing element. Studies in the literature show that alloys with predominance of β phase have more excellent mechanical compatibility with human bone². In this work, chemical, structural, and microstructural characterization of Ti-25Ta-70Zr alloy is presented.

EXPERIMENTAL

The ingot was obtained using an arc-melting furnace. Already melted, it was subjected to heat treatment in a vacuum to relieve residual melt stresses. The alloy was also hot rolled. For chemical analysis, energy-dispersive X-ray spectroscopy (EDS) and density measurements were made. The structural characterization of the alloy was performed using the X-ray diffraction technique. The microstructural characterization was performed in an optical and a scanning electron microscope. Microhardness measurements were also made.

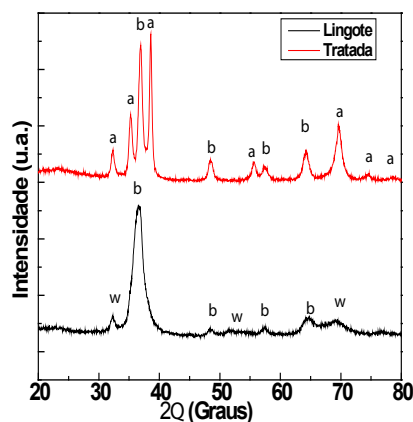


Figure 1: X-ray diffraction measurements for Ti-25Ta-70Zr alloys.

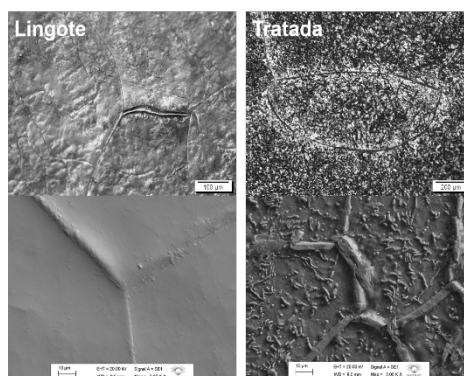


Figure 2: Optical and scanning electron microscope measurements for Ti-25Ta-70Zr alloys.

RESULTS AND DISCUSSION

The chemical composition results (EDS and density) showed that the produced alloy has excellent quality and stoichiometry. The structural characterization shows peaks of the ω and β phases to the alloy after melting. The heat treatment inhibited the ω phase and promoted the formation of the α phase. The micrographs showed microstructures formed by grains in both conditions (characteristic of β phase). It is possible to observe small intra-grain needles in the alloy after heat treatment, characterized by the α phase. The microhardness results showed that as-cast alloy has a hardness value of approximately 500 HV due to the existence of the ω phase. However, after the heat treatment, the ω phase was suppressed, reducing the hardness value to 272 HV.

ACKNOWLEDGMENTS

The authors thank Conselho Nacional de Desenvolvimento Científico e Tecnológico (CNPq)/Programa Institucional de Bolsas de Iniciação Científica (PIBIC) and Fundação de Amparo à Pesquisa do Estado de São Paulo (FAPESP) for financial support.

REFERENCES

1. Kuroda PAB, Buzalaf MAR, Grandini CR. Effect of molybdenum on structure, microstructure and mechanical properties of biomedical Ti-20Zr-Mo alloys. *Mater Sci Eng C*. 2016;67:511-5. <https://doi.org/10.1016/j.msec.2016.05.053>
2. Ho WF, Wu S-C, Hsu S-K, Li Y-C, Hsu H-C. Effects of molybdenum content on the structure and mechanical properties of as-cast Ti-10Zr-based alloys for biomedical applications. *Mater Sci Eng C*. 2012;32(3):517-22. <https://doi.org/10.1016/j.msec.2011.12.003>

Preparation and characterization of Ti-10Mo-5Mn-1Ag

Melissa Daniela de Almeida Nespeque^{1,*} , Mariana Luna Lourenço¹ , Carlos Roberto Grandini¹

1. Universidade Estadual Paulista “Júlio de Mesquita Filho” - Laboratório de Anelasticidade e Biomateriais – Bauru (SP), Brazil.

*Corresponding author: m.nespeque@unesp.br

INTRODUCTION

Over the years, titanium alloys have shown a desirable performance in the application as biomaterial¹. However, this raises a problem regarding the infections caused by the implant and the subsequent postoperative outcomes. In order to solve this, adding silver to the alloy can minimize these inconveniences. Silver is an element with potent antibacterial properties and improves the alloy's mechanical properties and corrosion resistance to be used as a biomaterial². After a theoretical study involving the molecular orbital Dv-xa theory, the Ti-10Mo-5Mn (wt%) alloy was prepared by arc melting and characterized chemically, structurally, microstructurally, and mechanically³. Furthermore, the same theoretical study and experimental procedure were done, adding 1.0 wt% of silver.

EXPERIMENTAL

The theoretical studies for the Ti-10Mo-5Mn-Ag alloys were made by varying the silver percentage from 0 to 2.0 wt% and obtaining the electronic parameters Md and Bo to predict silver's influence in alloy's microstructure. To prepare the Ti-10Mo-5Mn and Ti-10Mo-5Mn-1Ag ingots, both with 60 g of material in total, each element respected the stipulated proportions. The materials were then pickled and melted in an arc-melting furnace, with an argon atmosphere, to avoid contamination. After the melting, the ingots were subjected to chemical, structural (through X-ray diffraction measurements), and microstructural (by optical and scanning electron microscopy measurements) analysis.

RESULTS AND DISCUSSION

The percentages of silver analyzed indicated that the alloy's microstructure did not significantly change, with the β phase being predominant. Through the ingots' images, a good melting of the material is observed, as it keeps its silver and shiny appearance. The energy-dispersive X-ray spectroscopy (EDS) analysis showed that there was no contamination of other elements. Future characterizations will be done to conclude the microstructure of the alloy with silver.

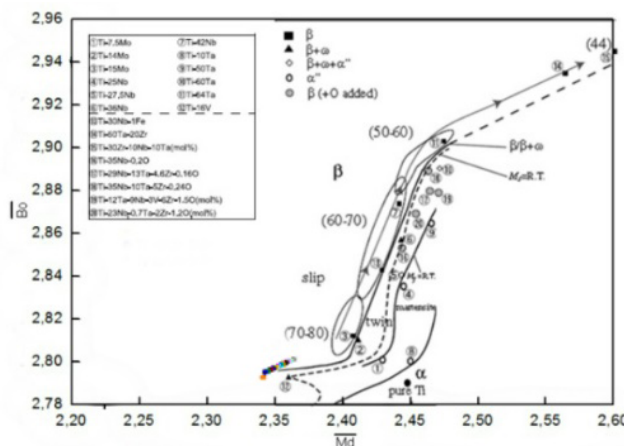


Figure 1: Md-Bo diagram for Ti-10Mo-5Mn-Ag alloys.

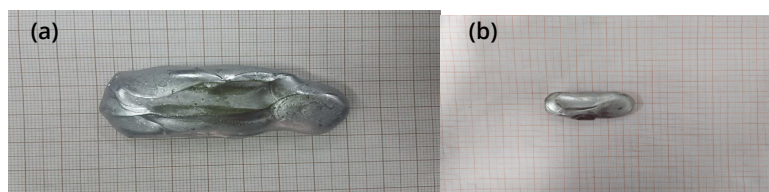


Figure 2: Ingots after melting: (a) Ti-10Mo-5Mn; (b) Ti-10Mo-5Mn-1Ag.

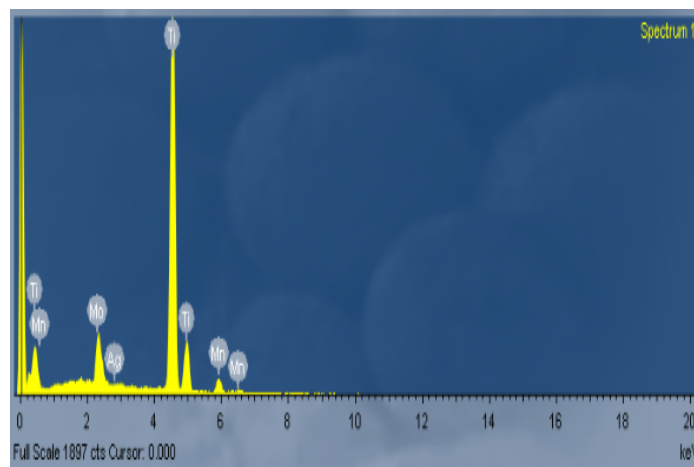


Figure 3: Energy-dispersive X-ray spectroscopy (EDS) analysis for Ti-10Mo-5Mn-1Ag alloy.

ACKNOWLEDGMENTS

The authors thank Coordenação de Aperfeiçoamento de Pessoal de Nível Superior (CAPES), Conselho Nacional de Desenvolvimento Científico e Tecnológico (CNPq), and Fundação de Amparo à Pesquisa do Estado de São Paulo (FAPESP) for financial support.

REFERENCES

1. Semiatin SL. An Overview of the Thermomechanical Processing of α/β Titanium Alloys: Current Status and Future Research Opportunities. *Met Mat Trans A*. 2020;51(5):2593-625. <https://doi.org/10.1007/s11661-020-05625-3>
2. Szaraniec B, Goryczka T. Structure and properties of Ti-Ag alloys produced by powder metallurgy. *J Alloys Compd*. 2017;709:464-72. <https://doi.org/10.1016/j.jallcom.2017.03.155>
3. Lourenço ML, Cardoso GC, Sousa KSJ, Donato TAG, Pontes FML, Grandini CR. Development of novel Ti-Mo-Mn alloys for biomedical applications. *Sci Rep*. 2020;10:6298. <https://doi.org/10.1038/s41598-020-62865-4>



Development of Ti-, Mo- and Zr-based alloy for biomedical applications

Israel Ramos Rodrigues^{1,2,*} , Renan Eduardo de Lima Lopes^{1,2} , Carlos Roberto Grandini^{1,2*} 

1. Universidade Estadual Paulista “Júlio de Mesquita Filho” - Laboratório de Anelasticidade e Biomateriais – Bauru (SP), Brazil.
2. Institute of Biomaterials, Tribocorrosion and Nanomedicine – Bauru (SP), Brazil.

*Corresponding author: betog@fc.unesp.br

INTRODUCTION

Ti is one of the most used metals as a manufacturing element for orthopedic implants¹. This element has interesting aspects, as excellent mechanical and biological properties, and it is interesting for biomedical applications. Ti, as a pure element, has dimorphism, that is, a compact hexagonal structure, alpha phase. It is stable until 862°C and for temperatures above it, it reveals a body-centered cubic structure, beta phase. Mo makes part of an element set, called β stabilizers. These elements, when mixed with Ti, reduce the transition temperature from α to β phase. Previous studies have argued that the concentration of Mo above 10% in weight has a β phase structure². Zr, when inserted in the alloy, increases the corrosion resistance, and decreases the melting point, and improves the biocompatibility of the alloy. In the presence of another β -stabilizer element, it also helps to stabilize the β phase. The alloys with the predominance of the β phase are the most desirable for biomedical applications due to their higher mechanical compatibility with the bone tissue³. This work presented the preparation and characterization of the Ti-10Mo-30Zr alloy aiming for biomedical applications.

EXPERIMENTAL

The ingots were prepared by arc-melting, and a homogenization heat treatment was made for 24 h at 1,000°C in a vacuum of 10⁻⁶ Torr and cooled at a rate of 10°C/min. The homogenized ingots were hot rolled at 1,000°C to obtain a regular format for future analyses. The samples were subject to density measurements and energy dispersive spectrometry (EDS). The samples were characterized by X-ray diffraction (XRD), optical microscope (OM), scanning electron microscope (SEM), Vickers microhardness, and elasticity modulus.

RESULTS AND DISCUSSION

The alloys' density values were higher than that of pure titanium, due to the addition of Zr and Mo. In XRD measurements, only peaks characteristics of the β phase were observed. In the OM and SEM micrographs, the grains are characteristic of the β phase. The EDS measurements reveal a right stoichiometry of the elements and no impurities contamination, which means that the alloy system agrees with the literature in the presence of β phase structure, even changing the Zr element concentration. Regarding microhardness, there was increase concerning pure titanium due to hardening of solid solution, and the modulus of elasticity was lower compared to the Ti-6Al-4V alloy already used as a biomaterial.



ACKNOWLEDGMENTS

The authors thank Coordenação de Aperfeiçoamento de Pessoal de Nível Superior (CAPES), Conselho Nacional de Desenvolvimento Científico e Tecnológico (CNPq) and Fundação de Amparo à Pesquisa do Estado de São Paulo (FAPESP) for financial support.

REFERENCES

1. Leyens C, Peters, M. Titanium and titanium alloys: fundamentals and applications. Weinheim: Wiley-VHC.; 2003.
2. Ho WF, et al. *J Mater Sci Mater Med.* 2012;19:3179-86.
3. Correa DRN, Kuroda PAB, Lourenço ML, Buzalaf MAR, Mendoza ME, Archanjo BS, et al. Microstructure and selected mechanical properties of aged Ti-15Zr-based alloys for biomedical applications. *Mat Sci Eng C.* 2018;91:762-71. <https://doi.org/10.1016/j.msec.2018.06.017>

Structural and microstructural characterization of the Ti-10Mo-40Zr alloy

Renan Eduardo de Lima Lopes^{1,2,*} , Israel Ramos Rodrigues^{1,2} , Carlos Roberto Grandini^{1,2} 

1. Universidade Estadual Paulista “Júlio de Mesquita Filho” - Laboratório de Anelasticidade e Biomateriais – Bauru (SP), Brazil.

2. Institute of Biomaterials, Tribocorrosion and Nanomedicine – Bauru (SP), Brazil.

*Corresponding author: renan.lopes@unesp.br

INTRODUCTION

Titanium is one of the most used biomedical applications elements due to its higher corrosion resistance and low specific mass, having particular application in hip replacement. Titanium has a crystalline structure called compact hexagonal (α phase). At 882°C, it goes through a transformation, with its structure changing from compact hexagonal to body-centered cubic (β phase). Molybdenum is a β stabilizer element. In other words, it helps to lower the temperature of the transition to the β phase. Zirconium is a neutral element. However, it has higher corrosion resistance. This work presented the preparation and characterization of the Ti-10Mo-40Zr alloy aiming for biomedical applications.

EXPERIMENTAL

The ingots were obtained through an arc-melting furnace. A homogenization heat treatment was made for 24 h at 1,000°C in a vacuum of 10⁻⁶ Torr and cooled at a rate of 10°C/min. The homogenized ingots were hot rolled at 1,000°C to obtain a regular format for future analyses. Chemically, the samples were characterized through density measurements using Archimedes principle and energy dispersive X-ray spectroscopy (EDS). The Ti-10Mo-40Zr sample was submitted to structural characterization through X-ray diffraction (XRD) and microstructural characterization through a scanning electron microscope (SEM). Mechanical properties were obtained by microhardness and elasticity modulus measurements.

RESULTS AND DISCUSSION

After melting, the ingot presented silver color, showing that the ingot was not contaminated with impurities. The alloy's density was 5,71 g/cm³, higher than pure titanium, due to the addition of heavy elements like zirconium and molybdenum. The X-ray diffraction (Fig. 1) shows only the peaks associated with the β phase, with a body-centered cubic crystalline structure. SEM results (Fig. 2) show high presence of the β phase, corroborating XRD measurements.

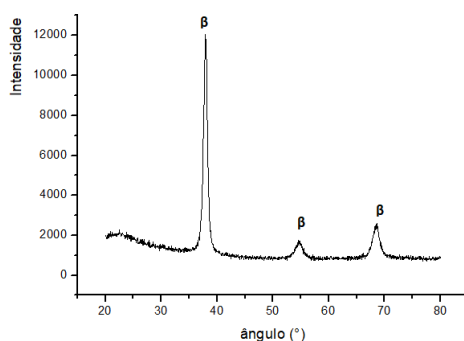


Figure 1: X-ray diffraction for Ti-10Mo-40Zr alloy.

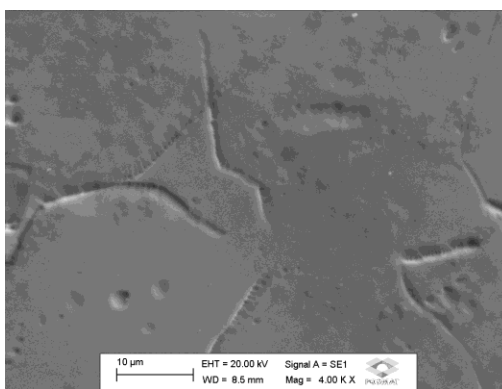


Figure 2: Scanning electron microscope micrograph for Ti-10Mo-40Zr alloy.

Regarding the EDS measurements, only the precursor elements were observed, showing that the proposed stoichiometry was respected and that the alloy was not contaminated. Results show that this alloy is a candidate for biomedical applications, needing future analyses of biological, chemical, and mechanical properties.

ACKNOWLEDGMENTS

The authors thank Coordenação de Aperfeiçoamento de Pessoal de Nível Superior (CAPES), Conselho Nacional de Desenvolvimento Científico e Tecnológico (CNPq) and Fundação de Amparo à Pesquisa do Estado de São Paulo (FAPESP) for financial support.

REFERENCES

1. Kuroda PAB, Buzalaf MAR, Grandini CR. Effect of molybdenum on structure, microstructure and mechanical properties of biomedical Ti-20Zr-Mo alloys. *Mater Sci Eng C*. 2016;67:511-5. <https://doi.org/10.1016/j.msec.2016.05.053>
2. Ho WF, Wu S-C, Hsu S-K, Li Y-C, Hsu H-C. Effects of molybdenum content on the structure and mechanical properties of as-cast Ti-10Zr-based alloys for biomedical applications. *Mater Sci Eng C*. 2012;32(3):517-22. <https://doi.org/10.1016/j.msec.2011.12.003>



Failure analysis of stiffened composite panels obtained by different adhesively bonding techniques and submitted to axial compression tests

Rita de Cássia Mendonça Sales^{1,2,*} , Geraldo Maurício Cândido¹, Maurício Vicente Donadon¹ 

1. Instituto Tecnológico de Aeronáutica - Divisão de Engenharia Aeronáutica – São José dos Campos (SP), Brazil.

2. Faculdade de Tecnologia de São José dos Campos Professor Jessen Vidal – São José dos Campos (SP), Brazil.

*Correspondence author: rita.sales@fatec.sp.gov.br

INTRODUCTION

Stiffened composite panels manufactured by adhesive bonding technology are increasingly being used in aerospace applications due to their enhanced mechanical performance with reduced number of parts in comparison with conventional riveted panels. An adequate design philosophy is desired to exploit the advantages of these panels moving from a conservative safe life to a damage tolerant philosophy allowing a damage existence in the structure in a non-critical condition¹. However, in order to benefit from a damage tolerant design philosophy, the damage growth must be well understood and predicted, to ensure that a critical damage size is never detected between inspections². Therefore, the aims of this work were to identify and to compare the compression failure modes of composite stiffened panels obtained by co-bonding and secondary bonding techniques after the post-buckling fatigue tests and the residual strength tests.

EXPERIMENTAL

The material used to manufacture the stiffened panels were a unidirectional carbon fiber and epoxy resin: T800/3900-2 (Toray®). An epoxy adhesive film EA 9695 (Loctite®) was used to bond stiffener and skin. The panels were loaded in compression using a testing frame with a hydraulic actuator with load capacity of 50 kN. All panels were subjected to fatigue tests up to 3.10^5 cycles. After the fatigue tests, the panels were subjected to a quasi-static compression load to analyze the residual strength. At last, the panels were visually inspected, and the failure modes were identified and compared. Images of regions with failure were taken using a Nikon D3100 camera equipped with 18-55 mm lenses.

RESULTS AND DISCUSSION

After the residual strength tests, failures were observed at skin, stiffener and skin-stiffener interface in the panels tested. The failures occurred at CB panel were in-plane shear (PS) followed by through the thickness shear (TS) at skin, and wedge splitting (WS) and longitudinal cracking (LC) at stiffener (Fig. 1). During the catastrophic failure in SB panels (Fig. 2), compression failure modes were observed at skin region were PS followed by TS, and delamination buckling (DB) at stiffener³. In both panels, a failure mechanism named fiber bridging was also observed in two regions: between the stiffener layers named SFB and at adhesive region named AFB. Changes at stiffness were noticed in both panels, but a second change was verified at SB panel during the axial compression tests. These changes were caused by the manufacturing process, as the SB panel underwent two curing processes, due adhesive film, which increases crosslinks and, consequently, stiffens the material.



Figure 1: Failure modes observed at CB panel after catastrophic failure.

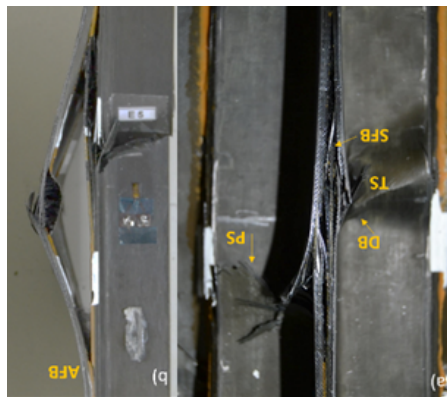


Figure 2: Failure modes observed at SB panel after catastrophic failure.

ACKNOWLEDGMENTS

Conselho Nacional de Desenvolvimento Científico e Tecnológico (CNPq) (Proc. 301069/2019-0), Coordenação de Aperfeiçoamento de Pessoal de Nível Superior (CAPES) (Proc. 88887.360818/2019-00) and Instituto Tecnológico de Aeronáutica (ITA).

REFERENCES

1. Mouritz AP. Introduction to aerospace materials. Woodhead; 2012.
2. Federal Aviation Administration. Aging Airplane Program: widespread fatigue damage. Federal United States: Aviation Administration; 2010.
3. Opelt CV, Cândido GM, Rezende MC. Compressive failure of fiber reinforced polymer composites: a fractographic study of the compression failure modes. Mater Today Commun. 2018;15:218-27. <https://doi.org/10.1016/j.mtcomm.2018.03.012>



Physical-chemical characterization of poly(methyloctadecylsiloxane) immobilized on titanized silica as a sorbent for solid-phase extraction

José Matheus Cardoso Santa Brígida¹, Carla Grazieli Azevedo da Silva^{1,*} 

¹.Universidade Federal de Mato Grosso (UFMT) - Department of Chemistry – Cuiabá (MT), Brazil.

*Correspondence author: carlag@live.com

INTRODUCTION

In the sample preparation of complex environmental aqueous matrices, for the determination of organic pollutants, as pesticides, the step of eliminating interferents that may compromise the quality and reliability of the analytical results due to the matrix effect is very important. Among the several techniques for solving problems related to the matrix effect in the extraction of complex samples, solid phase extraction (SPE) is the most used technique, due to its low consumption of organic solvents, complying with the principles of green chemistry, and the possibility to enhancing the concentrations of analytes to posterior instrumental analysis by gas or liquid chromatography (GC or LC)¹. SPE uses similar solid sorbent materials as in the stationary phases of LC, which have the function of extracting the analytes of interest from the matrices, being those based on silica modified with alkyl groups like C-18 or C-8².

EXPERIMENTAL

The preparation of the SPE materials were performed from the metallization of the chromatographic silica surface (particle diameter: 100 μm) with titanium (IV) butoxide. After, the poly(methyloctadecylsiloxane) (PMODS) was immobilized by thermal treatment, in an oven, in two experimental conditions: 100°C for 17.36h and 120°C for 16h. Afterwards, the materials were characterized by Fourier transform infrared (FTIR) spectroscopy using a KBr tablet (1% w/w) in the spectral range from 4,500 to 400 cm^{-1} and by the scanning electron microscopy (SEM) at different magnifications.

RESULTS AND DISCUSSION

The FTIR spectra of the sorbent materials (Fig. 1) showed absorption bands around 2,930 and 2,850 cm^{-1} , characteristics of aliphatic carbon³, and thus showing the presence of PMODS in the sorbent materials obtained at 100°C for 17.36 h and at 120°C for 16h, when compared to the spectra of the Ti metalized silica support (spectrum not shown). The SEM images indicated that the materials had irregular particle morphology with the mean size of 95 μm (Fig. 2a). The presence of PMODS coating the materials surface structure also could be observed by the SEM images, for the Si-Ti(PMODS) sorbent (Fig. 2b), showing a suitable hydrophobic layer coating for extracting pollutants, as the pesticides, from aqueous environmental samples, using the reversed phase separation mechanism.



Figure 1: Fourier transform infrared spectrum for solid phase extraction sorbent prepared at 120 °C for 12 h.

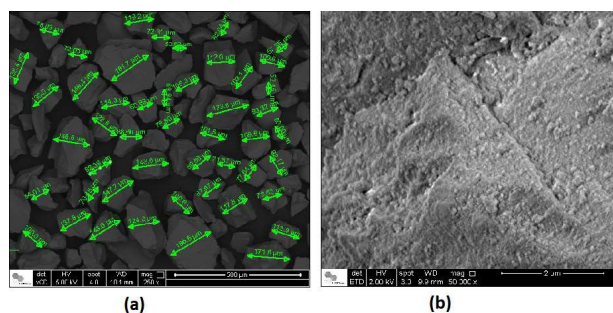


Figure 2: Scanning electron microscopy photomicrography: SiO₂ support using (a) the detection of the backscattered electrons at the magnification of 250× in and using (b) the detection of secondary electron at the magnification of 50,000× for Si-Ti(poly(methyloctadecylsiloxane)), both at 5 kV.

ACKNOWLEDGMENTS

The authors acknowledge Brazilian Nanotechnology National Laboratory and Fundação de Amparo à Pesquisa do Estado de Mato Grosso (FAPEMAT) for the research grant of José Matheus C. Santa Brígida.

REFERENCES

1. Jardim ICSF. Extração em fase sólida: fundamentos teóricos e novas estratégias para preparação de fases sólidas. *Scientia Chrom.* 2010;2(1):13-25.
2. Faria AM, Collins CH, Jardim ICSF. State-of-the-art in immobilized polymer stationary phases for high-performance liquid chromatography. *J Braz Chem Soc.* 2009;20(8):1385-98. <https://doi.org/10.1590/S0103-50532009000800002>
3. Faria AM, Collins KE, Collins CH. Enhanced stability stationary phases based on poly(methyltetradecylsiloxane) immobilized onto doubly titanized silica particles. *Chromatographia.* 2008;67(5-6):357-63. <https://doi.org/10.1365/s10337-008-0517-6>



AGRADECIMENTOS

O Comitê Organizador agradece a todos os participantes, aos patrocinadores e especialmente à CAPES, Fapesp e CNPq pelo apoio recebido para a realização do XLI CBrAVIC.

